A peer-reviewed version of this preprint was published in PeerJ on 14 October 2019.

View the peer-reviewed version (peerj.com/articles/7813), which is the preferred citable publication unless you specifically need to cite this preprint.

Smolyar I, Bromage T, Wikelski M. 2019. Layered patterns in nature, medicine, and materials: quantifying anisotropic structures and cyclicity. PeerJ 7:e7813 https://doi.org/10.7717/peerj.7813

Layered patterns in nature, medicine and materials: Quantification of anisotropic structures and cyclisity

I. Smolyar[a], T. Bromage[b], M. Wikelski[c]

[a]National Centers for Environmental Information/NOAA, 151 Patton Avenue, Asheville, NC 28801, USA. igorsmolyar8755@gmail.com
[b]Department of Biomaterials & Biomimetics and Basic Science & Craniofacial Biology, College of Dentistry, New York University, New York, NY 10003 USA. tim.bromage@nyu.edu
[c]Max-Planck Institute for Ornithology, Am Obstberg 1, D-78315 Radolfzell, Germany wikelski@orn.mpg.de
and
Dept. of Biology, Konstanz University, D-78467 Konstanz, Germany

Examples of layered patterns

Mars surface. Size in meters

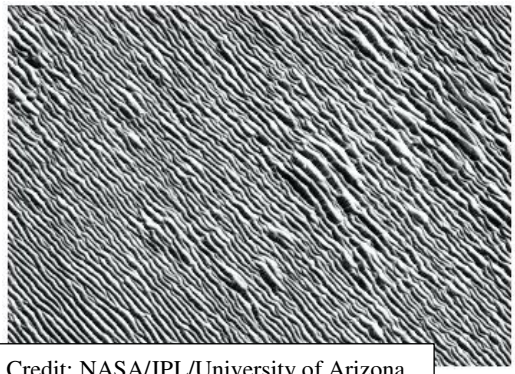

Credit: NASA/JPL/University of Arizona

Human bone. Size in microns

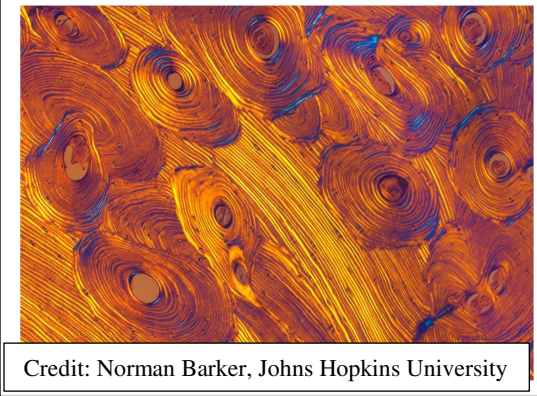

Credit: Norman Barker, Johns Hopkins University

Eutectic alloy. Size in microns

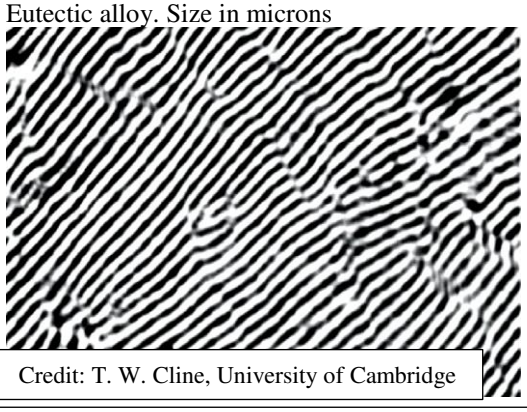

Credit: T. W. Cline, University of Cambridge

Fish skin. Size in centimeters

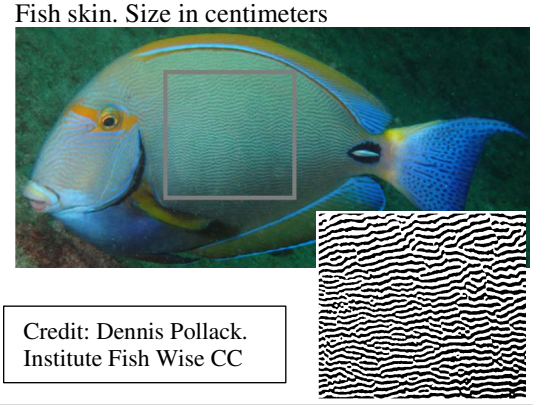

Credit: Dennis Pollack. Institute Fish Wise CC

35 figures are in the end of the manuscript

Basic concepts:

Figure 3. Layered pattern structure as graph and logical network

Figure 4. Quantification structural disorder in an anisotropic layered pattern

PeerJ Preprints | https://doi.org/10.7287/peerj.preprints.27451v2 | CC BY 4.0 Open Access | rec: 5 Jan 2019, publ: 5 Jan 2019

Abstract

Various natural patterns—such as terrestrial sand dune ripples, lamellae in vertebrate bones, growth increments in fish scales and corals, aorta and lamellar corpuscle of humans and animals—comprise layers of different thicknesses and lengths. Microstructures in manmade materials—such as alloys, perlite steels, polymers, ceramics, and ripples induced by laser on the surface of graphen—also exhibit layered structures. These layered patterns form a record of internal and external factors regulating pattern formation in their various systems, making it potentially possible to recognize and identify in their incremental sequences trends, periodicities, and events in the formation history of these systems. The morphology of layered systems plays a vital role in developing new materials and in biomimetic research. The structures and sizes of these two-dimensional (2-D) patterns are characteristically anisotropic: That is, the number of layers and their absolute thicknesses vary significantly in different directions.

The present work develops a method to quantify the morphological characteristics of layered patterns that accounts for anisotropy in the object of study. To reach this goal, we use Boolean functions and an N-partite graph to formalize layer structure and thickness across a 2-D plane and to construct charts of 1) "layer thickness vs. layer number" and 2) "layer area vs. layer number." We present a parameter for structural disorder in a layered pattern (DStr) to describe the deviation of a study object's anisotropic structure from an isotropic analog and illustrate that charts and DStr could be used as local and global morphological characteristics describing various layered systems such as images of, for example, geological, atmospheric, medical, materials, forensic, plants, and animals. Suggested future experiments could lead to new insights into layered pattern formation.

Keywords: 0-gravity, anisotropy of layered systems, biomimetics, Boolean functions, image processing, N-partite graph, structural anomaly, structural disorder of layered systems, world ocean

1. Introduction

Layered structures can be found in many natural patterns—including satellite images of the surfaces of Mars, Pluto (Fig. 1A), and Titan (Fig. 1B) and terrestrial tidal sand ripples—exhibit layered patterns of varying sizes, ranging from meters to hundreds of kilometers. Fish skin, fish scales, coral growth increments, leaf structures and flower surface microstructures, snake and spider skin (Fig. 2A, B), bird plumage patterns, three-dimensional (3-D) images of shells (Fig. 2C), clouds and lightning, human and animal hairs, and wild turkey wings (Fig. 2D) all exhibit patterns of this type. Other examples are microstructures in manmade materials and in lamella bones (Fig. 1C).

Natural layered patterns are attractive objects of study for specialists of different disciplines for several reasons. First, layer thickness and structure represent the cumulative effect of internal and external factors regulating pattern formation. Thus, layered patterns serve as a record of diverse events occurring in different space–time domains. This record makes it possible to link the morphology of layered patterns to external factors such as variability in the Earth's rotation (Pannella, 1972), climate cycles (Radebaugh et al., 2011; Ewing et al., 2014), and the state of the environment (Guyette and Rabeni, 1995; Costa et al., 2002).

Some soft tissues—including the human aorta, skeletal muscle (Fig. 2E), and Pacinian (lamellar) corpuscles—exhibit layered structures. Pacinian corpuscles are nerve endings in the skin responsible for detecting and locating skin deformations produced by air vibrations and skin contact (Kaas, 2012). Studying their morphological parameters has implications for the development of new technology for conveying speech and visual information through somatosensory channels (Rothenberg et al., 1977; Bau et al., 2010; Biswas et al., 2015). The human aorta has a layered (i.e., lamellar) structure (Fig. 14) that typifies the elastic lamina found in human and animal blood vessels. The study of aortic microstructure and age-related changes is an urgent area of medical research (Novotny et al., 2017; Tonar et al., 2015; Akhtar et al., 2011; Selçuk et al., 2015).

Additionally, analyzing layer morphology is an essential element of solving many problems in materials science, biomimetic, and forensic research. For instance, biometric research has

PeerJ Preprints | https://doi.org/10.7287/peerj.preprints.27451v2 | CC BY 4.0 Open Access | rec: 5 Jan 2019, publ: 5 Jan 2019

explored the structural properties of butterfly photonic systems (Vukusic and Sambles, 2003), flower surfaces (Barthlott et al., 2016; Huang et al., 2017), and snakeskin (Abdel-Aal and Mansori, 2011; Klein and Gorb, 2012). In materials science, a material's mechanical and physical characteristics are determined by its microstructure, which in many instances is layered (Moya, 1995; Mayer, 2005). Understanding the relationship between microstructure and these properties is vital for developing porous materials with new mechanical characteristics (Deville, 2018). In forensic research, morphological features of layered systems in hair and fingerprints can be used for identification purposes (Champod, 2015; Lee et al., 2014; De Marinis and Asprea, 2006).

The study and commercial applications of various categories of layered systems requires formalizing aspects of their analysis. One of the first steps toward this goal is quantitatively describing the morphology of a layered pattern. Formalizing this morphology is problematic because of the numerous breaks and confluences (i.e., bifurcations) in the layers of 2-D and 3-D objects (Blumberg, 2006). The number and thickness of these layers is a function of the direction in which they are measured; that is, they are anisotropic in both size (including thickness and area) and structure, thereby making it difficult to develop a formal procedure for their analysis.

Layered systems—irrespective of their nature or size—share several key elements, including the idea of layers, number of layers, and their thicknesses. If layers have no breaks or confluences (i.e., layers are structurally isotropic), then calculating the thickness, area, and number of these layers across a 2-D plane is a straightforward task. But if layers have breaks and confluences, quantifying a pattern's characteristics becomes problematic.

To address this problem, we have proposed an empirical model $M = \{BF, G(N), T_{M,N}\}$ of 2-D layered patterns, with the aim of providing tools to quantify the morphological features of anisotropic layered objects (Smolyar et al., 1987; Smolyar and Bromage, 2004; Smolyar, 2014; Smolyar et al., 2016). This model has three components: a Boolean function (BF) (Fig. 3B–D), an N-partite graph (G(N)) (Fig. 3A) to describe the 2-D structure of layers, and Table $T_{M,N}$, which comprises the thickness of layers along transects $R_1, \ldots, R_j, \ldots, R_N$, plotted from a pattern's lower margin to its upper margin. Transects $R_1, \ldots, R_j, \ldots, R_N$ are straight lines always

PeerJ Preprints | https://doi.org/10.7287/peerj.preprints.27451v2 | CC BY 4.0 Open Access | rec: 5 Jan 2019, publ: 5 Jan 2019

distributed evenly across a 2-D layered pattern. The concept of open/closed gates (Fig. 3B,C) makes it possible to describe all possible versions of layer structure using Boolean functions.

The second set of key elements shared by 2-D anisotropic layered systems are the concepts of layer structure across a 2-D plane and layer length, which are defined in terms of transects that cross a pattern from its lower to its upper margins (Fig. 4A). We introduce the concept of synchronizing layer formation across a 2-D plane in order to quantify the structure of layers and develop a procedure for plotting 1) "layer thickness vs. layer number" and 2) "layer area vs. layer number" (Smolyar et al., 2016). That is, to construct the structure of each layer across a 2-D plane, it is necessary to synchronize layer formation in the space–time domain. Because layers are anisotropic, more than one version of the layered structure could be used for synchronization, resulting in fuzziness in the charts for "layer thickness vs. layer number" and "layer area vs. layer number." Fuzziness is an unavoidable attribute when parameterizing anisotropic layered patterns. When describing the variability of layer size in anisotropic patterns across a 2-D plane, high accuracy and high confidence are mutually exclusive.

Smolyar et al. (2016) introduced the idea of an "index of confidence," which allows a compromise between detail and signal-to-noise ratio—either more detail and a lower signal-to-noise ratio or less detail and a higher signal-to-noise ratio—when describing the variability of layer thickness and area across *N* transects. It is therefore possible to plot robust charts for "layer thickness vs. layer number" and "layer area vs. layer number." These charts describe the global morphological characteristics of an entire 2-D layered pattern. For instance, if each layer (e.g., of tree rings, fish scales, lamellar bones, corals) is associated with the instant of time t_j in which it was formed, then a layer's thickness and area are measures of the growth rate of the layered system at that time. In this case, "layer thickness vs. layer number" and "layer area vs. layer number" are interpreted as growth-rate variability across the entire system of 2-D anisotropic layers.

Using model M = {BF, G(N), $T_{M,N}$} to analyze the growth-rate variability of lamella bones allows us to reveal cyclicity in bone formation not previously observed (Bromage et al., 2009). These results—as well as evidence that many factors controlling pattern formation are cyclic in

PeerJ Preprints | https://doi.org/10.7287/peerj.preprints.27451v2 | CC BY 4.0 Open Access | rec: 5 Jan 2019, publ: 5 Jan 2019

nature—motivate us to use M = {BF, G(N), $T_{M,N}$} to reveal and quantify cyclicity for layered objects when layer formation is not associated with a moment of time, t_j.

The present paper continues our previous work (Smolyar et al., 2016). The goals of the paper are two-fold: 1) develop a method for quantifying the structural characteristics of layered patterns and 2) examine the applicability of DStr and the empirical model M = {BF, G(N), $T_{M,N}$} for analyzing layered patterns of various categories. To reach these goals, we

- review layered patterns appearing in the realms of medicine, forensics, geology, botany, zoology, atmospheric science, and materials science in order to justify that similarities in the structural anisotropy of layers can be described by M = {BF, G(N), $T_{M,N}$};
- introduce a structural characteristic of layered patterns called "layers structural disorder" (DStr) and propose a fully automated method for its calculation. DStr serves as a measure of deviation from an isotropic prototype in patterns with anisotropic layered structure;
- illustrate that DStr is a universal characteristic applicable to any 2-D layered pattern, irrespective of nature and size, and could be used as a local and global defining characteristic of a layered pattern;
- illustrate the possibility of using an empirical model of layered patterns, M = {BF, G(N), $T_{M,N}$}, to quantify the variability of layer thickness across 2-D planes of images of objects of various categories.

Various examples underline the applicability of DStr and M = {BF, G(N), $T_{M,N}$} for quantifying the structural characteristics of various categories of living and non-living layered systems. We also give suggestions for further experiments that have the potential to help us better understand environmental influences on pattern formation. It is necessary to point out that using DStr and M = {BF, G(N), $T_{M,N}$} to gain insight into any particular layered system is outside of the scope of the present work.

In different publications, layers may be called growth lines, growth layers, circuli, bands, growth increments, lamellae, ripples, or ridges, depending on the object of study. The present work uses these terms synonymously.

PeerJ Preprints | https://doi.org/10.7287/peerj.preprints.27451v2 | CC BY 4.0 Open Access | rec: 5 Jan 2019, publ: 5 Jan 2019

2. Method

This section explains DStr and describes two structural extremes of anisotropic 2-D layered systems: minimal disorder (DStr = 0) and maximal disorder (DStr = 1).

2.1. Basic concept

A precise definition of anisotropy/isotropy depends on the object of study. Our definition of isotropic and anisotropic layered patterns comes from the study of growth increments in fish scales. Growth rates of fish scales vary in different directions, resulting in numerous breaks and confluences in growth layers, which are the source of anisotropy in fish scale growth layers because more than one possibility exists for describing layer structure across a 2-D plane (i.e., across N transects). In other words, the structure of layers is a function of the state of gates (Fig. 3B-D). Therefore, characteristics of anisotropy in a layered pattern are i) the possibility of more than one version of layer structure and ii) different lengths of layers, where length is defined as the number of transects crossing the layer. In an isotropic image, each layer is crossed all N transects (i.e., layers have no breaks and confluences), and only one possibility exists to describe the structure of each layer. Objects with isotropic layered structure are relatively rare. Hence, a general definition of anisotropy implies different properties in various different directions, and anisotropy in a layered system implies different properties in the directions of layers formation only.

2-D layered patterns consist of both isotropic (IC) and anisotropic (AC) components. We therefore define the DStr of a 2-D layered pattern as the measure of a pattern's deviation from isotropy. Because the N-partite graph, G(N), represents the structure of a layered pattern, AC and IC could be understood in terms of edges and vertices in G(N).

G(N) consists of a sequence of bi-partite graphs, $G(R_1,R_2)$, … $G(R_j,R_{j+1})$, … $G(R_{N-1},R_N)$, where $G(R_j,R_{j+1})$ is a bi-partite graph that describes the structure of a layered pattern situated between transects R_j and R_{j+1} (Fig. 3A). An isotropic layer here would imply that vertex $\mathbf{a}\in R_j$ connects only with vertex $\mathbf{b}\in R_{j+1}$ and $\mathbf{b}\in R_{j+1}$ connects only with $\mathbf{a}\in R_j$. Edge **ab** in $G(R_j,R_{j+1})$ is therefore an isotropic edge. TotalEdges denotes the total number of edges in $G(R_j,R_{j+1})$. The number of anisotropic edges in $G(R_j,R_{j+1})$ is equal to TotalEdges minus the number of isotropic edges.

PeerJ Preprints | https://doi.org/10.7287/peerj.preprints.27451v2 | CC BY 4.0 Open Access | rec: 5 Jan 2019, publ: 5 Jan 2019

Disorder (DGrp (R_j,R_{j+1})) of bi-partite graph G(R_j,R_{j+1}):

$$DGrp(R_j,R_{j+1}) = \text{anisotropic edges/ TotalEdges.}$$

Disorder of N-partite graph G(N):

(1) $$DGrp(R_1,R_N) = 1/(N-1)*\Sigma\ DGrp(R_j,R_{j+1}),\ j = 1, N.$$

Two questions follow from equation (1).

Question #1. From equation (1), it transpires that DGrp(R_1,R_N) depends on sampling density (i.e., the number of transects used to calculate DGrp(R_1,R_N)). How many transects should be used to quantify DGrp(R_1,R_N), which has not yet been technically defined? Section 2.2 answers this question.

Question #2. Following equation (1), DGrp(R_1,R_N) varies from 0 to 1. If DGrp(R_1,R_N) = 0, then the layered pattern is entirely isotropic; such layered images are easily visualized (Fig. 24). But what do entirely anisotropic patterns (that is, DGgr(R_1,R_N) = 1) look like? Section 2.3 tackles this issue.

2.2. Sampling density

Because the AC of a layered pattern are unevenly distributed in 2-D space, we examine multiple versions of sampling density to determine how many transects are necessary to quantify DStr. We plot the function y = f(x) (i.e., DStr = f(number of transects)), which describes dynamic changes in DStr when the number of transects tends to the maximum possible number. The area bounded by y = f(x) and the y-axis is the measure of DStr.

The choice of how many transects, R_1, …, R_j, …, R_N, to use to develop the empirical model M = (BF, G(N), $T_{M,N}$) plays an essential role in analyzing the structure of anisotropic layered patterns. Consider the proposed approach for constructing sets of transects used to describe model components BF, G(N), and $T_{M,N}$ and calculate DStr.

The general principle in choosing the number of transects is based on the fact that we do not know *a priori* how many transects will best describe the particular layered pattern within the

PeerJ Preprints | https://doi.org/10.7287/peerj.preprints.27451v2 | CC BY 4.0 Open Access | rec: 5 Jan 2019, publ: 5 Jan 2019

frame of finding a solution to the specific problem. In these circumstances, our choice is to examine as many different versions of transect sets. In the present work, all transects are straight lines, and the distance between two adjacent transects remains constant across all transects.

Figure 4 illustrates the procedure for constructing y = f(x) and calculating DStr. Fig. 4A depicts a layered pattern with structural anisotropy and a graph constructed for transects A, B, and C; Figure 4B depicts a graph for four transects. The initial layered pattern is presented as a raster graphic; thus, the size of the layered pattern is measured in terms of pixels. The minimum distance between two adjacent transects is 1 pixel. If the thickness of a transect is equal to 1 pixel, then the maximal number of transects is N_{max} = pattern width/2 (if the pattern width is divisible by 2), and N_{max} = (pattern width+1)/2 otherwise. The layered pattern in Fig. 4 has a maximum of 103 transects. We calculate DGrp for N = 3, 4, 5, … , 103, or 100 versions of transect sets (Fig. 4C) to plot y = f(x) and normalize the number of transects in order to present the results of the calculation in scale [0,1]; N_i(normalized) = N_i/N_{max} (Fig. 4D). By calculating DGrp for transect Set #1 = (R_1, R_2, R_3), Set #2 = (R_1, R_2, R_3, R_4), …, Set #100 = (R_1, R_2, … , R_{103}), we describe the variability of DStr across all possible transect versions. In this case, y = f(x) contains as much structural detail as possible for the layered pattern under study.

We refer to the number of transect sets used to plot y = f(x) and calculate DStr as "sampling density." Sampling density is "highest" if all possible versions of transect sets are used to construct y = f(x) and calculate DStr (Fig. 4D). Sampling density could be described as "medium" or "low" depending on the number of transect sets used to construct y = f(x). Fig. 22B illustrates how high, medium, and low sampling density affect the shape of y = f(x).

The coefficient of determination, R^2 (Draper and Smith, 1998), ranges from 0 to 1 and is used to estimate how well the partial-rational function $y = \boldsymbol{m}x^{\boldsymbol{k}}$ replicates y = f(x). If $R^2 = 1$, then $y = \boldsymbol{m}x^{-\boldsymbol{k}}$ is the approximation of y = f(x) with 0 error. We choose function $y = \mathbf{m}x^{-\mathbf{k}}$ to replicate y = f(x) for two reasons. First, it contains two numeric coefficients, **m** and **k**, so only two numeric values serve as global structural characteristics of the entire 2-D layered pattern. Second, for many-layered patterns, $R^2 \geq 0.93$ for $y = \mathbf{m}x^{-\mathbf{k}}$.

PeerJ Preprints | https://doi.org/10.7287/peerj.preprints.27451v2 | CC BY 4.0 Open Access | rec: 5 Jan 2019, publ: 5 Jan 2019

We use Microsoft Excel 2007 to calculate parameters $\boldsymbol{m}$ and $\boldsymbol{k}$ for $y = \boldsymbol{m}x^{-\boldsymbol{k}}$ and R^2 for $y = \boldsymbol{m}x^{-\boldsymbol{k}}$. Because $R^2 = 0.9962$, $y = 0.0228x^{-0.969}$ (Fig. 4D), thus equation (2) can be used to calculate DStr:

$$\mathrm{DStr} = \int_0^1 f(x)dx. \quad (2)$$

For the pattern in Fig. 4D, DStr = 0.08346.

2.3. Maximal structural disorder of layered patterns (DStr = 1)

Consider the appearance of a layered pattern with DStr = 1 (i.e., the layered pattern's has no IC): Each vertex situated along transect R_j connects with all vertices situated along R_{j+1}; thus, the bi-partite graph $G(R_j, R_{j+1})$ is complete. If the layered image consists of complete bi-partite graph sequences for all possible numbers of transects, then DStr = 1. It should be stressed that we do not use isolated vertices (i.e., those that are not connected to other vertices) in calculating DStr, because they do not form isotropic or anisotropic edges. One possible example of a pattern in which DStr approaches maximal structural disorder is stars in the night sky (Fig. 11A, B).

3. Results

We use images of living and non-living systems to justify applying the proposed method to quantify structural characteristics of a broad range of patterns. Section 3.1 presents results of calculating DStr, Section 3.2 presents the variability of layer size across a 2-D plane, and Section 3.3 presents experiments illustrating the sensitivity of these methods to detecting minor changes in layered structures.

3.1. Structural disorder of layered patterns

The algorithm for calculating DStr consists of the following steps:

1. The original layered image (in grayscale raster format) is converted into M = (BF, G(N), $T_{M,N}$) using the technology described in Smolyar, 2014 and Smolyar et al. (2016).
2. Transects $R_1, \ldots, R_j, \ldots, R_N$ are plotted and $DGrp(R_j,R_{j+1})$ is calculated (equation 1).
3. Step 2 is repeated P times, resulting in $DGrp(1,N_1)$, $DGrp(1,N_2)$, …, $DGrp(1,N_P)$.
4. The function y = f(x) is constructed and R^2 is calculated.
5. DStr for the entire sampling area is calculated (equation 2).

We consider DStr for layered images in seven categories: geology, atmosphere, materials, medicine, plants, animals, and forensics.

PeerJ Preprints | https://doi.org/10.7287/peerj.preprints.27451v2 | CC BY 4.0 Open Access | rec: 5 Jan 2019, publ: 5 Jan 2019

Geology (Figures 5–8). Sand dunes on the Martian surface form a record of the role of wind in climatic regime (Gardin et al., 2011; Diniega et al., 2017; Lapotre et al., 2016). Studying the structural characteristics of dunes and their changes over time is necessary to better understand Martian climatic systems and how they impact robotic and human activity on Mars. Figure 5 shows the structural similarities and differences among four parts of the sampling area. Parameter DStr for parts A – D indicates that part D has the most complicated layered structure, i.e deviation from isotropic layered object, since DStr(D)> DStr(B)> DStr(A)> DStr(C).

Figure 6A depicts structural anomalies in a layered system of the Martian surface. The DStr of the sampling area **a** is 10 times less than that of nearby area **b**, which exhibits structural anomaly with respect to area **a**. Figure 6B depicts the structural anomaly of sand ripples. The red sampling area exhibits structural anomaly with respect to nearby orange and blue areas. The DStr of the orange and blue areas is 2.3 times less than that of the red area.

Figure 7 shows a vertical section of underground soil structure, obtained by Ground Penetrating Radar, that demonstrates anisotropic layers that can be used to identify pipes, archeological artifacts, or soil composition in the study area (Robinson et al., 2013). The sampling area of Figure 7 is divided into four parts, and DStr is calculated for each part. Part D has the most complicated structure since DStr(D)> DStr(B)> DStr(A)> DStr(C).

Figure 8 shows significant differences between structures of sand ripples formed in the tidal zone at Inch on the Dingle Peninsula in Ireland. Knowledge of the dynamics and morphology of dunes and ripples is useful for managing beach ecosystems (Sloss et al., 2012; Passchier and Kleinhans, 2005).

Atmosphere (Figures 9–11). Altocumulus clouds (Fig. 9) and cloud-to-ground lightning (Fig. 10) are examples of atmospheric layered patterns. The morphology of these phenomena can be described in the same quantitative terms used for geologic and biological systems, namely, as a deviation from a layered object with isotropic structure. The structure of lightning could be described with different levels of detail. A satellite image of the United States at night and

PeerJ Preprints | https://doi.org/10.7287/peerj.preprints.27451v2 | CC BY 4.0 Open Access | rec: 5 Jan 2019, publ: 5 Jan 2019

357 another from the Hubble Space telescope (Fig. 11) illustrate what the chart for "DStr vs. number
358 of transects" looks like in images tending toward complete disorder.
359
360 Materials (Figure 12). Materials science is an attractive area for the application of M = {BF,
361 G(N), $T_{M,N}$} because the macro- and nanostructures of various materials exhibit layered
362 anisotropic patterns (Fig. 12) that define their properties. Thus, DStr could serve as a local and
363 global morphological parameter for describing material microstructures. DStr could also be used
364 to link structures and properties, an essential step in developing materials with desired
365 combinations of characteristics. Figure 12A exhibits images of a eutectic alloy, ion-induced
366 ripples (Lian et al., 2006), and perlite and their corresponding DStr parameters.
367
368 The morphology of the surface of black diamonds is an essential element in developing solar
369 energy conversion systems (Calvani et al., 2016). Figure 12B shows the dynamic of DStr as a
370 function of different treatments of the black diamond surface.
371
372 Medicine (Figures 13–15). Lamella bones (Fig. 13), the human aorta (Fig. 14), and an eye
373 angiogram (Fig. 15) are medical examples of layered patterns with structural anisotropy. Because
374 medical treatments affect their structures, estimating the influence of treatment necessitates
375 comparing the morphology of layered patterns before and after treatment (Novotny et al., 2017).
376 Structural disorder in the sampling area of bone B is much simpler than that in bone A (Fig. 13).
377 Sampling area B is uniform, whereas sampling area A includes a combination of bone and osteon
378 lamellar systems.
379
380 The aorta lamellar pattern in Figure 14 has uniform anisotropic structure since parts A, B, C, and
381 D have similar values of DStr. It is possible to consider an eye angiogram as a layered pattern
382 with structural anisotropy (Fig. 15). The structure of an eye angiogram with medium detail is
383 more complicated than that with low detail. DStr allows us to quantitatively describe this
384 difference.
385
386 Plants (Figures 16–17). Flower surfaces can be super hydrophobic and self-cleaning, features
387 that make their morphology an important object of biomimetic study (Barthlott et al., 2017).

PeerJ Preprints | https://doi.org/10.7287/peerj.preprints.27451v2 | CC BY 4.0 Open Access | rec: 5 Jan 2019, publ: 5 Jan 2019

Figure 16 shows the layered microstructure of the surface of a Rose petal divided into four sampling areas. Visual inspection of the sampling areas allows us to note that area B has the most complicated layer structure. Values of DStr for A, B, C, and D verify this observation.

Figure 17 depicts juvenile and adult leaves of an aquatic Madagascar Lace plant, which is an excellent model for studying programmed cell death in plants (Gunawardena et al., 2004; Dauphinee et al., 2017). We use the juvenile and adult vein systems in Madagascar Lace leaves to compare their morphology. The sampling area of the juvenile leaf is completely isotropic, DStr(lace juvenile leaf) = 0 (Fig. 17), whereas the sampling area of the adult leaf has a high degree of disorder, which is obvious from its pattern; DStr(lace adult leaf) = 0.7116 (Fig. 17).

Animals (Figures 18–21). The configuration of stripes on fish skin (Fig. 18) is a typical example of an anisotropic layered pattern. The formation of patterns on the surfaces of fish, shells, and mammals has been explained by a reaction–diffusion system (Turing, 1952; Meinhardt, 1989; Shoji et al., 2003). Results of calculating DStr for sampling areas A, B, C, and D imply that DStr(B)>DStr(C)>DStr(A)>DStr(D), indicating that area B has the most complicated structure and area D has the simplest structure among four sampling areas. This result inspires two questions: 1) Is the DStr of the right side of the fish similar to the DStr of the left side? 2) Could the morphology of stripes serve as a record of internal and external events in the life history of a fish? Model M = {BF, G(N), $T_{M,N}$} could be one tool to help to answer these questions.

The micro-ornamentation of snakes is broadly studied in biomimetic research due to unique combinations of surface features (Arnold, 2002; Gower, 2003; Filippov and Gorb, 2016). Figure 19 shows hierarchical layered microstructures in snake skin. Although the entire area of snake skin shown in Figure 19 has complicated morphology, sampling areas A and B have DStr close to isotropy because the DStr of A and B are very low: DStr(A) = 0.042 and DStr(B) = 0.063.

Plumage patterns in banded pitta, kingfisher, and owl (Fig. 20) offer examples of layered systems in bird plumage. DStr shows significant diversity in the structure of these layered systems: DStr(giant kingfisher) = 0.7591; DStr(banded kingfisher) = 0.0574. This result inspires us to ask whether parameters of layered structures might serve as phenotypic characteristics

PeerJ Preprints | https://doi.org/10.7287/peerj.preprints.27451v2 | CC BY 4.0 Open Access | rec: 5 Jan 2019, publ: 5 Jan 2019

(Gluckman and Mundy, 2016). Model M = {BF, G(N), $T_{M,N}$} could be used to test this hypothesis (i.e., examine the structural characteristics of birds' plumage patterns with respect to state of the environment).

Photonic systems of biological objects generate interest among scientists and engineers across various disciplines due to their unique ability to manipulate color using micro-structured surfaces (Starkey and Vukusic, 2013; Parker, 2000). Many photonic surfaces in flowers and animals exhibit lamellar structures (Vukusic and Sambles, 2003), such as the scales arranged in anisotropic layered patterns on the surfaces of morpho butterfly wings (Fig. 21A). We use DStr to compare the anisotropic characteristics of left and right wings. Figure 21B reports the results of DStr calculations for six sampling areas. The left and right wings of Morpho butterfly have similar structural characteristics: DStr is equal to 0.132 and 0.131, respectively. Could DStr be a characteristic of blue color nuances in Morpho butterflies? Do male and female Morpho butterflies have similar structural characteristic DStr? How do local/global structural anomalies in butterfly wings with respect to DStr affect butterfly color? Model M = {BF, G(N), $T_{M,N}$} could be used to answer these questions.

Forensic (Figures 22–23). The layered microstructures of human hair are much more complicated than those of some animals (Fig. 22A), which is confirmed by DStr(human), DStr(deer), DStr(mouse), and the corresponding charts for "structural disorder of hair = f(number of transects)." Figure 22B shows that high sampling density accounts for more structural details than low sampling density.

As Figure 23A indicates, the four basic categories of fingerprint patterns have distinctive structural characteristics that vary from DStr(plain arch) = 0.1021 to DStr(central pocket loop) = 0.1978. Distinctions between DStr among different categories of fingerprints substantially depend on the number of transects used to calculate DStr (Section 2.2). To define the number of transects that allow maximal differences among DStr in the four categories of fingerprints, we plot the chart (Fig. 23B) as DStr(central pocket loop) − DStr(plain arch) = f(number of transects). Nine transects allow the maximal possible differences between two categories of fingerprints; that is, DStr(central pocket loop) − DStr(plain arch) = 0.253, which is 2.6 times

PeerJ Preprints | https://doi.org/10.7287/peerj.preprints.27451v2 | CC BY 4.0 Open Access | rec: 5 Jan 2019, publ: 5 Jan 2019

more than the DStr(central pocket loop) and DStr(plain arch) comparison if equation (2) is used to calculate DStr. Sampling density and number of transects could complement DStr in forensic identification.

Excel file (Supplemental) presented raw data for calculation DStr and DStr = f(transect number).

3.2. Cyclic variability of layer size across 2-D plane

The algorithm for constructing chart for "layer thickness vs. layer number is identical to that used in Smolyar et al. (2016). The signal-to-noise ratio for charts (Figures 24-29) is equal to 6. The experiments described in this section examine the distribution of layer thickness across a sampling area in order to estimate whether average layer thickness accurately describes the morphological characteristics of 2-D layered systems.

Geology (Figures 24–25). Dune fields are an example of the layered patterns that exist throughout nature. Dune spacing (i.e., layer thickness) is a basic morphological characteristic of dune systems (Lancaster, 2009). Figures 24 and 25 show layered fragments of the surface of Mars that have isotropic structure (i.e., all fragments have DStr = 0), which allows us to describe the variability of layer thickness across the 2-D sampling area with high accuracy. Several transects are used to calculate average thickness of each layer. Charts of "layer thickness vs. layer number" show cyclic trends in the variability of layer thickness across the sampling area (Fig. 24 and 25). Similar cyclic trends in anisotropic structures are also observed on Mars and Earth (Smolyar et al., 2016).

Materials (Figure 26). Lamellar/rippled/layered patterns have been found in metals, alloys, insulators, semiconductors, and many others materials (Deville, 2018; Zuo et al., 2016; Moya, 1995). Lamellar thickness is a micromorphological characteristic that plays a central role in the relationship between a material's microstructure and its macro properties because "the unique properties of natural layered materials and nanocomposites are achieved through a fine control of the layer thickness" (Deville et al., 2007, p. 970). Figure 26A depicts an image of layered Al–Si composite with anisotropic structure. The chart of "layer thickness vs. layer number" shows cyclicity in the variability of layer thickness across the sampling area (Fig. 26B), which is

PeerJ Preprints | https://doi.org/10.7287/peerj.preprints.27451v2 | CC BY 4.0 Open Access | rec: 5 Jan 2019, publ: 5 Jan 2019

481 divided into parts A, B, C, and D (Fig. 26C) according to the uniform distribution of layer
482 thickness in each part (Fig. 26D). It follows that the chart of "layer thickness vs. layer number"
483 provides a more detailed description of a layered pattern's morphological characteristic than
484 average layer thickness.
485
486 Medicine (Figures 27). Figure 27 shows a Pacinian (lamellar) corpuscle (PC), a sensory receptor
487 in skin that is sensitive to contact and vibration. The anisotropic lamellar structure of PCs plays
488 an essential role in the function of the PC system; lamellar thickness and number of lamellae are
489 used to examine the link between the PC's material and morphological characteristics and its
490 response to vibration (Quindlen et al., 2017). We use 42 transects to plot the chart of "layer
491 thickness vs. layer number" (Fig. 27), which clearly demonstrates the cyclic nature of variability
492 in lamellar thickness across the sampling area.
493
494 Animals (Figures 28–29). The chart of "layer thickness vs. layer number" exhibits non-random
495 trends in the variability of layer thickness across bird feathers (Fig. 28). The chart and DStr could
496 potentially serve as morphological characteristics of birds with application to the study of their
497 life cycles. Striped patterns are often used to distinguish bird species from one another. In
498 particular, shrikes and their relatives are recognizable to birders by the peculiar differences in the
499 thickness and layering of their striped patterns, many of which are simply black and white.
500 Furthermore, there are often marked differences in the morphological features of feathers
501 between males and females of the same species, a dimorphism that is recognized both by the
502 animals themselves and by human observers (Gluckman 2014).
503
504 The morphology of orb (circular) spider webs (Fig. 29) is frequently studied not only because of
505 their superior mechanical properties but also as a source of information about spiders'
506 construction behaviors (Sensenig et al., 2010; Eberhard, 2014; Soler and Zaera, 2016). The orb
507 web represents a layered system with structural anisotropy: "One of the most relevant structural
508 traits of orb webs is their mesh width" (Zschokke and Nakata, 2015, p. 661). Mesh width (i.e.,
509 layer thickness) is used to understand the construction features of web systems and relate them to
510 spiders' behavior. For instance, Zschokke and Nakata (2015, p. 661) point out that "a closer look
511 at the orb webs reveals that mesh widths are not the same throughout the entire web." Charts

PeerJ Preprints | https://doi.org/10.7287/peerj.preprints.27451v2 | CC BY 4.0 Open Access | rec: 5 Jan 2019, publ: 5 Jan 2019

512 describing the variability of mesh width across the sampling area (Fig. 29) confirm this statement
513 and indicate cyclicity in the variability of mesh width across the sampling area. Thus, M = {BF,
514 G(N), $T_{M,N}$} could be used to generate a new set of structural characteristics describing the
515 anisotropy of an orb web and its segments.
516

517 **3.3. Sensitivity of DStr to minor structural changes**

518 Next, we examine how minor changes in layer structure affect DStr, using fingerprint (Fig. 30A),
519 fish scale (Fig. 30B), and an eye angiogram (Fig. 30C) as test objects. Let us denote
520 characteristics of images before and after structural changes by DStr(before changes) and
521 DStr(after changes). We describe the link between DStr(before changes) and DStr(after changes)
522 and structural changes in images in quantitative terms using the following procedure: First, we
523 describe the difference between DStr(before changes) and DStr(after changes) on a relative scale
524 (%). All changes in layer structure are marked in red. We denote the difference as Parameter-1.
525 Second, we describe (in %) the difference (in pixels) between the images before and after
526 changes. To do so, we calculate the number of black pixels in an image before changes (total
527 pixels before changes) and the total number of pixels that change color (white to black or vice
528 versa) as a result of structural changes (total pixel change). The ratio (%) of "total pixel
529 change/total pixels before changes" allows us to calculate the magnitude of structural changes in
530 an image. This ratio is denoted Parameter-2. The relation between Parameter-1 and Parameter-2
531 allows us to estimate the sensitivity of DStr to structural changes in the image. Results of
532 calculating Parameter-1 and Parameter-2 are

533 | | Parameter-1 | Parameter-2 |
534 | Fingerprint | 0.55% | 0.072% |
535 | Fish scale | 3.80% | 0.150% |
536 | Eye angiogram | 0.32% | 0.077% |
537 | Average | 1.56% | 0.10% |

538 The average ratio between Parameter-1 and Parameter-2 is 1.56:0.1, which implies that a 1%
539 structural change in layers results in a 15.6% change in DStr. This result provides evidence that
540 minor changes in layer structure are accompanied by substantially greater changes in DStr
541 values. This feature of M = {BF, G(N), $T_{M,N}$} could be positive or negative, as required by
542 application. For instance, if it is necessary to identify a fingerprint image of poor quality with

PeerJ Preprints | https://doi.org/10.7287/peerj.preprints.27451v2 | CC BY 4.0 Open Access | rec: 5 Jan 2019, publ: 5 Jan 2019

many gaps, then the sensitivity of DStr and y = f(x) to structural changes is a barrier. If the image is of a good quality and it is necessary to track minor changes in structure over time (Silvestro et al., 2010) or find structural differences between patterns of spider webs (Eberhard, 2014; Hesselberg, 2013; Blackledge and Zevenbergen, 2006) or aorta (Avolio et al., 1998; Zou and Zhang, 2009; Taghizadeh and Tafazzoli-Shadpour, 2017; Mattson and Zhang, 2017), for instance, then the sensitivity of M = {BF, G(N), $T_{M\,N}$} to structural changes is an advantage.

4. Discussion

4.1. Method summary

Model M = {BF, G(N), $T_{M,N}$} is an example of an empirical approach to studying anisotropic layered systems. Analyzing large datasets requires this procedure to be formalized. The developed method allows us to fully automate the conversion of a layered image into M = {BF, G(N), $T_{M,N}$} and to calculate the morphological characteristics of layered patterns (Smolyar, 2014; Smolyar et.al., 2016). The present work introduces the idea of structural disorder in layered systems. The fundamental difference between DStr and other approaches to quantifying structures (Adams et al., 2004) is that DStr measures the deviation of anisotropic layer structures from isotropy. Also, it is usual practice to choose parameters for describing patterns based on the specific characteristics of an object of study. DStr and charts of “layer thickness vs. layer number” and “layer area vs. layer number” can be used globally as well as locally to describe the morphological characteristics of any anisotropic layered pattern. This property of DStr and the charts allows us to formulate new questions, suggest new testable hypotheses about pattern formation, and identify links between properties and structures of study objects, extending areas of applications for analyzing various anisotropic layered systems.

It is transparent that the transition from layered to non-layered patterns occurs continuously and monotonously, which raises the question of whether it is possible to distinguish between layered and non-layered images. Let us consider how we can use DStr to answer this question. DStr could be defined in either of two ways: First, DStr is the area between y = 0 and the function y = f(x) (Fig. 4D). In this case, DStr is the measure of deviation of an anisotropic pattern from isotropy, denoted by DStr(deviation from isotropy). Second, DStr could be interpreted as the deviation of an anisotropic pattern from a system with maximal disorder (i.e., a chaotic system),

PeerJ Preprints | https://doi.org/10.7287/peerj.preprints.27451v2 | CC BY 4.0 Open Access | rec: 5 Jan 2019, publ: 5 Jan 2019

which is defined as the area between y = f(x) and y = 1, denoted DStr(deviation from chaos). Thus, y = f(x) divides a 1x1 square into two areas (Fig. 4D): DStr(deviation from isotropy) and DStr(deviation from chaos). Because the area of the square is equal to 1, thus

(3) Deviation of anisotropic layer structure from maximal order +
Deviation of anisotropic layered structure from maximal disorder = 1,

where

maximal order = isotropy in layers structure,

maximal disorder = chaos in layers structure.

Using equation (3), it is possible to quantitatively describe a layered pattern in the following manner: If DStr ≤ 0.5, then the structure of a pattern is more layered then chaotic; if DStr > 0.5, then the structure is more chaotic than layered. Therefore, DStr ≤ 0.5 is the maximal possible value for the characteristic of disorder in the structure of layered patterns. This is why a threshold of 0.5 is used to describe the difference between the structures of layered patterns in percentages (Section 4.2).

Let us consider some of the limitations of the proposed method. Many limitations are as yet unknown because the morphology of anisotropic layered patterns is a relatively new object of study. Thus, we list the most obvious limitations that follow from the image analyses presented in Section 3:

- Images of the Martian surface (Fig. 24) exhibit layered patterns as a result of processes occurring in different space–time domains. The proposed method does not provide tools to describe global structural parameters of this category of images.
- Many images presented in Section 3 consist of lines with simple shapes, but the images of the human aorta (Fig. 14) and Pacinian corpuscle (Fig. 27) have more complicated configurations. The proposed method ignores the shape of layers.
- It is necessary to quantify the spatial orientation of layers when developing new materials (Deville, 2018) and setting up correspondence between the morphology of layered systems and water temperature (Olson et al., 2012; Gilbert et al., 2017). The proposed method does not provide tools to quantify the preferential orientation of layers.
- Model M = {BF, G(N), $T_{M,N}$} does not account for the material properties of layers.

PeerJ Preprints | https://doi.org/10.7287/peerj.preprints.27451v2 | CC BY 4.0 Open Access | rec: 5 Jan 2019, publ: 5 Jan 2019

- All the transect versions used to calculate DStr are plotted in one direction, which is perpendicular (or quasi-perpendicular) to the layers.
- The problem of layered pattern normalization is outside the scope of this work.

4.2. Experimental results

We calculate DStr for images in seven categories: geology, atmosphere, materials, medicine, forensic, plants, and animals (Fig. 31). The leaves of Madagascar Lace plants demonstrate the highest level of structural diversion from fully isotropic layered pattern, with DStr = 0 to DStr = 0.7116. Landforms on Mars also demonstrate relatively high levels of structural diversion, from isotropic (DStr = 0) to anisotropic (DStr = 0.303). Experiments with tidal ripples, alloys, hairs, lightning, bones, eye angiograms, fingerprints, and bird plumage patterns illustrate the potential for DStr to be used as a global structural characteristic of the entire sampling area of layered patterns. Thus, it is reasonably safe to suggest that DStr is a universal characteristic that allows us to compare the structure of various categories of 2-D layered patterns, irrespective of size and origin.

If a sampling area can be divided into subareas, then DStr and the chart of "layer thickness vs. layer number" could serve as local structural characteristics of layered patterns. Experiments with Martian landforms (Fig. 5 and 6A), ground-penetrating radar sections (Fig. 7), fish skin (Fig. 18), and the human aorta (Fig. 14) demonstrate that DStr is distributed unevenly across sampling areas. Since DStr varies from 0 to ≤0.5 for layered patterns, it is possible to describe changes in DStr as percentages, which is more convenient for interpreting and estimating the degree of distinction between objects. For instance, segments C and D of the Martian landform in Figure 5 have DStr(C) = 0.193 and DStr(D) = 0.303, respectively. The percentage difference between DStr(C) and DStr(D) is

$$\mathrm{DStr(C)} - \mathrm{DStr(D)} = \mathrm{abs}\ [(0.193 - 0.303)/0.5] * 100\% = 22\%.$$

The 22% difference between DStr(C) and DStr(D) could be interpreted as low, medium, or high depending on the type of object under study and the problem statement.

Figure 6 shows an interesting example of uneven distribution of DStr across a Martian landform (Fig. 6A) and sand ripples (Fig. 6B). There is a 33% difference in DStr between sampling areas

PeerJ Preprints | https://doi.org/10.7287/peerj.preprints.27451v2 | CC BY 4.0 Open Access | rec: 5 Jan 2019, publ: 5 Jan 2019

A and B (Fig. 6A), which is characterized by substation disruption in layer structure. There is a 55% difference in DStr between the red and blue/orange sampling areas (Fig. 6B). The distinguishing features are obvious, and the differences in structure between areas A and B (Fig. 6A) and the red and blue/orange areas (Fig. 6B) are detectable with the naked eye. From a general point of view, Figure 6 is an example of structural anomalies in an anisotropic layered system. Such anomalies could exist in any category of object of study. For instance, structural anomalies in metal microstructure could be interpreted as cracks. Procedures for detecting structural anomalies in layered patterns could find applications in solving broad problems, especially in medicine and materials science.

The pattern of the human aorta (Fig. 14) is an example of a layered pattern with very complicated structural anisotropy that cannot be manually processed. Four segments—A, B, C, and D—show similar but not identical DStr (Fig. 14). There is a 4% difference between DStr(A) and DStr(D), which is probably close to the noise due to converting the initial color image to black and white.

Another application of DStr is describing local structures in Morpho butterfly wings (Fig. 21A). We assume that the left and right wings of flying objects have identical structures. In order to test whether DStr is suitable to test this assumption, we divide the left and right wings into symmetric segments (Fig. 21A). DStr are calculated and the symmetric segments are presented in charts for "DStr vs. number of transects" (Fig. 21B). The DStr differences between the symmetric segments do not exceed 2.8%, justifying our original assumption.

Fingerprints are another example of layered patterns. The structural characteristics of fingerprint ridges—such as bifurcation, trifurcation, and ridge ending and crossing—as well as peculiarities of their distribution across the 2-D plane are used for individual identification. Model M = {BF, G(N), $T_{M,N}$} allows us to account for tiny characteristics of the fingerprint image. Figure 23 illustrates the potential for using DStr to distinguish the structure of four basic categories of fingerprint patterns. Also, via open/closed gates (Fig. 3B and C), it is possible to reveal morphological characteristics of ridges that are most sensitive or robust to fingerprint identification. In this way, it may be possible to decrease uncertainty in fingerprint recognition.

PeerJ Preprints | https://doi.org/10.7287/peerj.preprints.27451v2 | CC BY 4.0 Open Access | rec: 5 Jan 2019, publ: 5 Jan 2019

Parameter DStr is the result of generalizing the sequence DGrp(N_1), …, DGrp(N_k), …, DGrp(N_{MAX}), where N_k is the number of transects used to calculate DGrp(N_k) (equation 2). Generalizing the sequence of DGrp(N_1), …, DGrp(N_k), …, DGrp(N_{MAX}) makes the result of the DStr calculation independent of the number of transects. In individual cases, DGrp(N_k) could also be used to quantify the structural disorder of 2-D anisotropic layered patterns. We illustrate this use of DGrp(N_k) with an example using the four categories of fingerprints depicted in Figure 23. The chart of "DStr vs. number of transects" (Fig. 23) makes it clear that structural differences among the four categories of fingerprints are distributed unevenly along the axis "number of transects." This raises a question about how many transects, N_k, are necessary to maximize the structural differences among fingerprints of different categories. The chart for "{DStr(Central pocket loop) − DStr(Plain arch)} vs. number of transects" (Fig. 23B) demonstrates that using nine transects maximizes the structural differences between central pocket loop and plain arch fingerprint patterns. If a different number of transects is used to calculate DStr (equation 2), then the structural distinction between these categories of fingerprints is

$$(0.198 - 0.102)/0.5*100\% = 19.2\%.$$

If nine transects (i.e., a fixed number of transects) are used to calculate the structural distinction between central pocket loop and plain arch patterns, the result is

$$0.25/0.5*100\% = 50\%.$$

Thus, applying nine transects increases the structural differences between central pocket loop and plain arch more than 2.6 times.

Experiments with fingerprints (Fig. 23A) illustrate that the chart for "DStr vs. number of transects," which is highly accurate (R^2>0.9), could be interpolated to a power function, $y=\mathbf{m}x^{-\mathbf{k}}$. Because DStr is sensitive to minor structural changes (Fig. 30A) and the four basic categories of fingerprints have substantially different **m** and **k** parameters, $y=\mathbf{m}x^{-\mathbf{k}}$ could serve as a unique fingerprint identification number. Using **m** and **k** would be sufficient to find in a database those fingerprints with identical **m** and **k** parameters or identify a relatively small set of fingerprints with similar **m** and **k** values. Images in a large database could be sorted according to **m** and **k** values in order to speed up fingerprint identification.

PeerJ Preprints | https://doi.org/10.7287/peerj.preprints.27451v2 | CC BY 4.0 Open Access | rec: 5 Jan 2019, publ: 5 Jan 2019

The geometrical configuration of chart DStr = f(number of transects) could be used as a morphological characteristic of layered patterns in addition to DStr and DStr for the fixed number of transects. We demonstrate on an image of human hair (Fig. 22B) how the variability of distance between transects (i.e., sampling density) could affect the shape of DStr = f(number of transects). Figure 22B shows that shape of the chart for DStr = f(number of transects) for low sampling density is much simpler than that of the chart for high sampling density. Thus, in addition to DStr, the shape of DStr = f(number of transects) itself could serve as a morphological characteristic of a 2-D layered pattern.

Complicated layered patterns in bird plumage (Fig. 20) are formed by multiple individual feathers that have, individually, relatively simple patterns. Thus, it is not quite clear whether layer thickness is distributed chaotically across the body or demonstrates trends similar to other layered systems (Fig. 24–27). We calculate DStr (Fig. 20) and the chart for "layer thickness vs. layer number" (Fig. 28) in order to analyze the morphology of these layers. Because DStr(Pitta, Owl) < 0.5, we conclude that the feather patterns form layers in these species. Charts for "layer thickness vs. layer number" (Fig. 28) exhibit trends in variability of layer thickness across pitta and owl bodies. These results justify the potential applicability of DStr and the chart for "layer thickness vs. layer number" for describing morphological characteristics of bird plumage. In this context, it should be noted that the distinction between layer thickness and layer number is also used by birds themselves to distinguish among different species, even in a generalized way. Sparrow hawks, which are among the most fearsome predators of small birds, particularly songbirds, have a particular pattern of feathers on the breast plumage. Sparrow hawks are mobbed by small birds all over the world, and the feather patterns alone suffice to entice small birds to engage in the mobbing behavior.

Cuckoos, on the other hand, are not predatory birds but throw the eggs of other birds out of their nests, replacing them with their own egg, which is then raised by the host bird. Cuckoos are also generally mobbed by small birds, as well as physically attacked whenever they approach (Davies and Welbergen, 2008). Most cuckoos have evolved layered feather patterns on their breast plumage that mimic those of sparrow hawks, helping them to mislead songbirds into thinking a dangerous predator (sparrow hawk) is in front of them, not a benign (but annoying) cuckoo

PeerJ Preprints | https://doi.org/10.7287/peerj.preprints.27451v2 | CC BY 4.0 Open Access | rec: 5 Jan 2019, publ: 5 Jan 2019

(Welbergen and Davies, 2011). This pattern mimicry has proven somewhat effective (Trnka and Prokop, 2012). However, it is important to note that some small bird species have learned to distinguish the subtle differences in layered patterns between predators and their cuckoo mimics and now differentially attack these two groups of enemies (Welbergen and Davies, 2008).

The structure and size of lamellar bone form a record of the state of internal and external factors responsible for lamellar formation over an organism's life history. The cyclicity of lamellae thickness (Bromage et.al., 2009) over the period of formation is a cumulative effect of many cyclic factors. Many hard tissues form incremental patterns at varying time scales. For instance, mammalian enamel and dentine develop according to a circadian rhythm, creating a pattern visible as daily microanatomical growth lines. These tissues, as well as those of bone, have also been observed in some mammals to contain longer-period developmental rhythms that scale with body mass (Bromage et al., 2012). These hard tissue rhythms are of substantial interest in mammal life history research, providing information about the duration and amplitude of periodic phenomena as well as about other natural history events occurring during bone and tooth formation, which for some species could not be obtained by other means.

In bone in particular, a specific tissue called lamellar bone may be found in many, if not most, mammals and many other vertebrates. Lamellar bone is profoundly incremental and thus of particular concern here because each layer, while representing a defined period of formation, can vary in width, the layers reflecting growth rate. The significance of such layers for biological research is that changes in their widths potentially reflect internal and external events in an organism's life history. It is also significant that this record is often preserved after an organism's death, either as resilient hard tissue or as a fossil. Incremental patterns are a primary source of information about the duration and amplitude of periodic phenomena as well as about other natural history events occurring during formation: Information about cyclicity, interactions between environmental and/or physiological cycles, and perturbations to the responding system are all inherently contained in these incremental patterns.

For instance, in a child growing during a period of drought, bone lamellae have been observed to diminish from approximately 6 µm to 4 µm in width over the 8- or 9-day period over which each

PeerJ Preprints | https://doi.org/10.7287/peerj.preprints.27451v2 | CC BY 4.0 Open Access | rec: 5 Jan 2019, publ: 5 Jan 2019

lamella is formed (Bromage et al., 2011). Seasonal rhythms, perhaps dependent on food availability, are also apparent in such studies of lamellar bone growth-rate variability.

Substantial areas of the Martian surface are covered by dunes and ripples formed by wind-blown sand (Kok, 2010). Images of Martian landforms such as Transverse Aeolian Ridges, sand dunes, and ripples are examples of 2-D anisotropic layered systems. Figures 24 and 25 show examples of isotropic Martian landforms. Charts of "layer thickness vs. layer number" for these landforms exhibit cyclicity in the variability of layer thickness across a 2-D plane. By averaging layer thickness across the entire sampling area, we lose some important morphological characteristics. A similar statement can be made for materials with layered microstructures.

Pearlite steel (Liu et al., 2016), alloy (Ivanchenko et al., 2008), ceramic (Deville, 2008), and thin films (Alberius et al., 2002) exhibit lamellar microstructures with various levels of anisotropy (i.e., numbers of bifurcations and breaks in the lamellar structure). The distribution of bifurcations and breaks across a 2-D sampling area plays an important role in quantifying the micromorphological features of lamellar systems (Ardel, 1999; Deville, 2018; Lia et al., 2017). Average lamellar thickness is one of the key parameters broadly used to characterize lamellar structure. Charts for "layer thickness vs. layer number" demonstrate cyclic variability of lamellar thickness across the 2-D plane. In this case, average lamellar thickness is not a precise morphological characteristic. For instance, the chart of "layer thickness vs. layer number" (Fig. 26) shows that the lamellar pattern has four blocks—A, B, C, and D—with distinctive lamellar thicknesses. This must be considered when searching for links between material properties and microstructures.

The variable cyclicity of layer thickness across the sampling area of an anisotropic layered system is to be expected because "the whole pattern [of nature] is of cycles within cycles within cycles" (Medawar and Medawar, 1983, p. 73). Model M = {BF, G(N), $T_{M,N}$} provides tools to reveal cyclicity in layered anisotropic environments.

PeerJ Preprints | https://doi.org/10.7287/peerj.preprints.27451v2 | CC BY 4.0 Open Access | rec: 5 Jan 2019, publ: 5 Jan 2019

4.3. Possible experimental tests

Many factors that contribute to the formation of layered patterns in living systems have cyclic natures. For instance, layers in growth systems are formed in direct response to cyclic environmental factors such as temperature (Goodwin et al., 2001; Izzo and Zydlewski, 2017), tides (Poulain et al., 2011), and light–dark rhythms (Scrutton, 1978; Smith, 2006). Cyclic planetary dynamics can also affect the formation of growth increments (Clark II, 1974; Pannella and MacClintock, 1968; Kahn and Pompea, 1978; Vanyo and Awramic, 1985). On the surfaces of Earth and Mars, winds are mainly responsible for the formation of dunes and ripples (Lapotre et al., 2016; Kok et al., 2012). It is reasonable to suggest that the cyclicity of layer thickness stems from the cyclicity of factors controlling layer formation, but this explanation is not always possible. Layered patterns are the cumulative result of many factors occurring in different space–time domains, not all of which are cyclic, and not all factors are known.

Notwithstanding the fact that each object of study has unique properties, the layers of various systems are all formed in the gravity fields of the massive rotating bodies of Earth, Mars, and other planets. Thus, it would be reasonable to explore the influence of zero-gravity (i.e., extreme external factors on layer formation). Let us consider some possible additional experiments that would help us better understand the mechanisms of layer formation. A promising approach would be to examine the influence of extreme external factors—such as zero-gravity, extreme temperature, radioactive contamination, low oxygen, and absence of light—on layer morphology. Empirical model M = {BF, G(N), $T_{M,N}$} is a suitable tool for such experiments since it is sensitive to minor structural changes (Fig. 30) and allows us to detect anomalies in layered systems.

<u>Experiment #1</u>: Examine the influence of zero-gravity on the formation of layered systems. Aquatic habitats for studying the lifecycle of freshwater fish are available on the International Space Station and could be used to investigate the influence of zero-gravity on scale formation in medaka fish (Chatani et al., 2015) and zebrafish (Aceto et al., 2015). Lamella bones of iguana (Smolyar et al., 2016), Madagascar Lace leaves (Fig. 17), and flower surfaces (Fig. 16) are other potential candidates for exploring the formation of anisotropic layers under zero-gravity conditions.

PeerJ Preprints | https://doi.org/10.7287/peerj.preprints.27451v2 | CC BY 4.0 Open Access | rec: 5 Jan 2019, publ: 5 Jan 2019

Experiment #2: Examine the influence of extreme temperatures—including drought, high/low air temperature, and high/low water temperature—on the formation of anisotropic growth increments. Extreme temperatures are a major environmental stress that affect the growth of terrestrial and marine living systems. For instance, "high temperature stress is a major environmental stress that limits plant growth, metabolism, and productivity worldwide. Plant growth and development involve numerous biochemical reactions that are sensitive to temperature" (Hasanuzzaman et al., 2013, p. 9643). Various marine and terrestrial layered living systems could be used to examine the influence of extreme temperature on the formation of layered systems.

Experiment #3: Examine the influence of radioactive contamination on layer formation. The areas around Chernobyl (Ukraine) and Fukushima (Japan) are natural laboratories for studying the influence of radioactive contamination on growth increments of various layered systems, including flower surfaces, spider webs, and butterfly wings. For instance, there is strong evidence that water contamination affects fish scale structures (Hidayati et al., 2013, Sultana et al., 2017).

Experiment #4: Examine the influence of the absence of light on the formation of fish scale growth increments. Sweetwater, Tennessee, where trout live without light in a cave lake, would be an ideal natural laboratory. Other candidates for experiments could be the scales of various categories of salt- and freshwater fish from aquariums permanently covered with light-tight material.

Experiment #5: Examine the influence of oxygen levels on the morphology of elastic lamellae in humans and animals. Since aorta distribute oxygenated blood to all parts of the body, it is possible to assume that environmental oxygen levels might affect aorta morphology (Fig. 14). One possible avenue for experimentation could be the aorta of human and animal populations subjected for many generations to high-altitude, low-oxygen conditions, such as those in the high-altitude Tibetan highlands (Simonson et al., 2010; He et al., 2016). Model M = {BF, G(N), $T_{M,N}$} could be used to compare the morphology of aortas formed in Tibet to those formed in sea-level oxygen environments.

PeerJ Preprints | https://doi.org/10.7287/peerj.preprints.27451v2 | CC BY 4.0 Open Access | rec: 5 Jan 2019, publ: 5 Jan 2019

4.4. Areas of application

Macro-, micro-, and nanostructures play a vital role in understanding pattern formation and relationships between processes and structures (Aizenberg and Fratzl, 2009). Central problems in studying layered objects—particularly in medicine (Novotny et al., 2017), materials science (Deville, 2018), and biomimetic research (Meyers et al., 2008; Gilbert et al., 2017)—are quantitatively describing the relationship between structure and properties, tracking structural changes over a period of time, and revealing structural anomalies. Experiments with various categories of layered systems justify the possibility of using M = {BF, G(N), $T_{M,N}$} to help to solve these problems.

Detecting structural anomalies in layered systems is necessary when solving a broad spectrum of medical and engineering problems. For instance, cracks are a typical example of anomalies in the lamellar structures of metals and alloys; anomalies in growth increments in tree rings allow us to reconstruct extreme environmental phenomena. Experiments with animal footprints on sand ripples and the layered surface of Mars (Fig. 6) provide evidence on the applicability of M = {BF, G(N), $T_{M,N}$} to reveal structural anomalies in layered systems.

Many layered objects—such as corals, fish scales and bivalve shells—are formed in the world ocean. Morphological characteristics of growth increments in these objects are a function of seawater parameters and changes in the space–time domain. Model M = {BF, G(N), $T_{M\,N}$} could be used to analyze growth increments of shells in a seawater environment. Our interest in the link between growth increments and the marine environment is based on available marine data products, new instrumental technology measuring the chemical composition of seawater, and recently published discoveries of relationships between the morphology of shell growth increments and seawater temperature (Gilbert et al., 2017).

<u>Marine data products.</u> The World Ocean Database (WOD) and International Comprehensive Ocean-Atmosphere Data Sets (ICOADS) are the world's largest freely available marine databases. WOD comprise 16+ million globally distributed profiles, beginning with instrumental observations in 1772 through the present (Levitus, 2012; Boyer et al., 2014). A profile is the set

PeerJ Preprints | https://doi.org/10.7287/peerj.preprints.27451v2 | CC BY 4.0 Open Access | rec: 5 Jan 2019, publ: 5 Jan 2019

of measurements of physical, hydrochemical, and plankton characteristics of seawaters on the surface and at various depths (Matishov et al., 2000).

ICOADS is an archive of global near-surface marine data, with over 456 million individual records since 1662 (Slutz et al. 1985; Smith and Reynolds, 2004; Wilkinson et al., 2011; Woodruff et al. 2011; Freeman et al., 2017). Each record is a set of sea-surface temperature (SST) and marine meteorological parameters such as wind speed and direction, humidity, sea-level pressure, cloud cover, sea state, sea ice, and descriptive information such as type and amount of cloud cover at different levels in the atmosphere. ICOADS and WOD are used to study local (Reagan et al., 2018; Seidov et al., 2017; Matishov et al., 2014: Kaplan et al., 1997; Ansell et al., 2006; Marullo et al., 2011) and global (Casey and Cornillon, 2001; Rayner et al., 2003; Garcia et al., 2005; Levitus et al., 2005; Ishii et al., 2005) climatic characteristics of the world ocean and its dynamics. Time series of sea characteristics at various depths, SST, and near-surface meteorology are used to study marine climate dynamics. Time series data are essential to study how "global climate change threatens global biodiversity, ecosystem function and human well-being" (Williams et al., 2008, p. 2621). WOD and ICOADS allow us to plot time series of temperature over 120+ years; WOD additionally includes time series of salinity for 80+ years.

<u>Seawater temperature as a function of chemical composition of growth increments</u>. Using WOD and readily available databases of layered objects, M = {BF, G(N), $T_{M,N}$} could be used to study growth patterns of marine life, such as corals and mollusks, which are used as proxies for environmental state (Sadler et al., 2014; Wanamaker et al., 2011; Reynolds et al., 2017, Carroll et al., 2009). Specifically, the link between seawater temperatures and the morphology and chemical composition of growth layers is a focus of sclerochronological and sclerochemical research (Butler and Schöne, 2017; Reynolds et al., 2016). The availability of WOD as well as large-scale coral and mollusk archives (Reynolds et al., 2017; Donner et al., 2017) allows us to compensate for the lack of water-temperature data before instrumental observations were established. Model M = {BF, G(N), $T_{M,N}$} could be used to formalize a procedure for the development of growth-rate variability (i.e., charts of "layer thickness vs. layer number" and "layer area vs. layer number"), which is essential to accurately reconstruct historical seawater temperatures.

PeerJ Preprints | https://doi.org/10.7287/peerj.preprints.27451v2 | CC BY 4.0 Open Access | rec: 5 Jan 2019, publ: 5 Jan 2019

One possible result of water temperature reconstruction could be long time-series of temperature variability in the Gulf Stream system from the East Coast of the United States to the Barents Sea (Wanamaker et al., 2011; Reynolds et al., 2013; Carroll et al., 2011; Carroll et al., 2014).

Seawater temperature as a function of growth increment morphology. Gilbert et al. (2017) developed a novel method that allows us to reconstruct present and past seawater temperature by analyzing the morphology of modern and fossil shells, which "complements the strength and compensates for the weaknesses of existing geochemical method" (p. 291). Model M = {BF, G(N), $T_{M,N}$} could be used to formalize some stages of layered image processing and account for the structural anisotropy of shells' growth increments. WOD could be used to define areas of the world ocean suitable to examine the influence of seawater parameters of different water masses on the development of shells' growth increments. Gilbert et al. (2017) hypothesized that factors such as salinity, pH, or nutrients can affect the morphology of shells' growth increments in addition to water temperature. Within the frame of this hypothesis it would be reasonable to examine the influence of seawater chemical composition on the development of shells' growth lines. The new method for measuring the chemical composition of fresh and saltwater could be used for this purpose.

Measuring periodic table in fresh and salt waters (Bäuchle,et al., 2018). Water is an accumulation of dissolved elements in the form of organic (typically carbon-hydrogen-based) and inorganic (non-organic) molecules. Given the importance of water to all life, it is astonishing that not a single aqueous sample has ever been measured for element concentrations across the breadth of the chemical periodic table. This dearth of research is not for the lack of want for knowledge but because technologies for detecting all elements in a water sample have been unwieldy and expensive to operate. A recently developed "simultaneous Mass Spectrometer" ICP-MS (si-ICP-MS) permits 71 inorganic elements to be detected in one evaluation from small sample volumes in seconds and at relatively low consumable and personnel costs.

To examine the potential of si-ICP-MS for evaluating environmental water, and for assessing its usefulness in studies of incremental structures, we first measured tap, well, rain, freshwater lake, river, seawater, and snow. Figure 32 depicts the distribution of fresh and saltwater samples.

PeerJ Preprints | https://doi.org/10.7287/peerj.preprints.27451v2 | CC BY 4.0 Open Access | rec: 5 Jan 2019, publ: 5 Jan 2019

Figure 33 shows that most of the periodic table is indeed represented in environmental water, which includes municipally treated tap water. This is fascinating because snow is essentially the same as all other fresh waters, which indicates that the atmosphere—after being scrubbed by snowflakes—is fundamental to the movement of elements at high latitudes and altitudes around the world. Seawater stands out as having higher abundances of elements overall.

The WOD, integrated with chemical composition of seawater, will thus allow us to examine the influence of a broad spectrum of seawater characteristics on the development of growth increments in marine life such as coral, fish scales, and shells. Additionally, the chemical composition of soil and air allows us to use $M = \{BF, G(N), T_{M,N}\}$ to quantify the correspondence between environment and growth patterns of terrestrial plants and animals.

To appreciate the relevance of such data to the study of incremental structures, we examined the lamellar bone of a subsistence fisherman who lived around a freshwater lake. We used a laser ablation system attached to the si-ICP-MS to measure the same elements measured from the lake water on which he made his living. We have made two interesting observations from this research: First, the inorganic spectrum of elements in the local water and in a bone from the fisherman were quite similar.

Second, we discovered that the lamellar increments of bone are formed on the same interval at which the growth increments in enamel, the striae of Retzius, are formed (Bromage et al., 2009). Striae of Retzius may be calibrated in absolute time, and in this fisherman that period was 8 days. Roughly 15 years of continuously formed lamellar bone were available from years for which we have meteorological data. In the example shown in Figure 34, we demonstrate, for instance, that from 1981 to 1995, the concentration of Strontium (Sr) varies cyclically in its ratio with Zinc (Zn).

Other examples in which marine data could relate to the structure of living organisms are birds' and turtles' morphology and their migration patterns across the world ocean (Fig. 35). Although the focus of the present work is the quantitative description of morphology of layered anisotropic patterns, nevertheless a proposed method could be potentially extended for processing morpholo-

PeerJ Preprints | https://doi.org/10.7287/peerj.preprints.27451v2 | CC BY 4.0 Open Access | rec: 5 Jan 2019, publ: 5 Jan 2019

gical characteristics of arbitrary images such as birds' feathers, backs, and footprints. New instrumental methods of monitoring birds' and turtles' migration on a global scale (e.g., the ICARUS project) provide us with tools to describe collective birds motion across the world ocean.

Bird migration. ICARUS, short for "International Cooperation for Animal Research Using Space," is a global collaboration of animal scientists to establish a novel satellite-based infrastructure (Cook et al., 2004; Wikelski et al., 2011) for Earth observation of small objects such as migratory birds, bats, or sea turtles (Pennisi, 2011). These findings will aid behavioral research, species protection, and research into the paths taken in the spread of infectious diseases. The information could even help predict ecological changes and natural disasters. In the process, ICARUS researchers will attach miniaturized transmitters to hundreds or thousands of animal species. These transmitters send measurement data via a CDMA-encoded signal (code-division multiple access) to a receiver station in space that transmits data to a ground station. The results will be published in a database that will be accessible to everyone at www.movebank.org

A miniaturized, solar-powered animal tag can communicate with the ICARUS equipment at the International Space Station from a distance of up to 800 kilometers, allowing it to record its absolute position at regular intervals using GPS and to acquire local temperatures, 3-D acceleration, and 3-D magnetometer values as well as pressure, altitude, and humidity, which give indications of the animal's behavior, internal and external state, and environmental conditions—all using a tag with a mass less than 5 grams and a volume of approximately 2 cm^3.

Integrated morphological characteristics of individual birds, their migration routes, WOD and ICOADS create a basis to formulate testable hypotheses of scientific and commercial value.

PeerJ Preprints | https://doi.org/10.7287/peerj.preprints.27451v2 | CC BY 4.0 Open Access | rec: 5 Jan 2019, publ: 5 Jan 2019

5. Conclusion

The anisotropic features of layered systems make them attractive objects of study from both scientific and commercial points of view. The empirical model M = {BF, G(N), $T_{M,N}$} is an example of the engineering approach (Reeves and Fraser, 2009) to studying pattern formation in nature and beyond.

Various layered systems presented in this paper exhibit surprising levels of structural similarity, what Ball (2009, p. 177) called nature's use of "not the Law of Pattern but a palette of principles".

The key element of the present work is the notion of structural disorder in 2-D layered systems (DStr), which is applicable to any layered object, irrespective of size or nature. Equation (3), which shows that layered patterns comprise anisotropic and isotropic components, provides a foundation for formalizing DStr. Equation (3) could potentially be used to extend the applicability of DStr to quantify the morphological characteristics of arbitrary 2-D binary patterns.

Acknowledgment

The authors thank Amy Bekkerman of Precision Edits for help in preparing the manuscript. We would like to acknowledge Galina Vovna and Boris Ravvin for their discussions. The views and opinions expressed in this article are those of I. Smolyar and do not necessarily reflect the official policy or position of NOAA.

PeerJ Preprints | https://doi.org/10.7287/peerj.preprints.27451v2 | CC BY 4.0 Open Access | rec: 5 Jan 2019, publ: 5 Jan 2019

1020 **References**

1021 Abdel-Aal, H.A., and M.E. Mansori. 2011. "Reptilian Skin as a Biomimetic Analogue for the
1022 Design of Deterministic Tribosurfaces." In *Biomimetics -- Materials, Structures and*
1023 *Processes*, edited by P. Gruber, D. Bruckner, C. Hellmich, H.B. Schmiedmayer, H.
1024 Stachelberger, and I. Gebeshuber, 51–79. Berlin: Springer. http://doi.org/10.1007/978-3-642-
1025 11934-7_4.
1026 Aceto, J., R. Nourizadeh-Lillabadi, R. Marée, N. Dardenne, N. Jeanray, L. Wehenkel, P.
1027 Aleström, J.J.W.A. van Loon, M. Muller. 2015. "Zebrafish Bone and General Physiology Are
1028 Differently Affected by Hormones or Changes in Gravity." *PLoS One* 10(6): e0126928.
1029 http://doi.org/10.1371/journal.pone.0126928.
1030 Adams, D.C., F.J. Rohlf, and D.E. Slice. 2004. "Geometric Morphometrics: Ten Years of
1031 Progress Following the 'Revolution.'" *Ital. J. Zool.* 71: 5–16.
1032 http://doi.org/10.1080/11250000409356545.
1033 Aizenberg, J., and P. Fratzl. 2009." Biological and Biomimetic Material." *Adv. Mater*. 21: 387–
1034 388. http://doi.org/10.1002/adma.200803699.
1035 Akhtar, R., M.J. Sherratt, J.K. Cruickshank, and B. Derby. 2011. "Characterizing the Elastic
1036 Properties of Tissues." *Mater. Today* 14(3): 96–105. http://doi.org/10.1016/S1369-
1037 7021(11)70059-1.
1038 Alberius, P.C.A., K.L. Frindell, R.C. Hayward, E.J. Kramer, G.D. Stucky, and B.F. Chmelka.
1039 2002. "General Predictive Syntheses of Cubic, Hexagonal, and Lamellar Silica and Titania
1040 Mesostructured Thin Films." *Chem. Mater.* 14(8): 3284–3294.
1041 http://doi.org/10.1021/cm011209u.
1042 Ansell, T.J., P.D. Jones, R.J. Allan, D. Lister, D.E. Parker, M. Brunet, A. Moberg, J. Jacobeit, P.
1043 Brohan, N.A. Rayner, E. Aguilar, H. Alexandersson, M. Barriendos, T. Brandsma, N.J. Cox,
1044 P.M. Della-Marta, A. Drebs, D. Founda, F. Gerstengarbe, K. Hickey, T. Jónsson, J. Luterbacher,
1045 Ø. Nordli, H. Oesterle, M. Petrakis, A. Philipp, M.J. Rodwell, O. Saladie, J. Sigro, V. Slonosky,
1046 L. Srnec, V. Swail, A.M. García-Suárez, H. Tuomenvirta, X. Wang, H. Wanner, P. Werner, D.
1047 Wheeler, and E. Xoplaki. 2006. "Daily Mean Sea Level Pressure Reconstructions for the
1048 European–North Atlantic Region for the Period 1850–2003." *J. Clim.* 19: 2717–2742.
1049 http://doi.org/10.1175/JCLI3775.1.

Ardell, A.J. 1999. "Microstructural Stability at Elevated Temperatures." *J. Eur. Ceram. Soc.* 19: 2217–2231. http://doi.org/10.1016/S0955-2219(99)00094-1.

Arnold, E.N. 2002. "History and Function of Scale Microornamentation in Lacertid Lizards." *J. Morphol.* 252(2): 145–169. http://doi.org/10.1002/jmor.1096.

Avolio, A., D. Jones, and M. Tafazzoli-Shadpour. 1998. "Quantification of Alterations in Structure and Function of Elastin in the Arterial Media." *Hypertens*. 32: 170–175. http://doi.org/10.1161/01.HYP.32.1.170.

Ball, P. 2009. *Branches: Nature's Patterns. A Tapestry in Three Parts*. Oxford, UK: Oxford University Press.

Barthlott, W., M. Mail, and C. Neinhuis, 2016. "Superhydrophobic Hierarchically Structured Surfaces in Biology: Evolution, Structural Principles and Biomimetic Applications." *Phil. Trans. A Math. Phys. Eng. Sci.* 374(2073): 20160191. http://doi.org/10.1098/rsta.2016.0191.

Barthlott, W., M. Mail, B. Bhushan, and K. Koch. 2017. "Plant Surfaces: Structures and Functions for Biomimetic Innovations." *Nano-Micro Lett.* 9(23): 1–40. http://doi.org/10.1007/s40820-016-0125-1.

Bau, O., I. Poupyrev, A. Israr, and C. Harrison. 2010. "TeslaTouch: Electrovibration for Touch Surfaces." In *Proceedings of the 23nd Annual ACM Symposium on User Interface Software and Technology, New York, NY, October 3–6*, 283–292. New York: ACM. http://doi.org/10.1145/1866029.1866074.

Bäuchle, Melanie, Tina Lüdecke, Sasan Rabieh, Khemet Calnek, Timothy G. Bromage. (2018). Quantification of 71 detected elements from Li to U for aqueous samples by simultaneous-inductively coupled plasma-mass spectrometry. RSC Adv., 2018, 8, 37008-37020 http://doi: 10.1039/C8RA07070A.

Biswas, A., M. Manivannan, and M,A. Srinivasan. 2015. "Multiscale Layered Biomechanical Model of the Pacinian Corpuscle." *IEEE Transactions on Haptics* 8: 31–42. http://doi.org/10.1109/TOH.2014.2369416.

Blackledge, T.A., and J.M. Zevenbergen. 2006. "Mesh Width Influences Prey Retention in Spider Orb Webs." *Ethol.* 112: 1194–1201. http://doi.org/10.1111/j.1439-0310.2006.01277.x.

Blumberg, D.G. 2006. "Analysis of Large Aeolian (Wind-Blown) Bedforms Using the Shuttle Radar Topography Mission (SRTM) Digital Elevation Data." *Remote Sens. Environ*. 100(2): 179–189. http://doi.org/10.1007/s00223-009-9221-2.

Boyer, T.P., H.E. Garcia, R.A. Locarnini, M.M. Zweng, A.V. Mishonov, J.R. Reagan, J.I. Antonov, O.K. Baranova, M.M. Biddle, D.R. Johnson and C.R. Paver. 2014. "2013 World Ocean Atlas Aids High-Resolution Climate Studies." *Eos, Trans. Am. Geophys. Union* 95(41): 369–370, http://doi.org/10.1002/2014EO410002.

Bromage, T.G., R.S. Lacruz, R. Hogg, H.M. Goldman, S.C. McFarlin, J. Warshaw, W. Dirk, A. Perez-Ochoa, I. Smolyar, D.H. Enlow, and A. Boyde. 2009. "Lamellar Bone Is an Incremental Tissue Reconciling Enamel Rhythms, Body Size, and Organismal Life History." *Calcif. Tissue Int.* 84(5): 388–404. http://doi.org/10.1007/s00223-009-9221-2.

Bromage, T.G., R.T. Hogg, R.S. Lacruz, and C. Hou. 2012. "Primate Enamel Evinces Long Period Biological Timing and Regulation of Life History." *J. Theor. Biol.* 305: 131–144. http://doi.org/10.1016/j.jtbi.2012.04.007.

Bromage, T.G., Y.M. Juwayeyi, I. Smolyar, B. Hu, S. Gomez, V.J. Scaringi, S. Chavis, P. Bondalapati, K. Kaur, and J. Chisi. 2011. "Signposts Ahead: Hard Tissue Signals on Rue Armand de Ricqlès." *C. R. Palevol.* 10: 499–507. http://doi.org/10.1016/j.crpv.2011.01.009.

Butler, P.G., and B.R. Schöne. 2017. "New Research in the Methods and Applications of Sclerochronology." *Palaeogeogr. Palaeoclim. Palaeoecol.* 465(B): 295–299. http://doi.org/10.1016/j.palaeo.2016.11.013.

Calvani, P., A. Bellucciab, M. Girolamia, S. Orlandoc, V. Valentinia, R. Poliniad, and D.M. Trucchia. 2016. "Black Diamond for Solar Energy Conversion." *Carbon*. 105: 401–407. http://doi.org/10.1016/j.carbon.2016.04.017.

Carroll, M.L., B.J. Johnson, G.A. Henkes, K.W. McMahon, A. Voronkov, W.G. Ambrose, and S.G. Denisenko. 2009. "Bivalves as Indicators of Environmental Variation and Potential Anthropogenic Impacts in the Southern Barents Sea." *Mar. Pollut. Bull.* 59(4–7): 193–206. http://doi.org/10.1016/j.marpolbul.2009.02.022.

Carroll, M.L., W.G. Ambrose Jr., B.S. Levin, W.L. Locke V, G.A. Henkes, H. Hop, and P.E. Renaud. 2011. "Pan-Svalbard Growth Rate Variability and Environmental Regulation in the Arctic Bivalve *Serripes groenlandicus*." *J. Mar. Syst.* 88(2): 239–251. http://doi.org/10.1016/j.jmarsys.2011.04.010.

Carroll, M.L., W.G. Ambrose Jr., W.L. Locke, V. Stuart, K. Ryan, and B.J. Johnson. 2014. "Bivalve Growth Rate and Isotopic Variability across the Barents Sea Polar Front." *J. Mar. Syst.* 130: 167–180. http://doi.org/10.1016/j.jmarsys.2013.10.006.

1112 Casey, K.S., and P. Cornillon. 2001. "Global and Regional Sea Surface Temperature Trends." *J.*
1113 *Clim.* 14: 3801–3818. http://doi.org/10.1175/1520-0442(2001)014<3801:GARSST>2.0.CO;2.
1114 Champod, C. 2015. "Fingerprint Identification: Advances since the 2009 National Research
1115 Council Report." *Phil. Trans. R. Soc. B* 370: 20140259. http://doi.org/10.1098/rstb.2014.0259.
1116 Chatani, M., A. Mantoku, K. Takeyama, D. Abduweli, Y. Sugamori, K. Aoki, K. Ohya, H.
1117 Suzuki, S. Uchida, T. Sakimura, Y. Kono, F. Tanigaki, M. Shirakawa, Y. Takano, and A. Kudo.
1118 2015. "Microgravity Promotes Osteoclast Activity in Medaka Fish Reared at the International
1119 Space Station." *Sci. Rep*. 5: 14172. http://doi.org/10.1038/srep14172.
1120 Cooke, S.J., S.G. Hinch, M. Wikelski, R.D. Andrews, L.J. Kuchel, T.G. Wolcott, P.J. Butler.
1121 2004. "Biotelemetry: A Mechanistic Approach to Ecology." Trends Ecol. Evol. 19(6): 334–343.
1122 http://doi.org/10.1016/j.tree.2004.04.003.
1123 Costa, A., H. Pereira, and Â. Oliveira. 2002. "Influence of Climate on the Seasonality of Radial
1124 Growth of Cork Oak during a Cork Production Cycle." *Ann. For. Sci.* 59(4): 429–437.
1125 http://doi.org/10.1051/forest:2002017.
1126 Dauphinee, A.N., J.I. Fletcher, G.L. Denbigh, C.R. Lacroix, and A.H.L.A.N. Gunawardena.
1127 2017. "Remodelling Of Lace Plant Leaves: Antioxidants and ROS Are Key Regulators of
1128 Programmed Cell Death." *Planta* 246(1): 133–147. http://doi.org/10.1007/s00425-017-2683-y.
1129 Davies, N.B., and J.A. Welbergen, 2008. "Cuckoo–Hawk Mimicry? An Experimental Test."
1130 *Proc. Royal Soc. B Biol. Sci.* 275: 1817–1822. http://doi.org/1098/rspb.2008.0331.
1131 De Marinis, A.M., and Asprea, A. 2006. "Hair Identification Key of Wild and Domestic
1132 Ungulates from Southern Europe." *Wildl. Biol*. 12: 305–320. http://doi.org/10.2981/0909-
1133 6396(2006)12%5B305:HIKOWA%5D2.0.CO;2.
1134 Deville, S. 2008. "Freeze-Casting of Porous Ceramics: A Review of Current Achievements and
1135 Issues." *Adv. Eng. Mater.* 10(3): 155–169. http://doi.org/10.1002/adem.200700270.
1136 Deville, S. 2018. "The Lure of Ice-Templating: Recent Trends and Opportunities for Porous
1137 Materials." *Scr. Mater*. 147: 119–124. http://doi.org/10.1016/j.scriptamat.2017.06.020.
1138 Deville, S., A. Tomsia, and E. Saiz. 2007. "The Materials that Came in from the Cold: Nacre-like
1139 Bioceramics through Freezing." In *Proceedings of the 10th International Conference of the*
1140 *European Ceramic Society, Berlin, June 17–21*, 969–975. Baden-Baden, Germany: Göller.

1141 Diniega, S., M. Kreslavsky, J. Radebaugh, S. Silvestro, M. Telfer, and D. Tirschg. 2017. "Our
1142 Evolving Understanding of Aeolian Bedforms, Based on Observation of Dunes on Different
1143 Worlds." *Aeolian Res.* 26: 5–27. http://doi.org/10.1016/j.aeolia.2016.10.001.
1144 Donner, S.D., G.J.M. Rickbeil, and S.F. Heron. 2017. "A New, High-Resolution Global Mass
1145 Coral Bleaching Database." *PLoS ONE* 12(4): e0175490.
1146 http://doi.org/10.1371/journal.pone.0175490.
1147 Draper, N.R., and H. Smith. 1998. *Applied Regression Analysis*, 3rd ed. New York, NY: Wiley.
1148 Eberhard, W.G. 2014. "A New View of Orb Webs: Multiple Trap Designs in a Single Structure."
1149 *Biol. J. Linn. Soc. Lond.* 111: 437–449. http://doi.org/10.1111/bij.12207.
1150 Ewing, R.C., A.G. Hayes, and A. Lucas. 2014. "Sand Dune Patterns on Titan Controlled by
1151 Long-Term Climate Cycles." *Natur. Geosci.* 8: 15–19. http://doi.org/10.1038/ngeo2323.
1152 Filippov, A.E., S.N. Gorb. 2016. "Modelling of the Frictional Behavior of the Snake Skin
1153 Covered by Anisotropic Surface Nanostructures." *Sci. Rep.* 6:23539.
1154 http://doi.org/10.1038/srep23539.
1155 Freeman, E., S.D. Woodruff, S.J. Worley, S.J. Lubker, E.C. Kent, W.E. Angel, D.I . Berry, P.
1156 Brohan, R. Eastman, L. Gates, W. Gloeden, Z. Ji, J. Lawrimore, N.A. Rayner, G. Rosenhagen,
1157 and S.R. Smith. 2017: "ICOADS Release 3.0: A Major Update to the Historical Marine Climate
1158 Record." *Int. J. Climatol.* 37: 2211–2237 http://doi.org/10.1002/joc.4775.
1159 Garcia, H.E., T.P. Boyer, S. Levitus, R.A. Locarnini, and J.I. Antonov. 2005. "Climatological
1160 Annual Cycle of Upper Ocean Oxygen Content Anomaly." *Geophys. Res. Lett*, 32: L09604.
1161 http://doi.org/10.1029/2004GL022286.
1162 Gardin, E., P. Allemand, C. Quantin, S. Silvestro, and C. Delacourt. 2011. "Dune Fields on
1163 Mars: Recorders of a Climate Change?" *Planet. Space Sci*. 60: 314–321.
1164 http://doi.org/10.1016/j.pss.2011.10.004.
1165 Gilbert, P.U.P.A., K.D. Bergmann, C.E. Myers, M.A. Marcus, R.T. DeVol, C.-Y. Sun, A.Z.
1166 Blonsky, E. Tamre, J. Zhao, E.A. Karan, N. Tamura, S. Lemer, A.J. Giuffre, G. Giribet, J.M.
1167 Eiler, and A.H. Knoll. 2017. "Nacre Tablet Thickness Records Formation Temperature in
1168 Modern and Fossil Shells." *Earth Planet. Sci. Letter*, 460: 281–292.
1169 http://doi.org/10.1016/j.epsl.2016.11.012.
1170 Gluckman, T.-L. 2014. "Pathways to Elaboration of Sexual Dimorphism in Bird Plumage
1171 Patterns." *Biol. J. Linn. Soc.* 111: 262–273. https://doi.org/10.1111/bij.12211.

1172 Gluckman, T.-L. and N.I. Mundy. 2016. "Evolutionary Pathways to Convergence in Plumage
1173 Patterns." *BMC Evol. Biol*. 16:172. http://doi.org/10.1186/s12862-016-0741-x.
1174 Goodwin, D.H., K.W. Flessa, B.R. Schone, and D.L. Dettman. 2001. "Cross-Calibration of Daily
1175 Growth Increments, Stable Isotope Variation, and Temperature in the Gulf of California Bivalve
1176 Mollusk *Chione cortezi*: Implications for Paleoenvironmental Analysis." *PALAIOS* 16(4): 387–
1177 398. http://doi.org/10.1669/0883-1351(2001)016<0387:CCODGI>2.0.CO;2.
1178 Gower, D.J. 2003. "Scale Micro Ornamentation of Uropeltid Snakes." *J. Morphol.* 258:249–268.
1179 http://doi.org/10.1002/jmor.10147.
1180 Gunawardena, A.H.L.A.N., J.S. Greenwood, and N.G. Dengler. 2004. "Programmed Cell Death
1181 Remodels Lace Plant Leaf Shape during Development." *Plant Cell* 16(1): 60–73.
1182 http://doi.org/10.1105/tpc.016188.
1183 Guyette, R.P., and C.F. Rabeni. 1995. "Climate Response among Growth Increments of Fish and
1184 Trees." *Oecologia* 104(3): 272–279. http://doi.org/10.1007/BF00328361.
1185 Hasanuzzaman, M., K. Nahar, M.M. Alam, R. Roychowdhury, and M. Fujita. 2013.
1186 "Physiological, Biochemical, and Molecular Mechanisms of Heat Stress Tolerance in Plants."
1187 *Int. J. Mol. Sci.* 14(5): 9643–9684. http://doi.org/10.3390/ijms14059643.
1188 He, Y., S. Yu, J. Hu, Y. Cui, P. Liu. 2016. "Changes in the Anatomic and Microscopic Structure
1189 and the Expression of HIF-1α and VEGF of the Yak Heart with Aging and Hypoxia." *PLoS ONE*
1190 11(2): e0149947. http://doi.org/10.1371/journal.pone.0149947.
1191 Hesselberg, T. 2013. "Web-Building Flexibility Differs in Two Spatially Constrained Orb
1192 Spiders." *J. Insect Behav*. 26: 283–303. http://doi.org/10.1007/s10905-012-9335-7.
1193 Hidayati, D., N. Sulaiman, S. Othman, and B.S. Ismail. 2013. "Fish Scale Deformation Analysis
1194 Using Scanning Electron Microscope: New Potential Biomarker in Aquatic Environmental
1195 Monitoring of Aluminum and Iron Contamination." *AIP Conf. Proc.* 1571(1): 563.
1196 http://doi.org/10.1063/1.4858714.
1197 Huang, X., Y. Hai, and W.-H. Xie. 2017. "Anisotropic Cell Growth-Regulated Surface
1198 Micropatterns in Flower Petals." *Theor. Appl. Mech. Lett.* 7(3): 169–174.
1199 http://doi.org/10.1016/j.taml.2017.03.004.
1200 Ishii, M., A. Shouji, S. Sugimoto, and T. Matsumoto. 2005. "Objective Analyses of Sea-Surface
1201 Temperature and Marine Meteorological Variables for the 20th Century Using ICOADS and the
1202 Kobe Collection." *Int. J. Climatol*. 25: 865–879 http://doi.org/10.1002/joc.1169.

Ivanchenko, V., T. Pryadko, V. Dekhtyarenko, and T. Kosorukova. 2008. "Hydrogen Absorbing Properties of a Ti–Zr–Mn Eutectic Alloy." *Chem. Met. Alloys* 1: 133–136.

Izzo, L.K., and J. Zydlewski. 2017. "Retrospective Analysis of Seasonal Ocean Growth Rates of Two Sea Winter Atlantic Salmon in Eastern Maine Using Historic Scales." *Mar. Coast. Fish.* 9: 357–372. http://doi.org/10.1080/19425120.2017.1334723.

Kaas, J.H. 2012. "Somatosensory System." In *The Human Nervous System*, 3rd ed., edited by J.K. Mai and G. Paxinos. Amsterdam: Elsevier. http://doi.org/10.1016/B978-0-12-374236-0.10030-6.

Kahn, P.G.K., and S. M. Pompea. 1978. "Nautiloid Growth Rhythms and Dynamical Evolution of the Earth-Moon System." *Nature* 275: 606–611. http://doi.org/10.1038/275606a0.

Kaplan, A., Y. Kushnir, M.A. Cane, and M.B. Blumenthal. 1997. "Reduced Space Optimal Analysis for Historical Data Sets: 136 Years of Atlantic Sea Surface Temperatures." *J. Geophys. Res.* 102(C13): 27835–27860. http://doi.org/10.1029/97JC01734.

Klein, M.-C.G., and S.N. Gorb. 2012. "Epidermis Architecture and Material Properties of the Skin of Four Snake Species." J. *R. Soc. Interface* 9: 3140–3155. http://doi.org/10.1098/rsif.2012.0479.

Kok, J. 2010. "Difference in the Wind Speeds Required for Initiation versus Continuation of Sand Transport on Mars: Implications for Dunes and Dust Storms." *Phys. Rev. Lett*. 104: 074502. http://doi.org/10.1103/PhysRevLett.104.074502.

Kok, J.F., E.J.R. Parteli, T.I. Michaels, and D. Bou Karam. 2012. "The Physics of Wind-Blown Sand and Dust." *Rep. Prog. Phys*. 75: 106901. http://doi.org/10.1088/0034-4885/75/10/106901.

Lancaster, N. 2009. "Dune Morphology and Dynamics." In *Geomorphology of Desert Environments*, edited by A.J. Parsons and A.D. Abrahams. Dordrecht: Springer, 557–595. http://doi.org/10.1007/978-1-4020-5719-9_18.

Lapotre, M.G.A., R.C. Ewing, M P. Lamb, W.W. Fischer, J P. Grotzinger, D.M. Rubin, K.W. Lewis, M.J. Ballard, M. Day, S. Gupta, S.G. Banham, N.T. Bridges, D.J. Des Marais, A.A. Fraeman, J.A. Grant, K.E. Herkenhoff, D.W. Ming, M.A. Mischna, M.S. Rice, D.Y. Sumner, A.R. Vasavada, and R.A. Yingst. 2016. "Large Wind Ripples on Mars: A Record of Atmospheric Evolution." *Science* 353(6294): 55–58. http://doi.org/10.1126/science.aaf3206.

Lee, E., T.-Y. Choi, D. Woo, M.-S. Min, S. Sugita, and H. Lee. 2014. "Species Identification Key of Korean Mammal Hair." *J. Vet. Med. Sci*. 76(5): 667–675. http://doi.org/10.1292/jvms.13-0569.

Levitus, S., 2012. "The UNESCO/IOC/IODE Global Oceanographic Data Archaeology and Rescue (GODAR) Project CODATA." *Data Sci. J.* 11: 46–71. http://doi.org/10.2481/dsj.012-014.

Levitus, S., J.I. Antonov, and T.P. Boyer. 2005. "Warming of the World Ocean, 1955–2003." *Geophys. Res. Lett.* 32: L02604. http://doi.org/10.1029GL021592.

Li, X., F. Bottler, R. Spatschek, B, A. Schmitt, M. Heilmaier, and F. Stein. 2017. "Coarsening Kinetics of Lamellar Microstructures: Experiments and Simulations on a Fully-Lamellar Fe-Al in situ Composite." *Acta Mater*. 127(1): 230–243. http://doi.org/10.1016/j.actamat.2017.01.041.

Lian, J., W. Zhou, Q.M. Wei, L.M. Wang, L.A. Boatner, R.C. Ewing. Simultaneous formation of surface ripples and metallic nanodots induced by phase decomposition and focused ion beam patterning. ***Appl***. *Phys. Lett.*, 88 (9) (2006) 93112. https://doi.org/10.1063/1.2181203

Liu, H., ,Z. Dai, J. Xu, B. Guo, X. He. 2014. "Effect Of Silica Nanoparticles/Poly(Vinylidene Fluoridehexafluoropropylene) Coated Layers on the Performance of Polypropylene Separator for Lithium-Ion Batteries." *J. Energy Chem*. 23 (5): 582–586. http://doi.org/10.1016/S2095-4956(14)60188-1.

Liu, S., F. Zhang, Z. Yang, M. Wang, and C. Zheng. 2016. "Effects of Al and Mn on the Formation and Properties of Nanostructured Pearlite in High-Carbon Steels." *Mater. Des.* 93: 73–80. http://doi.org/10.1016/j.matdes.2015.12.134.

Reagan, James, Dan Seidov and Tim Boyer,2018: Water vapor transfer and near-surface salinity contrasts in the north Atlantic Ocean, *Sci. Rep.*, **8**, 8830, http://dx.doi.org/10.1038/s41598-018-27052-6.

Robinson, M., C. Bristow, J. McKinley, and A. Ruffell. 2013. "1.5.5. Ground Penetrating Radar." In *Geomorphological Techniques, Part 1* (Online edition), edited by S.J. Cook, L.E. Clarke, and J.M. Nield, 1–26. London: British Society for Geomorphology.

Mansfield, K.L., J. Wyneken, W.P. Porter, J. Luo. 2014. "First Satellite Tracks of Neonate Sea Turtles Redefine the 'Lost Years' Oceanic Niche." *Proc. Biol. Sci.* 281(1781): 20133039. http://doi.org/10.1098/rspb.2013.3039.

1262 Marullo, S., V. Artale, and R. Santoleri. 2011. "The SST Multidecadal Variability in the
1263 Atlantic–Mediterranean Region and Its Relation to AMO." *J. Clim.* 24: 4385–4401.
1264 http://doi.org/10.1175/2011JCLI3884.1.
1265 Matishov, G.G., P. Makarevich, S. Timofeev, L. Kuznetsov, N. Druzhkov, V. Larionov, et al.
1266 2000. *Biological Atlas of the Arctic Seas 2000: Plankton of the Barents and Kara Seas.* NOAA
1267 Atlas NESDIS 39. Washington, DC: U.S. Government Printing Office.
1268 Matishov, G.G., S.V. Berdnikov, A.P. Zhichkin, S.L. Dzhenyuk, I.V. Smolyar, V.V. Kulygin, et
1269 al. 2014. *Atlas of Climatic Changes in Nine Large Marine Ecosystems of the Northern*
1270 *Hemisphere (1827–2013).* NOAA Atlas NESDIS 78, edited by G.G. Matishov, K. Sherman, and
1271 S. Levitus. Washington, DC: U.S. Government Printing Office.
1272 http://doi.org/10.7289/V5Q52MK5.
1273 Mattson, J., and Y. Zhang. 2017. "Structural and Functional Differences Between Porcine Aorta
1274 and Vena Cava." *J. Biomech. Eng.* 139: 071007. http://doi.org/10.1115/1.4036261.
1275 Mayer, G. 2005. "Rigid Biological Systems as Models for Synthetic Composites." *Science*
1276 310(5751): 1144–1147. http://doi.org/10.1126/science.1116994.
1277 Medawar, P.B., and J.S. Medawar. 1983. *Aristotle to Zoos. A Philosophical Dictionary of*
1278 *Biology*. Cambridege, MA: Harvard University Press.
1279 Meinhardt, H. 1989. "Tailoring and Coupling of Reaction-Diffusion Systems to Obtain
1280 Reproducible Complex Pattern Formation during Development of Higher Organism." *Appl.*
1281 *Math. Comp.* 32: 103–135. http://doi.org/10.1016/0096-3003(89)90090-8.
1282 Meyers, M.A., A.M. Hodge, and R.K. Roeder. 2008. "Biological Materials Science and
1283 Engineering: Biological Materials, Biomaterials, and Biomimetics." *JOM* 60: 21–22.
1284 http://doi.org/10.1007/s11837-008-0066-3.
1285 Moya, J.S. 1995. "Layered Ceramics." *Adv. Mater*. 7(2): 185–189.
1286 http://doi.org/10.1002/adma.19950070219.
1287 Novotny, R., D. Slizova, J. Hlubocky, O. Krs, J. Spatenka, J. Burkert, R. Fiala, P. Mitas, P.
1288 Mericka, M. Spacek, Z. Hlubocka, and J. Lindner. 2017. "Cryopreserved Human Aortic Root
1289 Allografts Arterial Wall: Structural Changes Occurring during Thawing." *PLoS ONE* 12(4):
1290 e017500. http://doi.org/10.1371/journal.pone.0175007.

Olson, I.C., R. Kozdon, J.W. Valley, and P.U.P.A. Gilbert. 2012. "Mollusk Shell Nacre Ultrastructure Correlates with Environmental Temperature and Pressure." *J. Am. Chem. Soc.* 134 (17): 7351–7358. http://doi.org/10.1021/ja210808s.

Pannella, G. 1972. "Paleontological Evidence on the Earth's rotational history since early Precambrian." *Astrophys. Space Sci.* 16: 212–237. http://doi.org/10.1007/BF00642735.

Pannella, G., and C. Macclintock. 1968. "Biological and Environmental Rhythms Reflecting in Molluscan Shell Growth." *J. Paleont. Met.* 42: 64–80. http://doi.org/10.1017/S0022336000061655.

Parker, A.R. 2000. "515 Million Years of Structural Color." *J. Opt. A*. 2: R15–R28. http://doi.org/10.1088/1464-4258/2/6/201.

Passchier, S., and M. G. Kleinhans. 2005. "Observations of Sand Waves, Megaripples, and Hummocks in the Dutch Coastal Area and Their Relation to Currents and Combined Flow Conditions." *J. Geophys. Res.* 110: F04S15. http://doi.org/10.1029/2004JF000215.

Pennisi, E. 2011. "Global Tracking of Small Animals Gains Momentum." *Sci*. 334(6059): 1042. http://doi.org/ 10.1126/science.334.6059.1042.

Poulain, C., A. Lorrain, J. Flye-Sainte-Marie, E. Amice, E. Morize, and Y. M. Paulet. 2011. "An Environmentally Induced Tidal Periodicity of Microgrowth Increment Formation in Subtidal Populations of the Clam *Ruditapes philippinarum*." *J. Exp. Mar. Biol. Ecol.* 397(1): 58–64. http://doi.org/10.1016/j.jembe.2010.11.001.

Quindlen, J.C., E.T. Bloom, L.E. Ortega, A.T. Moeller, and V.H. Barocas. 2017. "Micropipette Aspiration of the Pacinian Corpuscle." *J. Biomech.* 63: 104–109. http://doi.org/10.1016/j.jbiomech.2017.08.005.

Radebaugh, J., A. Le Gall , R.D. Lorenz, J.I. Lunine, and the Cassini RADAR Team. 2011. "Stabilized Dunes on Titan as Indicators of Climate Change." *EPSC Abs.* 6: 1–3.

Rayner, N.A., D.E. Parker, E.B. Horton, C.K. Folland, L.V. Alexander, D.P. Rowell, E.C. Kent, and A. Kaplan. 2003. "Global Analyses of Sea Surface Temperature, Sea Ice, and Night Marine Air Temperature, Sea Ice, and Night Marine Air Temperature since the Late Nineteenth Century." *J. Geophys. Res,* 108: 4407. http://doi.org/10.1029/2002JD002670.

Reagan, James, Dan Seidov and Tim Boyer,2018: Water vapor transfer and near-surface salinity contrasts in the north Atlantic Ocean, *Sci. Rep.*, **8**, 8830, http://dx.doi.org/10.1038/s41598-018-27052-6.

Reeves, G.T., and S.E. Fraser. 2009. "Biological Systems from an Engineer's Point of View." *PLoS Biol.* 7(1): e1000021. http://doi.org/10.1371/journal.pbio.1000021.

Reynolds, D.J., C.A. Richardson, J.D. Scourse, P.G. Butler, P. Hollyman, A. Román-González, and I.R. Hall. 2017. "Reconstructing North Atlantic Marine Climate Variability Using an Absolutely-Dated Sclerochronological Network." *Palaeogeo. Palaeoclim. Palaeoecol.* 465 Part B(1): 333–346. http://doi.org/10.1016/j.palaeo.2016.08.006.

Reynolds, D.J., J.D. Scourse, P.R. Halloran, A.J. Nederbragt, A.D. Wanamaker, P.G. Butler, C.A. Richardson, J. Heinemeier, J. Eiriksson, K.L. Knudsen, and I.R. Hall. 2016. "Annually Resolved North Atlantic Marine Climate over the Last Millennium." *Nat. Comm.* 7: 1–11. http://doi.org/10.1038/ncomms13502.

Reynolds, D.J., P.G. Butler, S.M. Williams, J.D. Scourse, C.A. Richardson, A.D. Wanamaker Jr., W.E.N. Austin, A.G. Cage, M.D.J. Sayer. 2013. "A Multiproxy Reconstruction of Hebridean (NW Scotland) Spring Sea Surface Temperatures between AD 1805 and 2010." *Palaeogeo. Palaeoclim. Palaeoecol.* 386: 275–285. http://doi.org/10.1016/j.palaeo.2013.05.029.

Rothenberg, M., R.T. Verrillo, S.A. Zahorian, M.L. Brachman, and S.J, Bolanowski Jr. 1977. "Vibrotactile Frequency for Encoding a Speech Parameter." *J. Acoust. Soc. Am.* 62(4): 1003–1012. http://doi.org/10.1121/1.381610.

Sadler, J., G.E. Webb, L.D. Nothdurft, and B. Dechnik. 2014. "Geochemistry-Based Coral Palaeoclimate Studies and the Potential of 'Non-Traditional' (Non-Massive *Porites*) Corals: Recent Developments and Future Progression." *Earth-Sci. Rev.* 139: 291–316. http://doi.org/10.1016/j.earscirev.2014.10.002.

Scrutton, C.T. 1978. "Periodic Growth Features in Fossil Organisms and the Length of the Day and Month." In *Tidal Friction and the Earth's Rotation*, edited by P. Broche and J. Sundermann, 154–196. Berlin: Springer-Verlag. http://doi.org/10.1007/978-3-642-67097-8_12.

Seidov, D., A. Mishonov, J. Reagan, and R. Parsons 2017. "Multidecadal Variability and Climate Shift in the North Atlantic Ocean." *Geophys. Res. Lett.* 44:4985–4993. http://doi.org/10.1002/2017GL073644.

Selçuk, E.B., M. Sungu, H. Parlakpinar, N. Ermiş, E. Taslıdere, N. Vardı, M. Yalçinsoy, M. Sagır, A. Polat, M. Karatas, and B. Kayhan-Tetik. 2015. "Evaluation of the Cardiovascular Effects of Varenicline in Rats." *Drug Design, Dev. Ther.* 9: 5705–5717. http://doi.org/10.2147/DDDT.S92268.

Sensenig, A., I. Agnarsson, and T.A. Blackledge. 2010. "Behavioural and Biomaterial Coevolution in Spider Orb Webs." *J. Evol. Biol*. 23(9): 1839–1856. http://doi.org/10.1111/j.1420-9101.2010.02048.x.

Shaffer, S.A., Y. Tremblay, H. Weimerskirch, D. Scott, D.R. Thompson, P.M. Sagar, H. Moller, G.A. Taylor, D.G. Foley, B.A. Block, and D.P. Costa. 2006. "Migratory Shearwaters Integrate Oceanic Resources across the Pacific Ocean in an Endless Summer." *Proc. Natl. Acad. Sci.* 103(34): 12799–12802. http://doi.org/10.1073/pnas.0603715103.

Shoji, H., A. Mochizuki, Y. Iwasa, M. Hirata, T. Watanabe, S. Hioki, and S. Kondo. 2003. "Origin of Directionality in the Fish Stripe Pattern." *Dev. Dyn.* 226(4): 627–33. http://doi.org/10.1002/dvdy.10277.

Silvestro, S., L.K. Fenton, D.A. Vaz, N.T. Bridges, G.G. Ori. 2010. "Ripple Migration and Dune Activity on Mars: Evidence for Dynamic Wind Processes." *Geophys. Res. Lett.* 37: L20203. http://doi.org/10.1029/2010GL044743.

Simonson, T.S., Y. Yang, C.D. Huff, H. Yun, G. Qin, D.J. Witherspoon, and Z. Bai. 2010. "Genetic Evidence for High-Altitude Adaptation in Tibet." *Science* 329(5987): 72–75. http://doi.org/10.1126/science.1189406.

Sloss, C.R., P. Hesp, and M. Shepherd. 2012. "Coastal Dunes: Aeolian Transport." *Nat. Educ. Knowl.* 3(10): 21.

Slutz, R.J., S.J. Lubker, J.D. Hiscox, S.D. Woodruff, R.L. Jenne, R.H. Joseph, P.M. Steurer, and J.D. Elms. 1985. *Comprehensive Ocean-Atmosphere Data Set: Release 1*. NTIS PB86-105723. Boulder, CO: NOAA Environmental Research Laboratories, Climate Research Program.

Smith, T.M. 2006. "Experimental Determination of the Periodicity of Incremental Features in Enamel." *J. Anat*. 208(1): 99–113. http://doi.org/10.1111/j.1469-7580.2006.00499.x.

Smith, T.M., and R.W. Reynolds. 2004. "Improved Extended Reconstruction of SST (1854–1997)." *J. Clim.* 17: 2466–2477. http://doi.org/10.1175/1520-0442(2004)017<2466:IEROS>2.0.CO;2.

Smolyar, I., T. Bromage, and M. Wikelski. 2016. "Quantification of Layered Patterns with Structural Anisotropy: A Comparison of Biological and Geological Systems." *Heliyon*, 2(3): e00079. http://doi.org/10.1016/j.heliyon.2016.e00079.

Smolyar, I.V. 2014. *System and Method for Quantification of Size and Anisotropic Structure of Layered Patterns*. U.S. Patent 8,755,578, issued June 17, 2014.

Smolyar, I.V., and T.G. Bromage. 2004. "Discrete Model of Fish Scale Incremental Pattern: A Formalization of the 2D Anisotropic Structure." *ICES J. Mar. Sci.* 61(6): 992–1003. http://doi.org/10.1016/j.icesjms.2004.07.013.

Smolyar, I.V., I. Ermolaeva, and A. Chernitsky. 1987. *Mathematical Model of Fish Scales and Algorithms for their Analysis.* Apatity, Russia: Kola Science Center, Russian Academy of Sciences.

Soler, A., and R. Zaera. 2016. "The Secondary Frame in Spider Orb Webs: The Detail that Makes the Difference." *Sci. Rep.* 6: 31265. http://doi.org/10.1038/srep31265.

Starkey, T., and P. Vukusic. 2013. "Light Manipulation Principles in Biological Photonic Systems." *Nanophotonics* 2: 289–307. http://doi.org/10.1515/nanoph-2013-0015.

Sultana, S., A. Siddique, S. Sultana, S. Mahboob, K. Al-Ghanim, and Z. Ahmed. 2017. "Fish Scales as a Non-Lethal Tool of the Toxicity of Wastewater from the River Chenab." *Environ. Sci. Pollut. Res.*24:2464–2475. http://doi.org/10.1007/s11356-016-7962-9.

Taghizadeh, H., and M. Tafazzoli-Shadpour. 2017. "Characterization of Mechanical Properties of Lamellar Structure of the Aortic Wall: Effect of Aging." *J. Mech. Behav. Biomed. Mater.* 65: 20–28. http://doi.org/10.1016/j.jmbbm.2016.08.011.

Tonar, Z., T. Kubíková, C. Prior, E. Demjén, V. Liška, M. Králíčková, and K. Witter. 2015. "Segmental and Age Differences in the Elastin Network, Collagen, and Smooth Muscle Phenotype in the Tunica Media of the Porcine Aorta." *Ann. Anat*. 201: 79–90. http://doi.org/10.1016/j.aanat.2015.05.005.

Trnka, A., and P. Prokop. 2012. "The Effectiveness of Hawk Mimicry in Protecting Cuckoos from Aggressive Hosts." *Anim. Behav*. 83: 263–268. http://doi.org/10.1016/j.anbehav.2011.10.036

Turing, A.M. 1952. "The Chemical Basis of Morphogenesis." *Phil. Transact. Royal Soc. B Biol. Sci.* 237(641): 37–72. http://doi.org/10.1098/rstb.2014.0218.

Vanyo, J.P., and S.M. Awramik. 1985. "Stromatolites and Earth-Sun-Moon Dynamics." *Precambrian Res.* 29(1–3): 121–142. http://doi.org/10.1016/0301-9268(85)90064-6.

Vukusic, P., and J.R. Sambles. "Photonic Structures in Biology." *Nature* 424: 852–855. http://doi.org/10.1038/nature01941.

Wanamaker, A.D. Jr., S. Hetzinger, and J. Halfar. 2011. "Reconstructing Mid- to High-Latitude Marine Climate and Ocean Variability Using Bivalves, Coralline Algae, and Marine Sediment

1415 Cores from the Northern Hemisphere." *Palaeogeo. Palaeoclim. Palaeoecol*. 302(1–2): 1–9.
1416 http://doi.org/10.1016/j.palaeo.2010.12.024.
1417 Welbergen, J.A., and N.B. Davies. 2008. "Reed Warblers Discriminate Cuckoos from
1418 Sparrowhawks with Graded Alarm Signals that Attract Mates and Neighbours." *Anim. Behav*.
1419 76: 811–822. https://doi.org/10.1016/j.anbehav.2008.03.020.
1420 ———. 2011. "A Parasite in Wolf's Clothing: Hawk Mimicry Reduces Mobbing of Cuckoos by
1421 Hosts." *Behav. Ecol*, 22: 574–579. http://doi.org/10.1093/beheco/arr008.
1422 Wilkinson, C., S.D. Woodruff, P. Brohan, S. Claesson, E. Freeman, F. Koek, S.J. Lubker, C.
1423 Marzin, and D. Wheeler. 2011. "Recovery of Logbooks And International Marine Data: The
1424 RECLAIM Project." *Int. J. Climatol.* 31: 968–979 http://doi.org/10.1002/joc.2102.
1425 Wikelski, M., R.W. Kays, N.J. Kasdin, K. Thorup, J.a. Smith, and G.W. Swenson. 2010. "Going
1426 Wild: What a Global Small-Animal Tracking System Could Do for Experimental Biologists." J.
1427 Exp. Biol. 210(2): 181–186. https://doi.org/10.1242/jeb.02629.
1428 Williams, S.E., L.P. Shoo, J.L. Isaac, A.A. Hoffmann, and G. Langham. 2008. "Towards an
1429 Integrated Framework for Assessing the Vulnerability of Species to Climate Change." *PLoS*
1430 *Biol.* 6(12): e325. http://doi.org/10.1371/journal.pbio.0060325.
1431 Woodruff, S.D., S.J. Worley, S.J. Lubker, Z. Ji, J.E. Freeman, D.I. Berry, P. Brohan, E.C. Kent,
1432 R.W. Reynolds, S.R. Smith, and C. Wilkinson. 2011. "ICOADS Release 2.5: Extensions and
1433 Enhancements to the Surface Marine Meteorological Archive." *Int. J. Climatol.* 31: 951–967
1434 http://doi.org/10.1002/joc.2103.
1435 Zuo, X., C. Zhao, L. Zhang, and E. Wang. 2016. "Influence of Growth Rate and Magnetic Field
1436 on Microstructure and Properties of Directionally Solidified Ag-Cu Eutectic Alloy." *Mater.* 9(7):
1437 569. http://doi.org/10.3390/ma9070569.
1438 Zou, Y., and Y. Zhang. 2009. "An Experimental and Theoretical Study on the Anisotropy of
1439 Elastin Network." *Ann. Biomed. Eng.* 37: 1572–1583. http://doi.org/10.1007/s10439-009-9724-z.
1440 Zschokke, S., and K. Nakata. 2015. "Vertical Asymmetries in Orb Webs." *Biol. J. Linn. Soc.*
1441 114(3): 659–672, http://doi.org/10.1111/bij.12456.

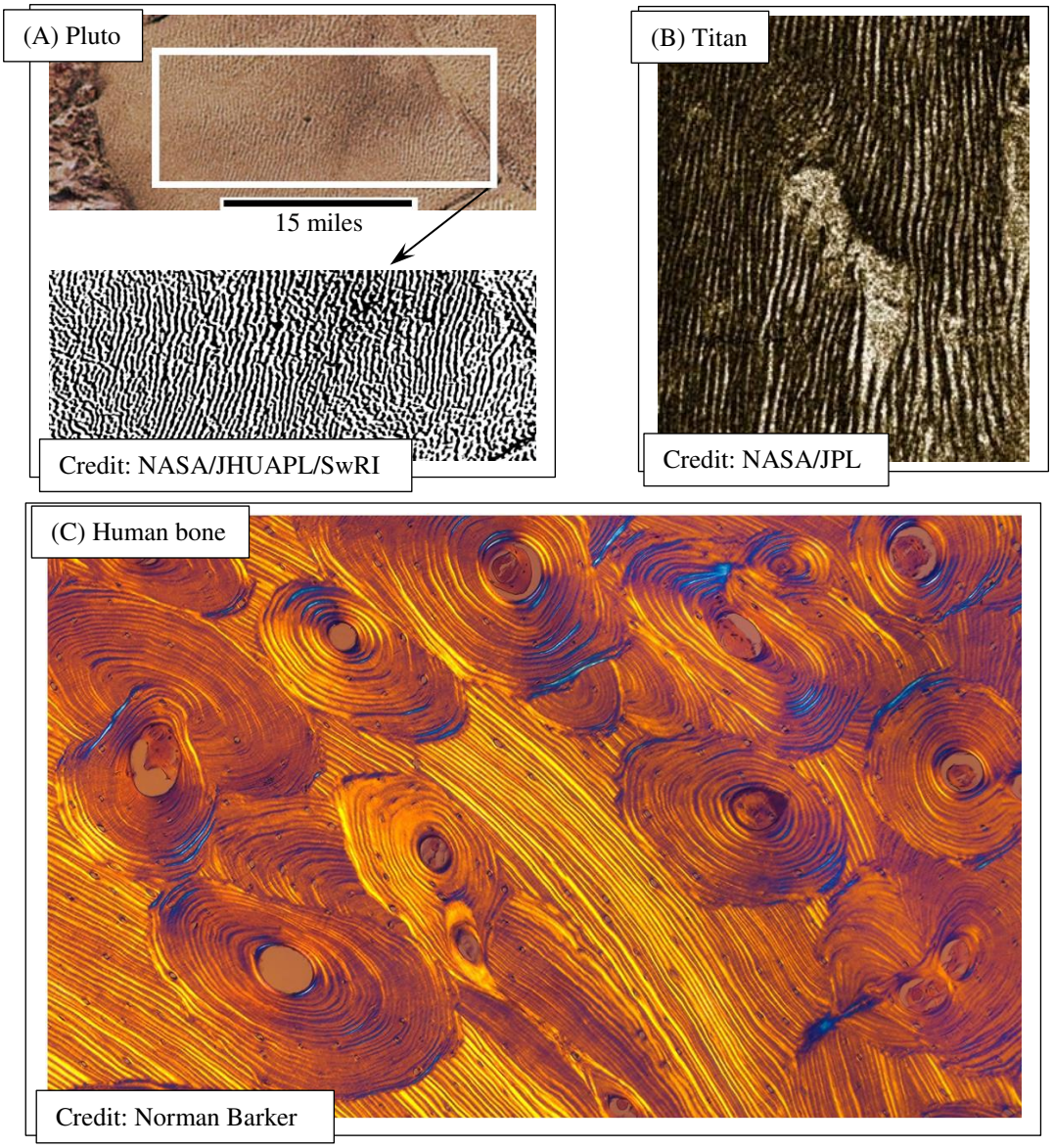

Figure 1. Living and non-living layered systems.
Structure of layers and variability of its thickness and chemical composition across 2D plane is the record of the internal and external factors responsible for patterns formation. These layered patterns form a record of internal and external factors regulating pattern formation in their various systems, making it potentially possible to recognize and identify in their incremental sequences trends, periodicities, and events in the formation history of these systems. Recent discoveries are:

Baleen whale cortisol levels reveal a physiological response to 20th century whaling. S. J. Trumble, S. A. Norman, D. D. Crain, F. Mansouri, Z. C. Winfield, R. Sabin, C. W. Potter, C. M. Gabriele & S. Usenko. Nature Communications, volume 9, Article number: 4587 (2018). http://doi: 10.1038/s41467-018-07044-w

Nacre Tablet Thickness Records Formation Temperature in Modern and Fossil Shells. Gilbert, P.U.P.A., K.D. Bergmann, C.E. Myers, M.A. Marcus, R.T. DeVol, C.-Y. Sun, A.Z. Blonsky, E. Tamre, J. Zhao, E.A. Karan, N. Tamura, S. Lemer, A.J. Giuffre, G. Giribet, J.M. Eiler, and A.H. Knoll. 2017. *Earth Planet. Sci. Letter*, 460: 281–292. http://doi.org/10.1016/j.epsl.2016.11.012.

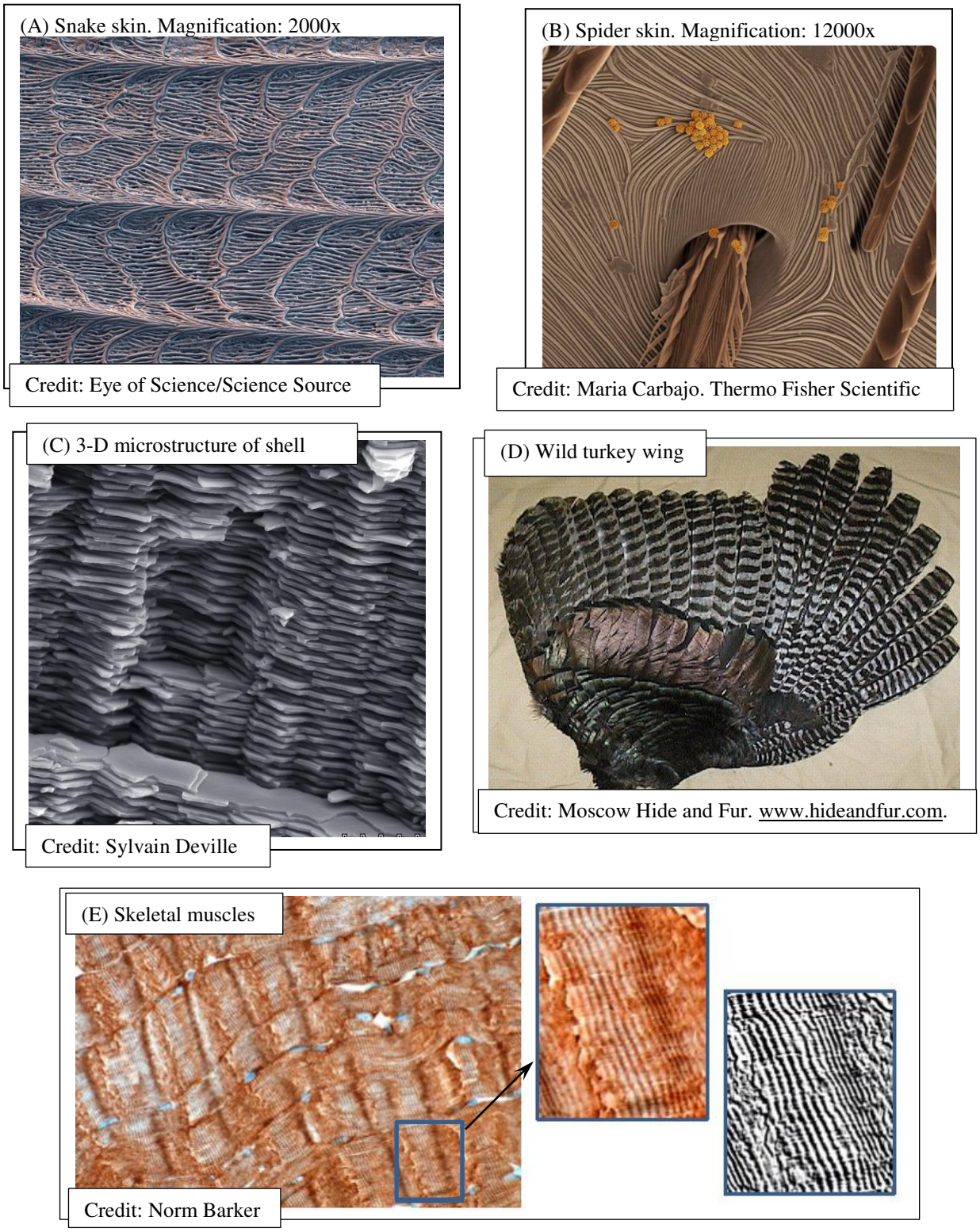

Figure 2. 3D and 2D layered systems

PeerJ Preprints | https://doi.org/10.7287/peerj.preprints.27451v2 | CC BY 4.0 Open Access | rec: 5 Jan 2019, publ: 5 Jan 2019

(A)

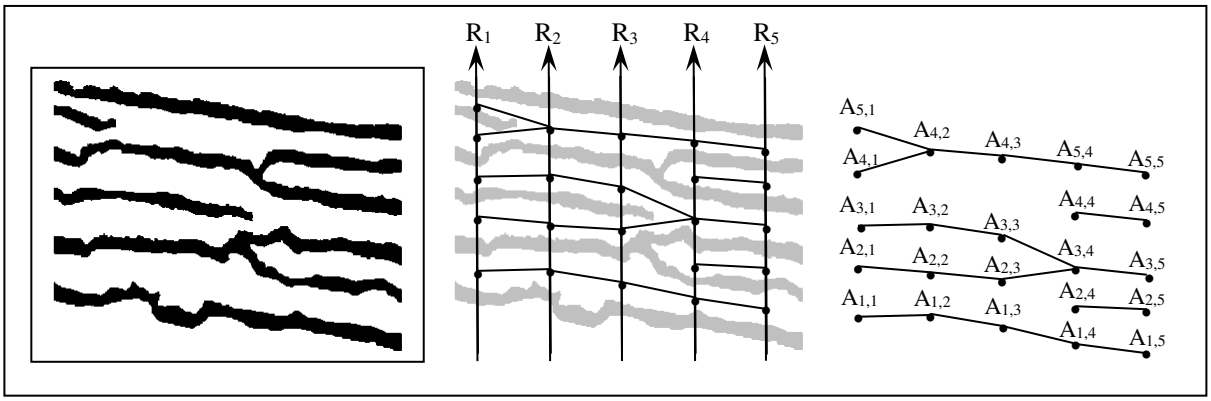

(B)

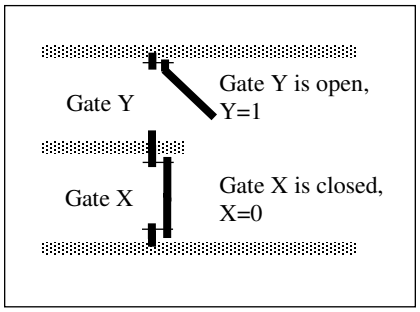

(C)

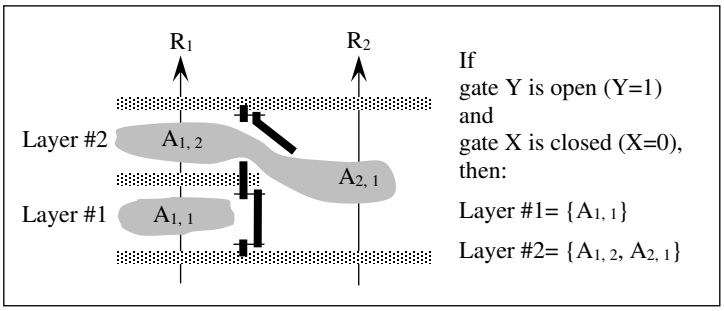

(D)

State of gates		Structure of layers		
X	**Y**	**Layer #1**	**Layer #2**	**Layer #3**
0	0	$A_{1,1}$	$A_{2,1}$	$A_{1,2}$
0	1	$A_{1,1}$	$A_{1,2}$, $A_{2,1}$	-
1	0	$A_{1,1}$, $A_{2,1}$	$A_{1,2}$	-
1	1	This state of gates violated properties of layers		

Figure 3. Structure of layered patterns as graphs (A) and logical network (B) – (D)
Empirical model M = {G(N), BF, $T_{M,N}$} of a layered pattern comprising N-partite graph G(N), Boolean Function (BF) and thickness of layers along transects R_1, …, R_N presented in the table $T_{M,N}$. Proposed methods allows us to fully automate conversion of a binary layered patterns into M = {G(N), BF, $T_{M,N}$}:

Quantification of Layered Patterns with Structural Anisotropy: A Comparison of Biological and Geological Systems. Smolyar, I.V., T. Bromage, M. Wikelski. 2016. Heliyon, 2(3): e00079. doi.org/10.1016/j.heliyon. 2016. e00079.

System and Method for Quantification of Size and Anisotropic Structure of Layered Patterns. Smolyar, I.V. 2014. U.S. Patent 8,755,578, issued June 17, 2014.

PeerJ Preprints | https://doi.org/10.7287/peerj.preprints.27451v2 | CC BY 4.0 Open Access | rec: 5 Jan 2019, publ: 5 Jan 2019

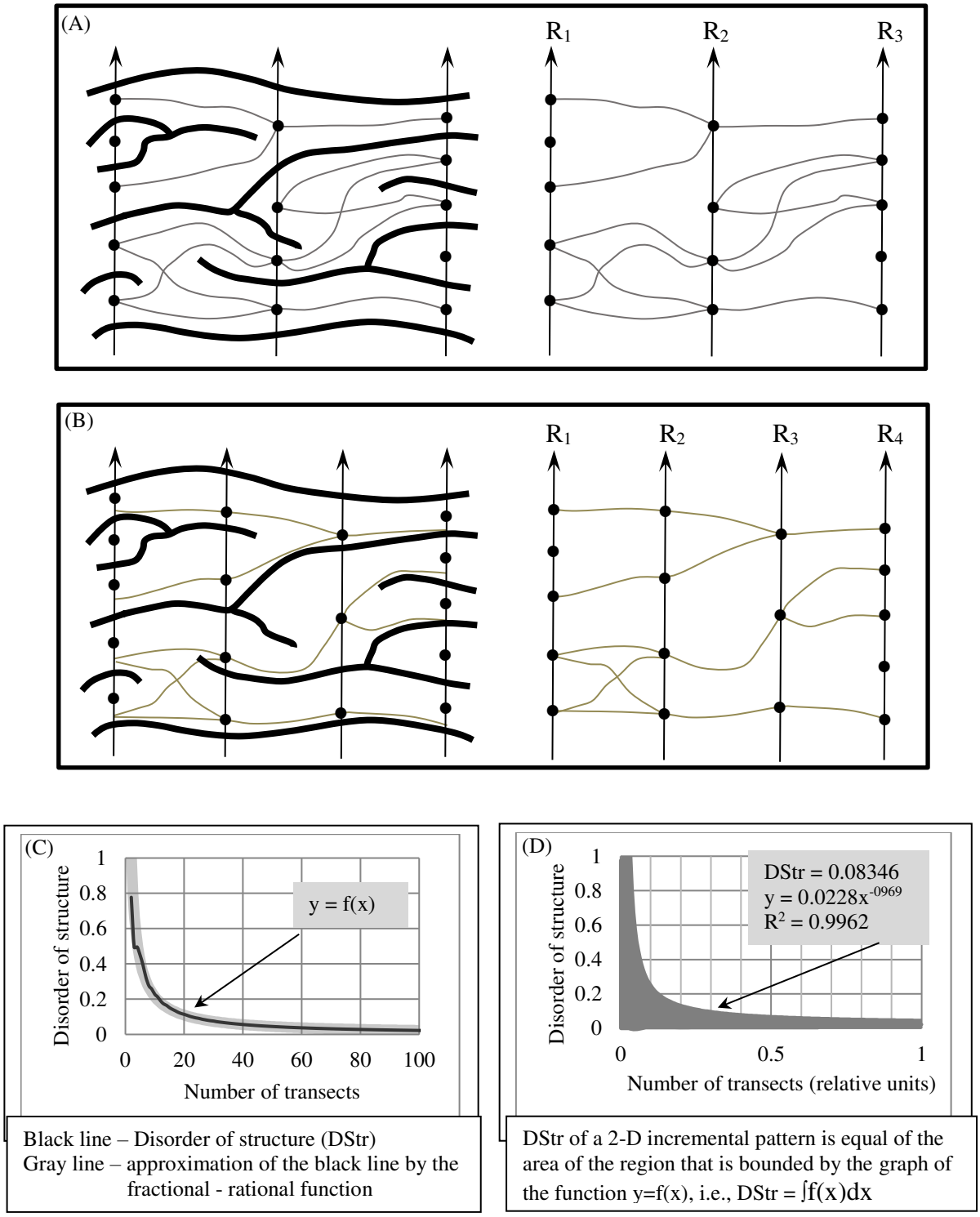

Figure 4. Quantifying structural disorder (DStr) in an anisotropic layered pattern.
DStr to describe the deviation of a study object's anisotropic structure from an isotropic analog.

PeerJ Preprints | https://doi.org/10.7287/peerj.preprints.27451v2 | CC BY 4.0 Open Access | rec: 5 Jan 2019, publ: 5 Jan 2019

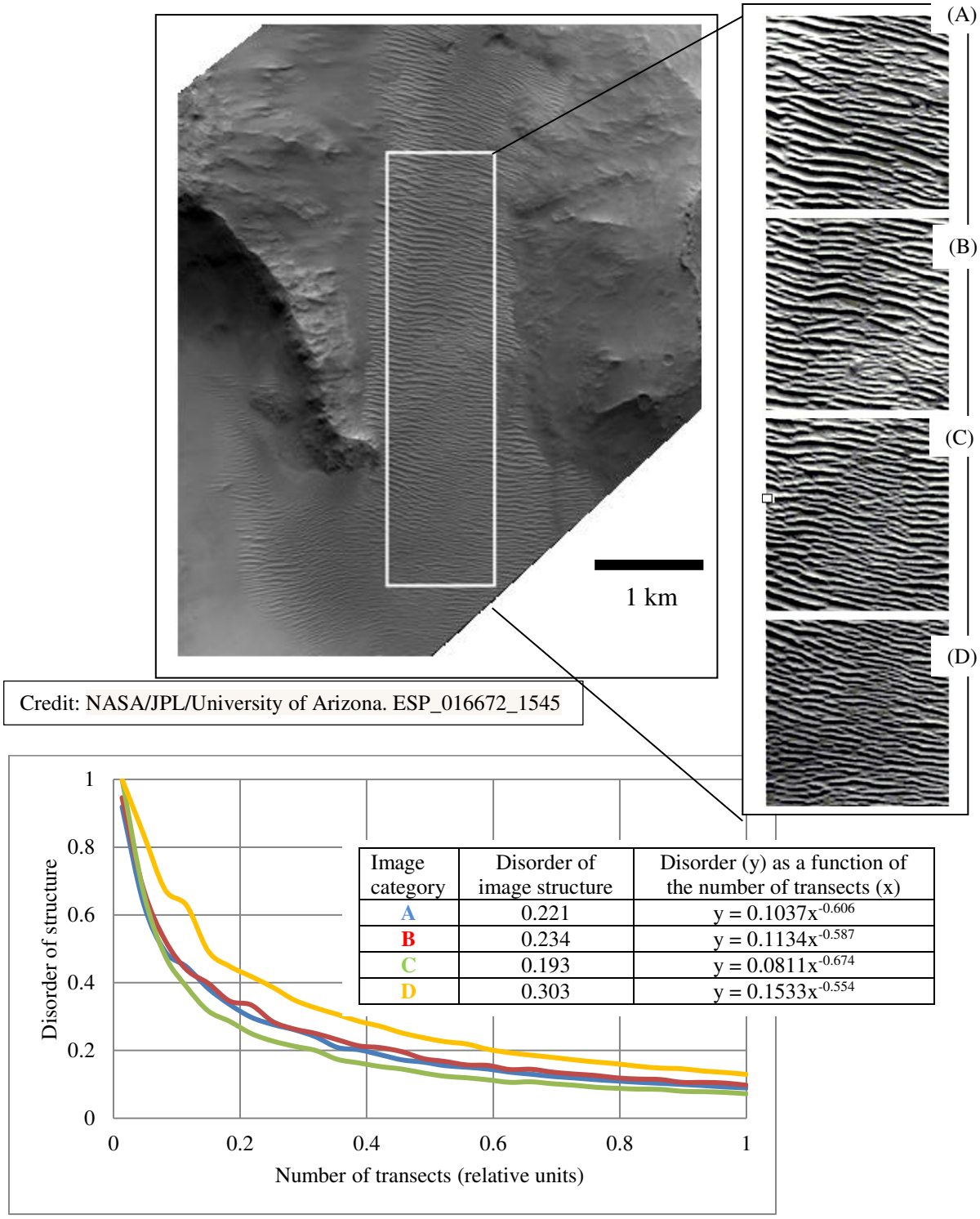

Image category	Disorder of image structure	Disorder (y) as a function of the number of transects (x)
A	0.221	$y = 0.1037x^{-0.606}$
B	0.234	$y = 0.1134x^{-0.587}$
C	0.193	$y = 0.0811x^{-0.674}$
D	0.303	$y = 0.1533x^{-0.554}$

Figure 5. Structural disorder on the Martian surface

PeerJ Preprints | https://doi.org/10.7287/peerj.preprints.27451v2 | CC BY 4.0 Open Access | rec: 5 Jan 2019, publ: 5 Jan 2019

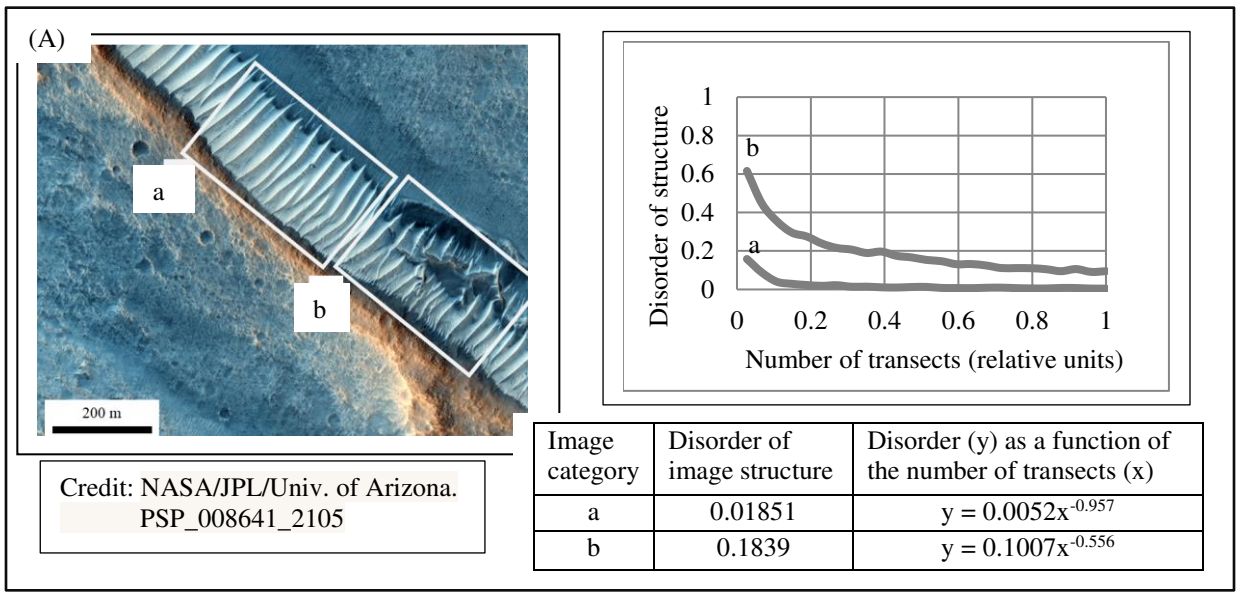

Credit: NASA/JPL/Univ. of Arizona. PSP_008641_2105

Image category	Disorder of image structure	Disorder (y) as a function of the number of transects (x)
a	0.01851	$y = 0.0052x^{-0.957}$
b	0.1839	$y = 0.1007x^{-0.556}$

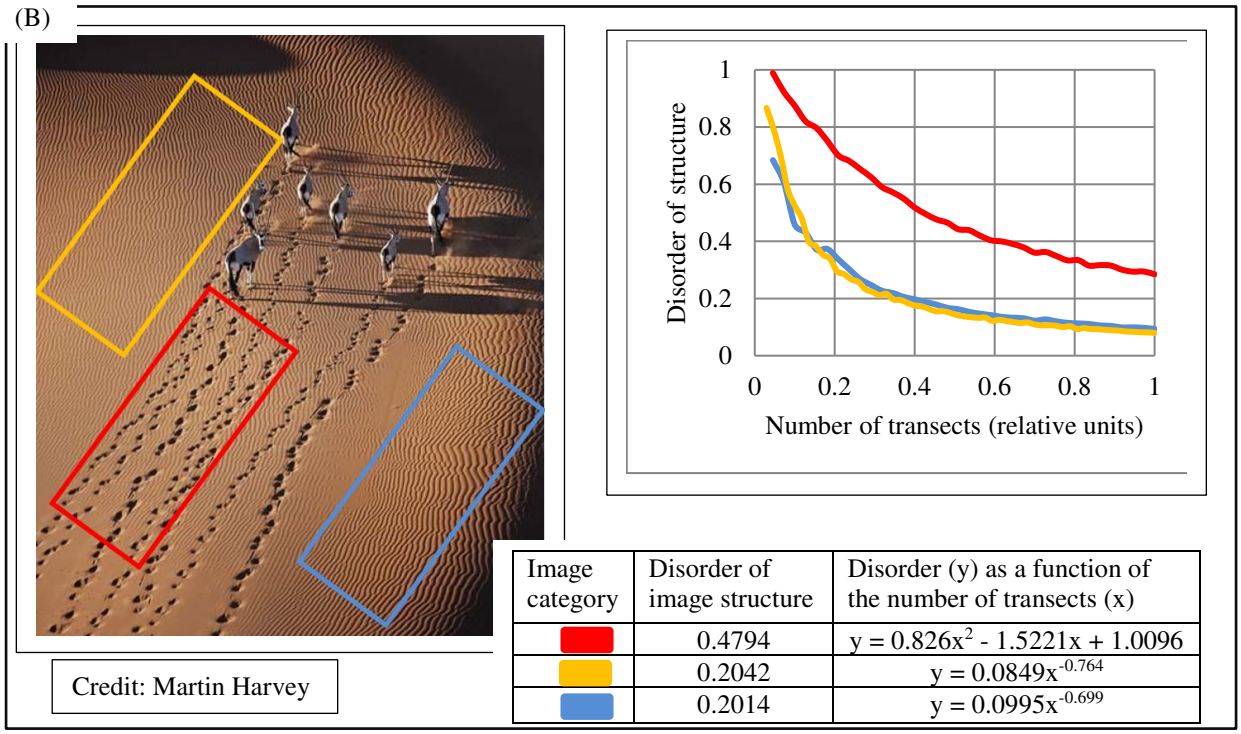

Credit: Martin Harvey

Image category	Disorder of image structure	Disorder (y) as a function of the number of transects (x)
	0.4794	$y = 0.826x^2 - 1.5221x + 1.0096$
	0.2042	$y = 0.0849x^{-0.764}$
	0.2014	$y = 0.0995x^{-0.699}$

Figure 6. Morphological characteristics of structural anomalies
Figure 6A. Martian surface structural anomaly
Figure 6B. Dunes sand ripples structural anomaly

Figure 6A depicts structural anomalies in a layered system of the Martian surface. The DStr of the sampling area a is 10 times less than that of nearby area b, which exhibits structural anomaly with respect to area a. Figure 6B depicts the structural anomaly of sand ripples. The red sampling area exhibits structural anomaly with respect to nearby orange and blue areas. The DStr of the orange and blue areas is 2.3 times less than that of the red area.

PeerJ Preprints | https://doi.org/10.7287/peerj.preprints.27451v2 | CC BY 4.0 Open Access | rec: 5 Jan 2019, publ: 5 Jan 2019

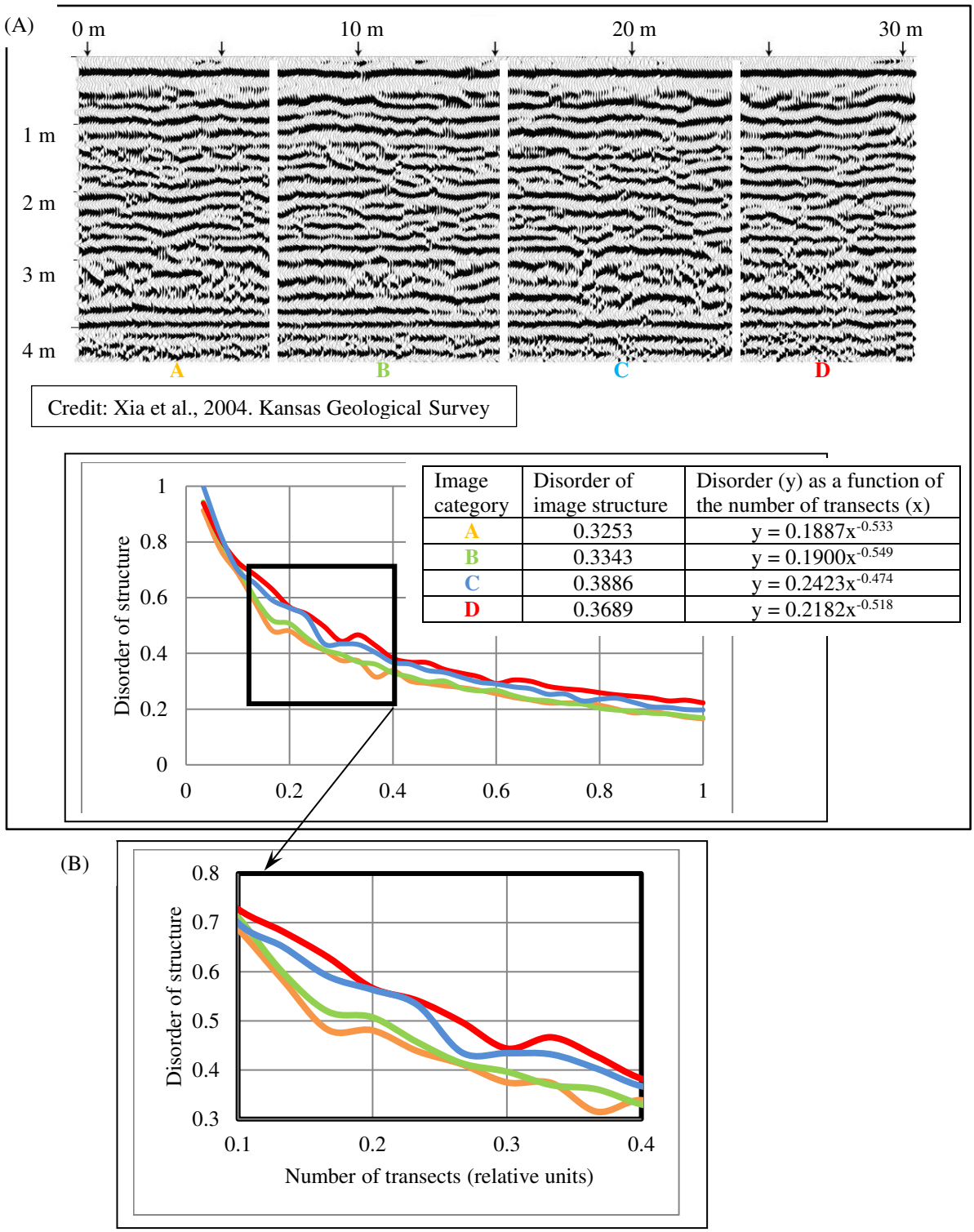

Image category	Disorder of image structure	Disorder (y) as a function of the number of transects (x)
A	0.3253	$y = 0.1887x^{-0.533}$
B	0.3343	$y = 0.1900x^{-0.549}$
C	0.3886	$y = 0.2423x^{-0.474}$
D	0.3689	$y = 0.2182x^{-0.518}$

Figure 7. Ground penetrating radar section
Figure 7A. Structural disorder in round penetrating radar section
Figure 7B. Fragment of the equation DStr = f(number of transects)
Fig. 7B shows that numbers of transects more than 0.1 and less than 0.4 maximize structural differences between segments A, B, C and D.

PeerJ Preprints | https://doi.org/10.7287/peerj.preprints.27451v2 | CC BY 4.0 Open Access | rec: 5 Jan 2019, publ: 5 Jan 2019

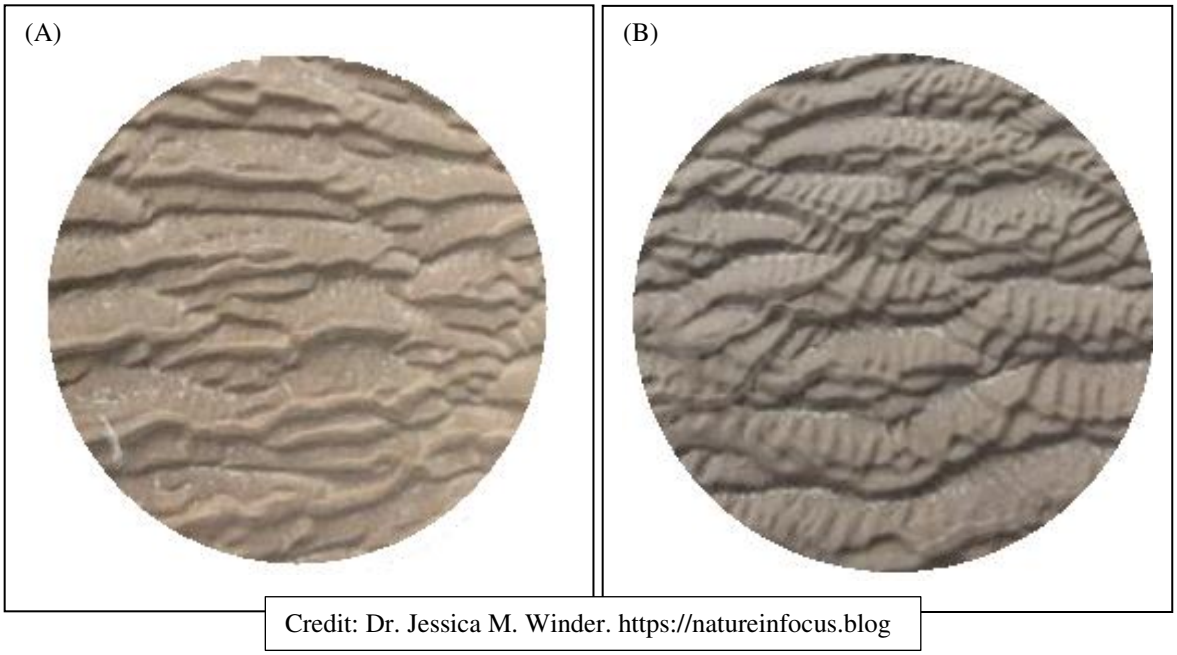

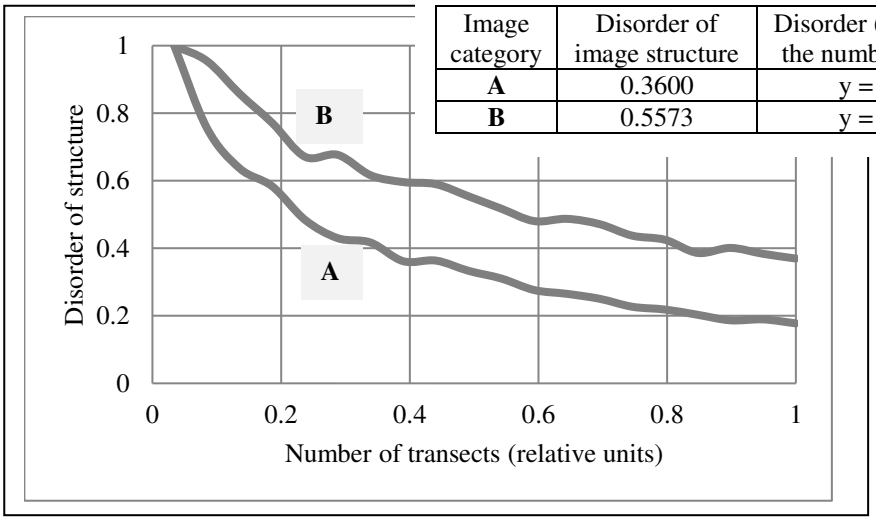

Image category	Disorder of image structure	Disorder (y) as a function of the number of transects (x)
A	0.3600	$y = 0.2046x^{-0.542}$
B	0.5573	$y = 0.4100x^{-0.329}$

Figure 8. Structural disorder in sand ripples at tidal zone. Diameter of images ~0.3 m

PeerJ Preprints | https://doi.org/10.7287/peerj.preprints.27451v2 | CC BY 4.0 Open Access | rec: 5 Jan 2019, publ: 5 Jan 2019

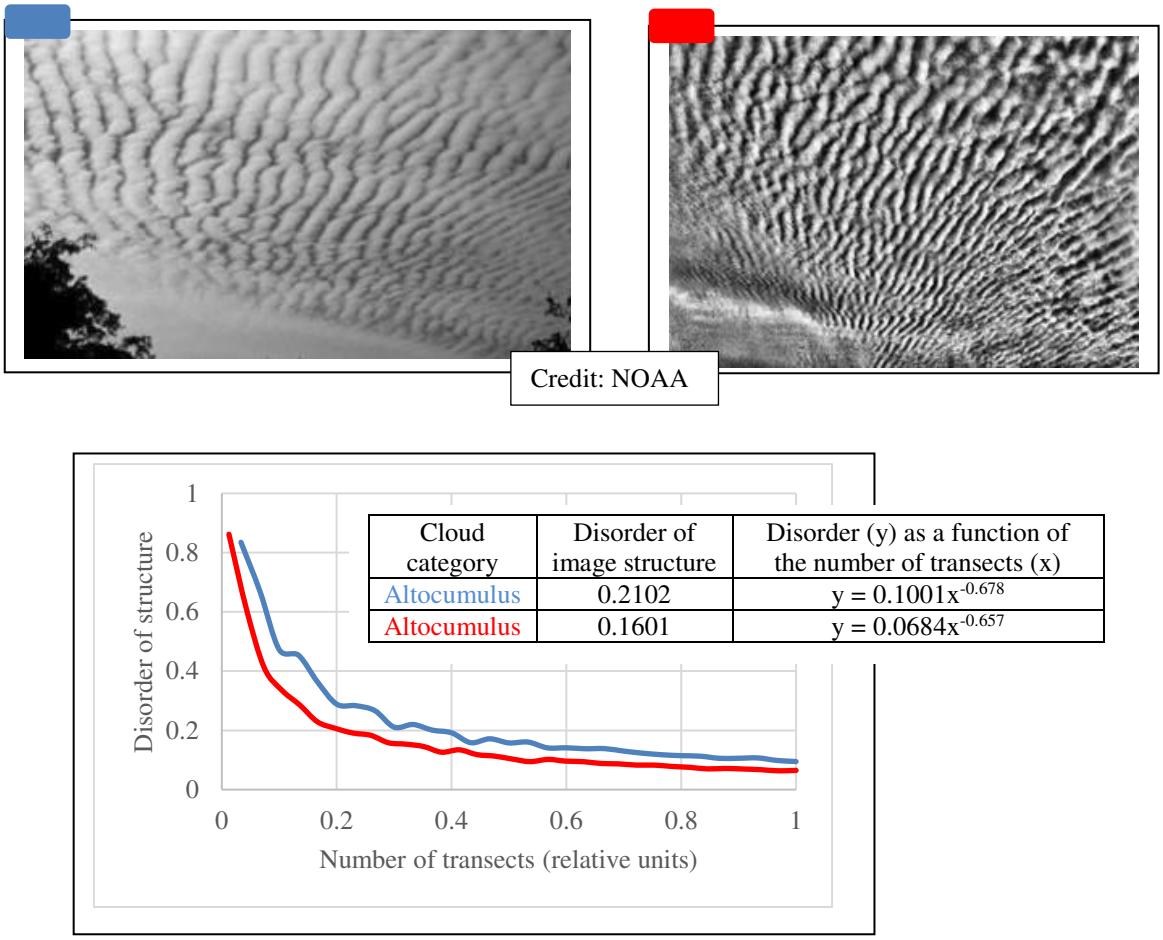

Cloud category	Disorder of image structure	Disorder (y) as a function of the number of transects (x)
Altocumulus	0.2102	$y = 0.1001x^{-0.678}$
Altocumulus	0.1601	$y = 0.0684x^{-0.657}$

Figure 9. Structural disorder in clouds

.

PeerJ Preprints | https://doi.org/10.7287/peerj.preprints.27451v2 | CC BY 4.0 Open Access | rec: 5 Jan 2019, publ: 5 Jan 2019

Credit: C. Clark. NOAA Photo Library, NOAA Central Library; OAR/EPL/National Severe Storm Laboratory (NSSL)

Details: Low

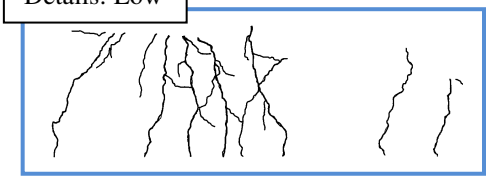

Details: Medium

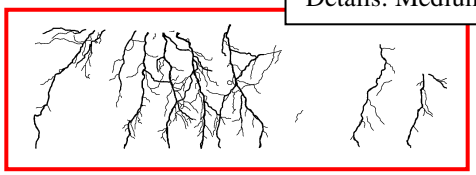

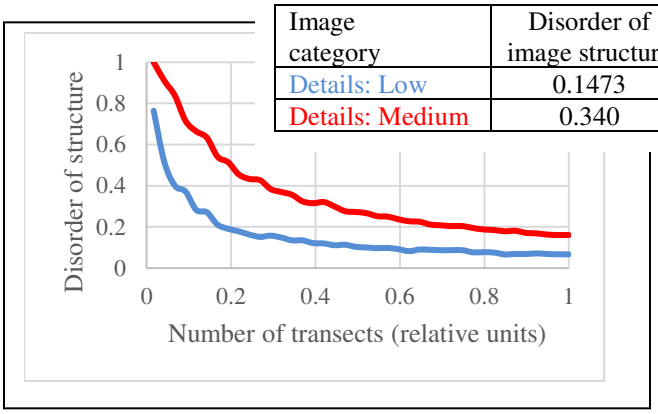

Image category	Disorder of image structure	Disorder (y) as a function of the number of transects (x)
Details: Low	0.1473	$y = 0.0671x^{-0.647}$
Details: Medium	0.340	$y = 0.1794x^{-0.548}$

Figure 10. Structural disorder in lightning

PeerJ Preprints | https://doi.org/10.7287/peerj.preprints.27451v2 | CC BY 4.0 Open Access | rec: 5 Jan 2019, publ: 5 Jan 2019

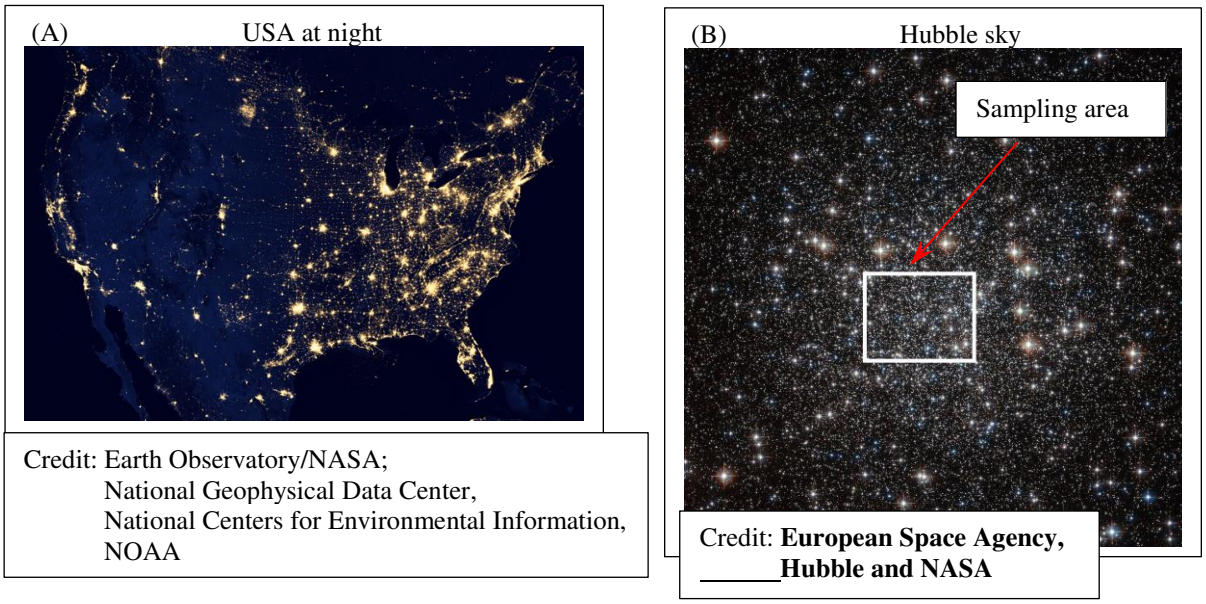

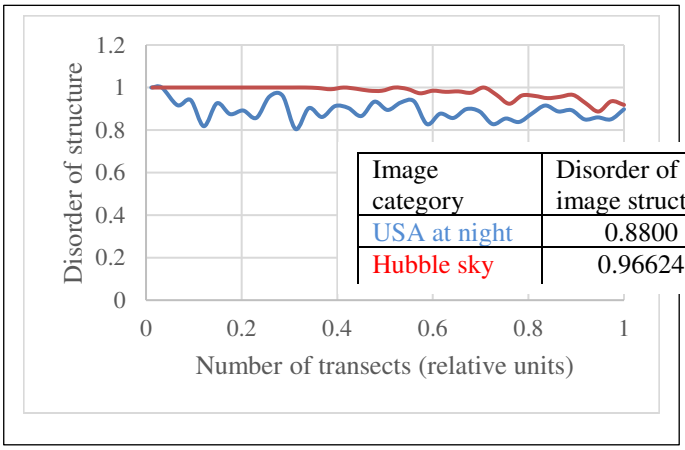

Image category	Disorder of image structure	Disorder (y) as the function of the number of transects (x)
USA at night	0.8800	y = 0.88
Hubble sky	0.96624	y = 0.97

Figure 11. Images of high-level structural disorder
Figure 11A. Structural disorder in satellite image of USA at night
Figure 11B. Structural disorder in photograph from Hubble space telescope

PeerJ Preprints | https://doi.org/10.7287/peerj.preprints.27451v2 | CC BY 4.0 Open Access | rec: 5 Jan 2019, publ: 5 Jan 2019

(A)

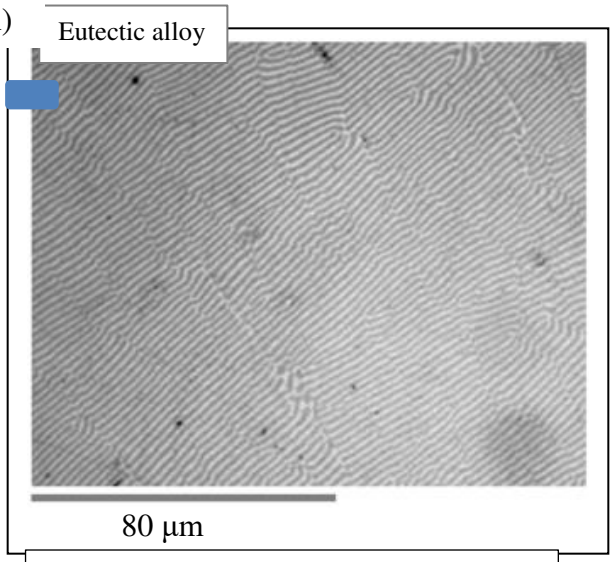

Credit: T. W. Cline, University of Cambridge

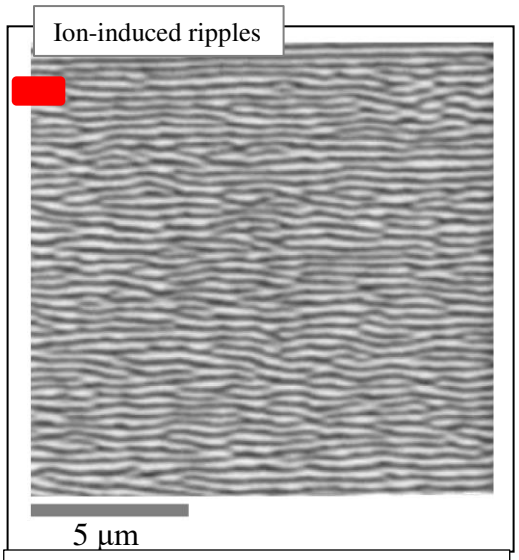

Credit: Lian et al. Applied Physical Letters, 88, 093112, 2006

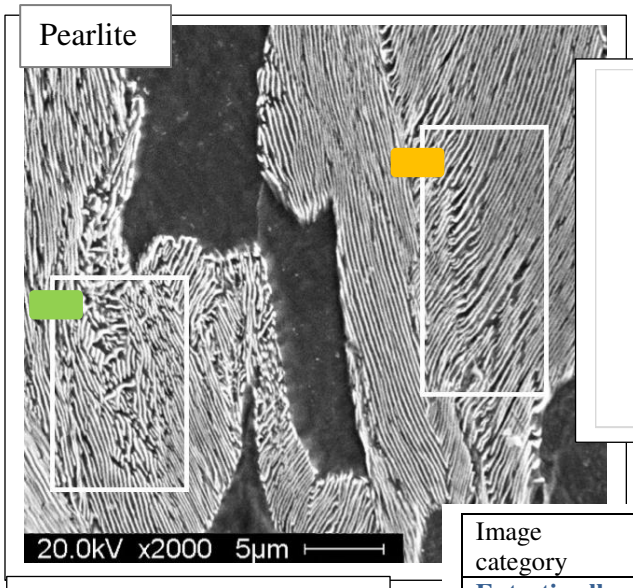

Credit: https://commons.wikimedia.org/w/index.php?title=File:Pearlite.jpg&oldid=264833343.(last visited May 8, 2018)

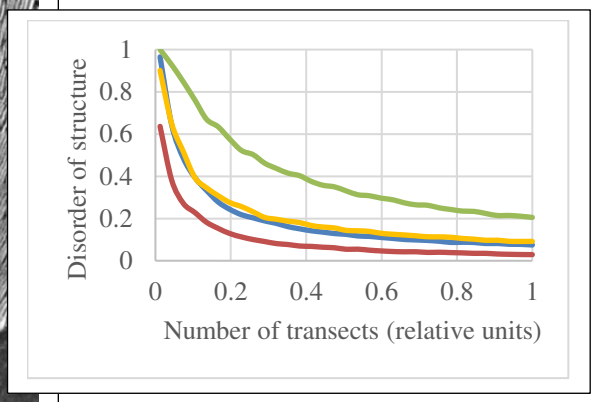

Image category	Disorder of image structure	Disorder (y) as a function of the number of transects (x)
Eutectic alloy	0.1835	$y = 0.0795x^{-0.649}$
Ion-induced ripples	0.0936	$y = 0.0313x^{-0.846}$
Pearlite	0.2027	$y = 0.0974x^{-0.588}$
Pearlite	0.4014	$y = -1.7325x^3 + 3.7322x^2 - 2.8391x + 1.0228$

Figure 12. Structural disorder of man-made layered materials
Figure 12A. Structural disorder in lamellar alloys
Figure 12B. Structural disorder in black diamonds
See next page

PeerJ Preprints | https://doi.org/10.7287/peerj.preprints.27451v2 | CC BY 4.0 Open Access | rec: 5 Jan 2019, publ: 5 Jan 2019

(B)

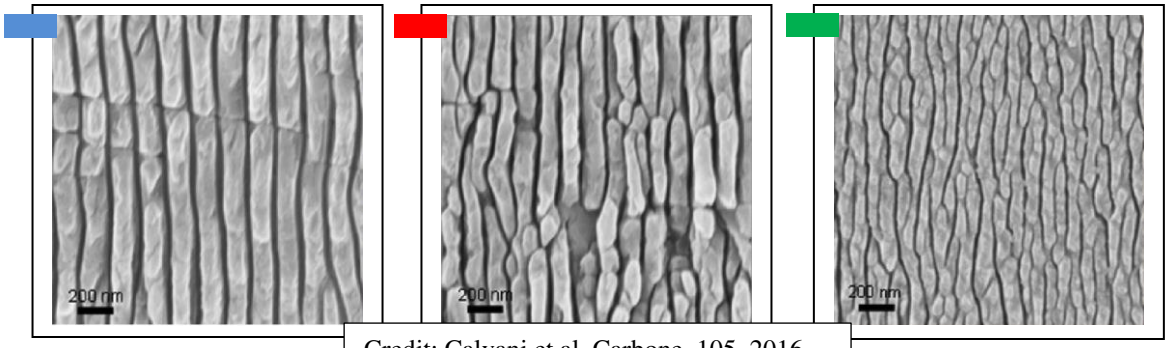

Credit: Calvani et al. Carbone, 105, 2016.

Black diamonds of different treatments	Disorder of image structure	Disorder (y) as a function of the number of transects (x)
Treatment #1	0.1357	$y = 0.0683x^{-0.596}$
Treatment #2	0.1425	$y = 0.0763x^{-0.556}$
Treatment #3	0.2835	$y = 0.1508x^{-0.555}$

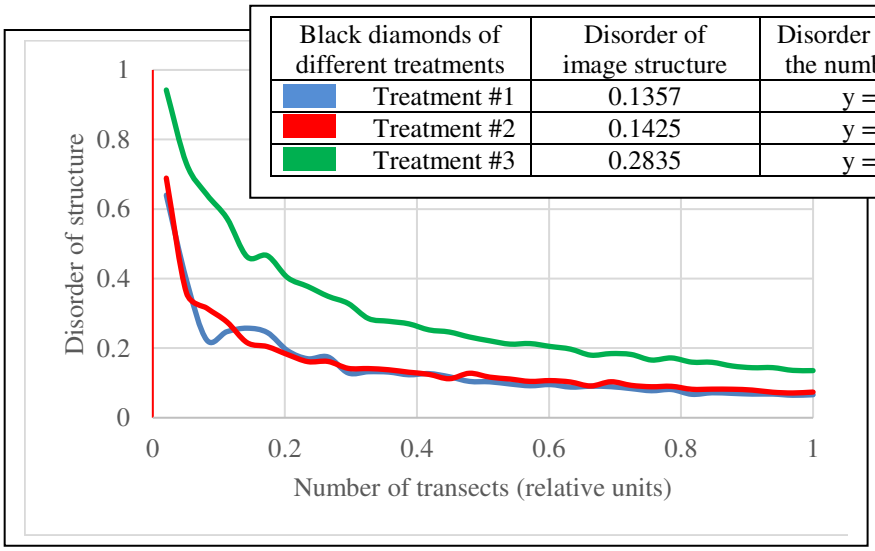

Figure 12B. Structural disorder in black diamonds

Materials science is an attractive area for the application of M = {BF, G(N), $T_{M,N}$} because the macro- and nanostructures of various materials exhibit layered anisotropic patterns (Fig. 12) that define their properties. Thus, DStr could serve as a local and global morphological parameter for describing material microstructures. DStr could also be used to link structures and properties, an essential step in developing materials with desired combinations of characteristics.

PeerJ Preprints | https://doi.org/10.7287/peerj.preprints.27451v2 | CC BY 4.0 Open Access | rec: 5 Jan 2019, publ: 5 Jan 2019

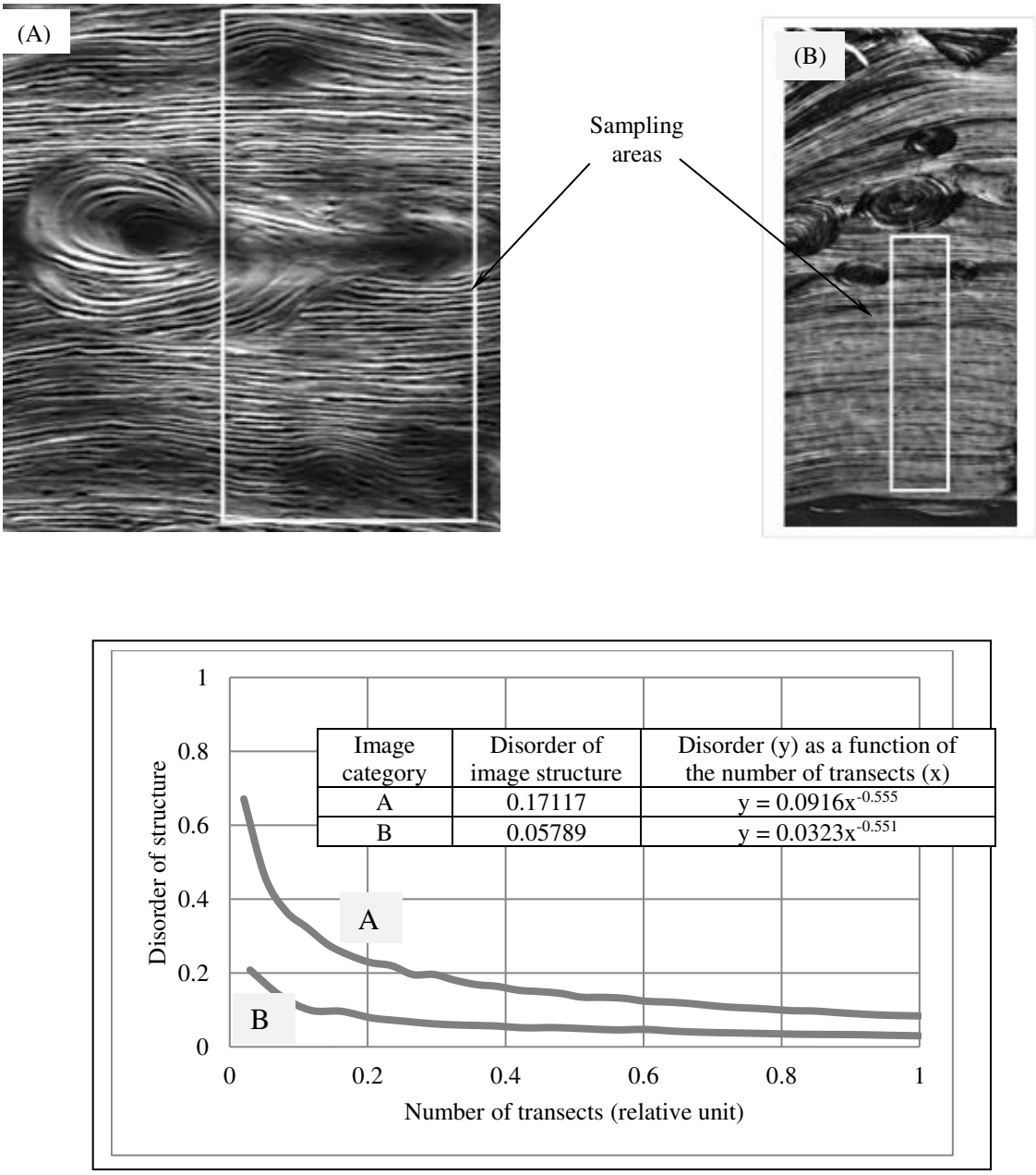

Figure 13. Structural disorder in lamella bones

PeerJ Preprints | https://doi.org/10.7287/peerj.preprints.27451v2 | CC BY 4.0 Open Access | rec: 5 Jan 2019, publ: 5 Jan 2019

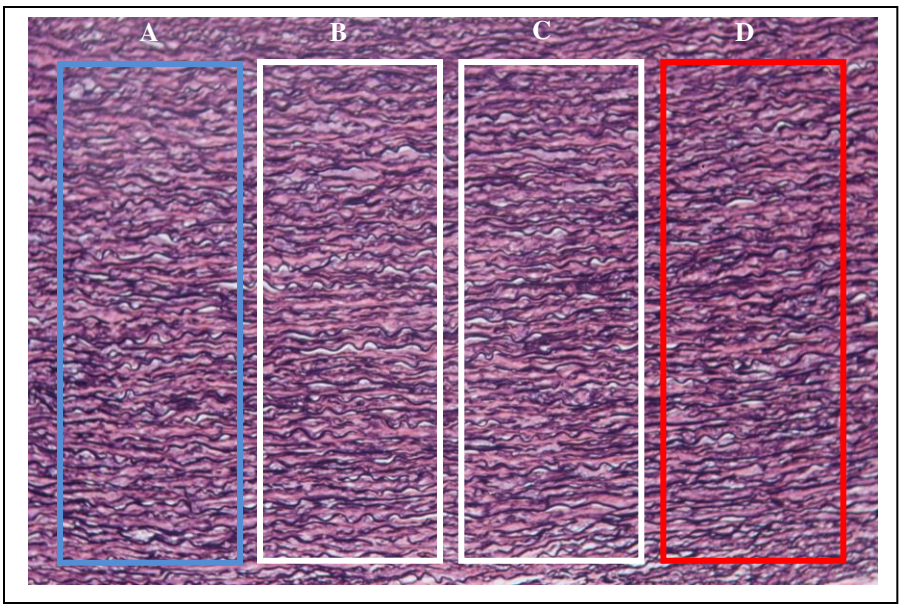

Credit: Donna Charley-Johnson, Triarch Incorporated

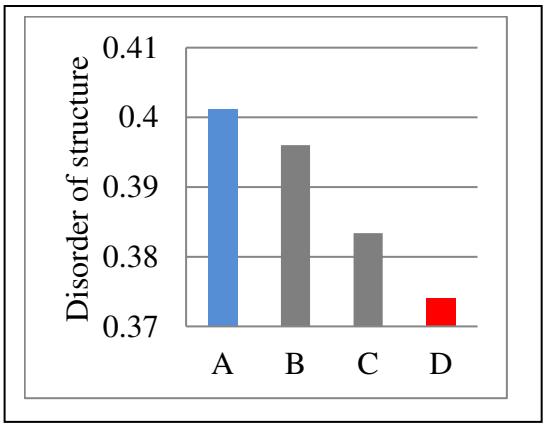

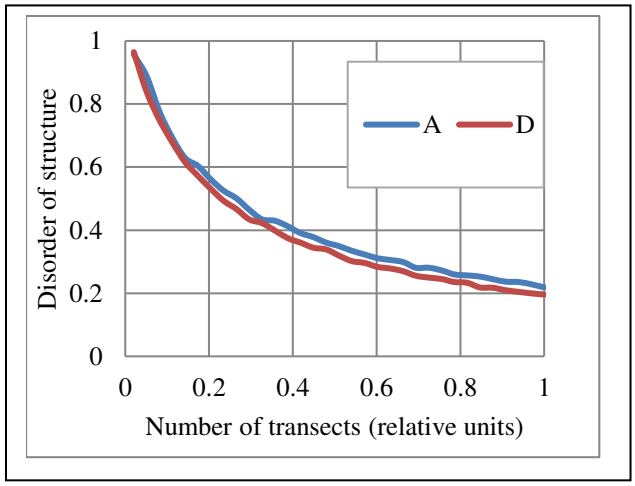

Figure 14. Structural disorder in lamellar human aorta

PeerJ Preprints | https://doi.org/10.7287/peerj.preprints.27451v2 | CC BY 4.0 Open Access | rec: 5 Jan 2019, publ: 5 Jan 2019

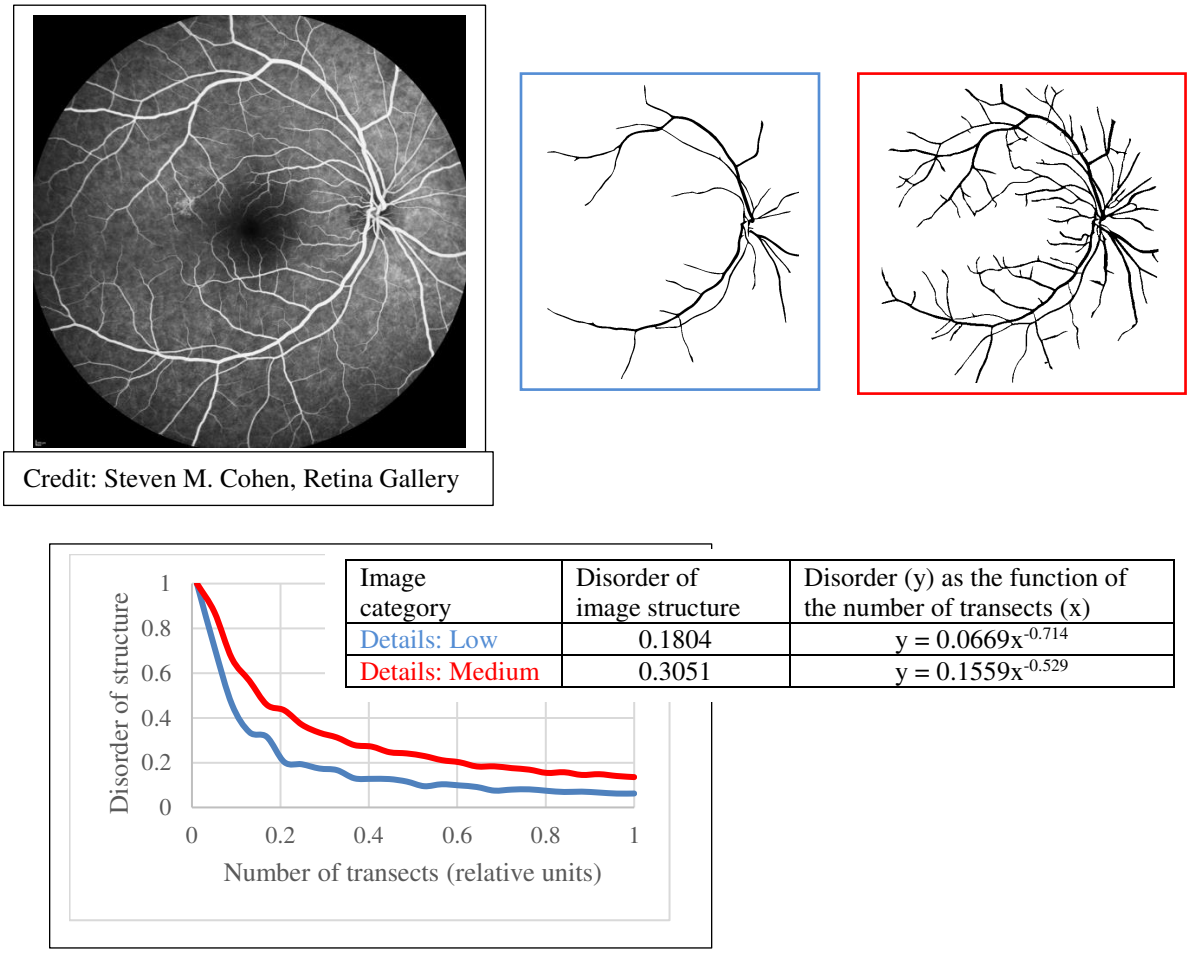

Image category	Disorder of image structure	Disorder (y) as the function of the number of transects (x)
Details: Low	0.1804	$y = 0.0669x^{-0.714}$
Details: Medium	0.3051	$y = 0.1559x^{-0.529}$

Figure 15. Structural disorder in human eye angiogram

PeerJ Preprints | https://doi.org/10.7287/peerj.preprints.27451v2 | CC BY 4.0 Open Access | rec: 5 Jan 2019, publ: 5 Jan 2019

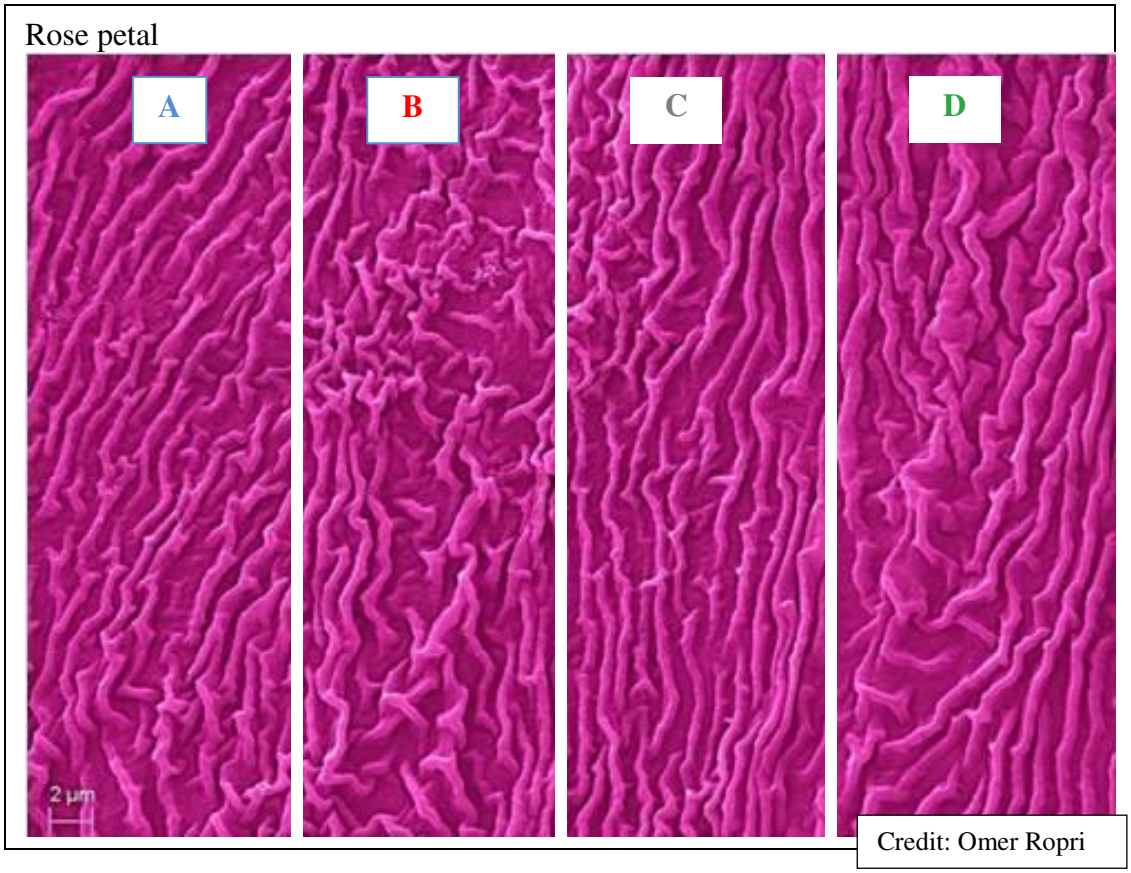

Image category	Disorder of image structure	Disorder (y) as a function of the number of transects (x)
A	0.367	$y = 0.2216x^{-0.451}$
B	0.471	$y = -1.2057x^3 + 2.5767x^2 - 2.0958x + 0.9771$
C	0.261	$y = 0.1399x^{-0.538}$
D	0.317	$y = 0.1742x^{-0.518}$

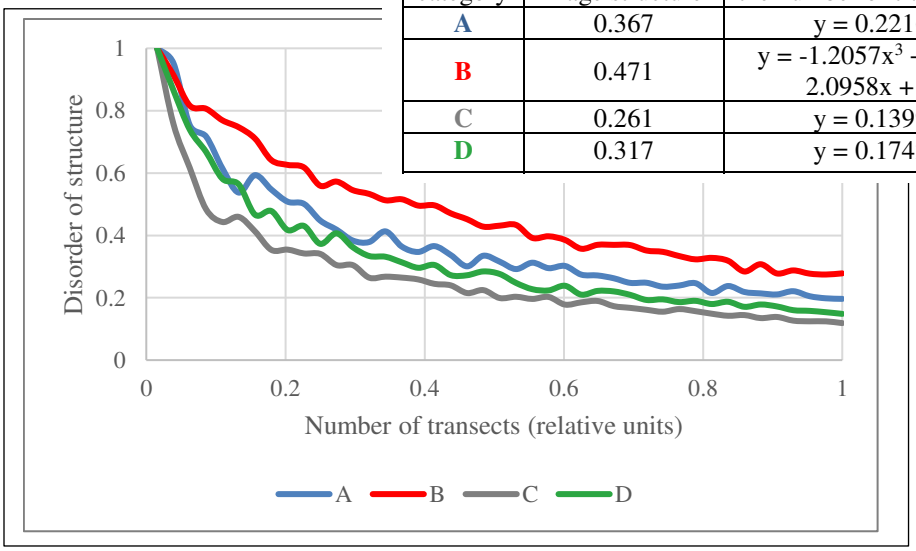

Figure 16. Structural disorder in flower surfaces

PeerJ Preprints | https://doi.org/10.7287/peerj.preprints.27451v2 | CC BY 4.0 Open Access | rec: 5 Jan 2019, publ: 5 Jan 2019

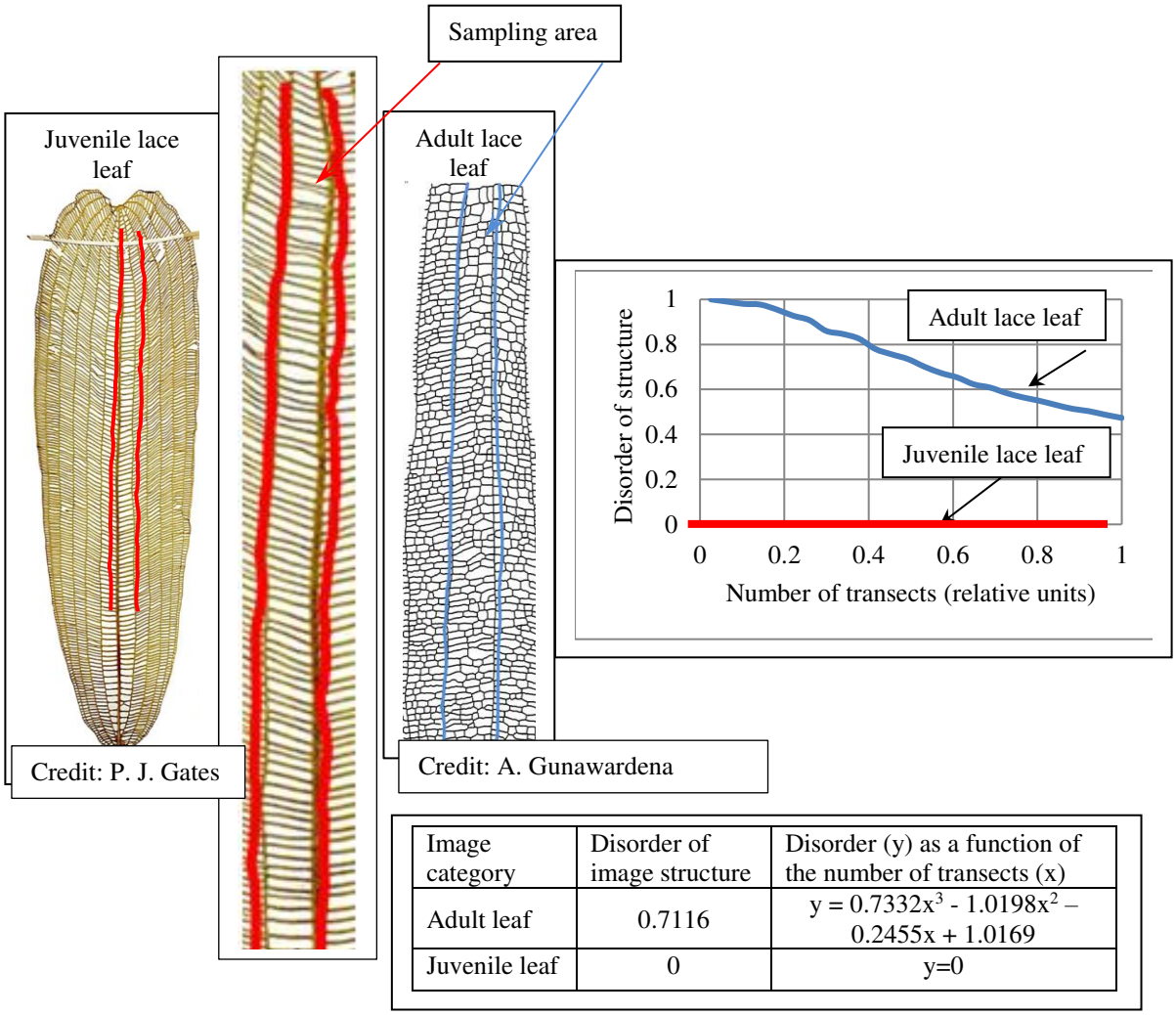

Image category	Disorder of image structure	Disorder (y) as a function of the number of transects (x)
Adult leaf	0.7116	$y = 0.7332x^3 - 1.0198x^2 - 0.2455x + 1.0169$
Juvenile leaf	0	y=0

Figure 17. Structural disorder in leaf system

PeerJ Preprints | https://doi.org/10.7287/peerj.preprints.27451v2 | CC BY 4.0 Open Access | rec: 5 Jan 2019, publ: 5 Jan 2019

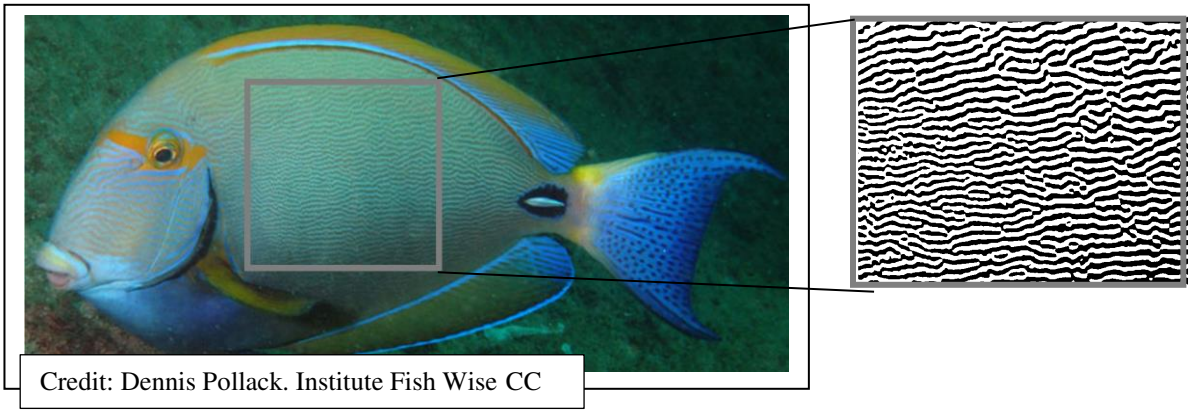

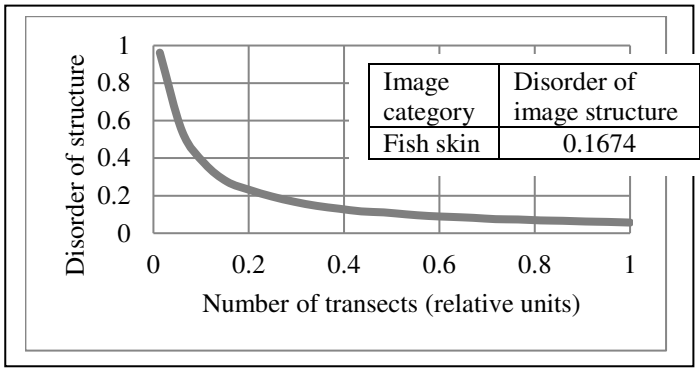

Image category	Disorder of image structure	Disorder (y) as the function of the number of transects (x)
Fish skin	0.1674	$y=0.0634x^{-0.716}$

Image category	Disorder of image structure	Disorder (y) as a function of the number of transects (x)
A	0.1578	$y = 0.0657x^{-0.755}$
B	0.1939	$y = 0.0811x^{-0.753}$
C	0.1697	$y = 0.0719x^{-0.744}$
D	0.1393	$y = 0.0598x^{-0.735}$

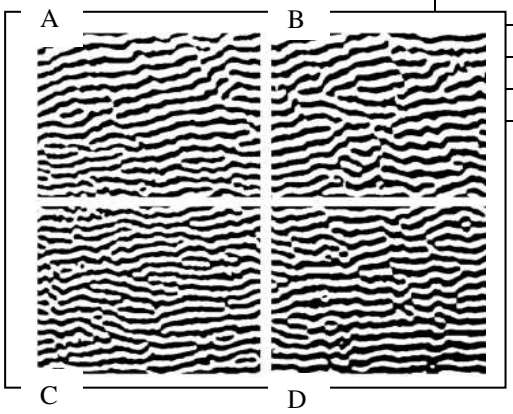

Figure 18. Structural disorder in fish skin

The configuration of stripes on fish skin (Fig. 18) is a typical example of an anisotropic layered pattern. The formation of patterns on the surfaces of fish, shells, and mammals has been explained by a reaction–diffusion system (Turing, 1952; Meinhardt, 1989; Shoji et al., 2003). Results of calculating DStr for sampling areas A, B, C, and D imply that DStr(B)>DStr(C)>DStr(A)>DStr(D), indicating that area B has the most complicated structure and area D has the simplest structure among four sampling areas. This result inspires two questions: 1) Is the DStr of the right side of the fish similar to the DStr of the left side? 2) Could the morphology of stripes serve as a record of internal and external events in the life history of a fish? Model M = {BF, G(N), $T_{M,N}$} could be one tool to help to answer these questions.

PeerJ Preprints | https://doi.org/10.7287/peerj.preprints.27451v2 | CC BY 4.0 Open Access | rec: 5 Jan 2019, publ: 5 Jan 2019

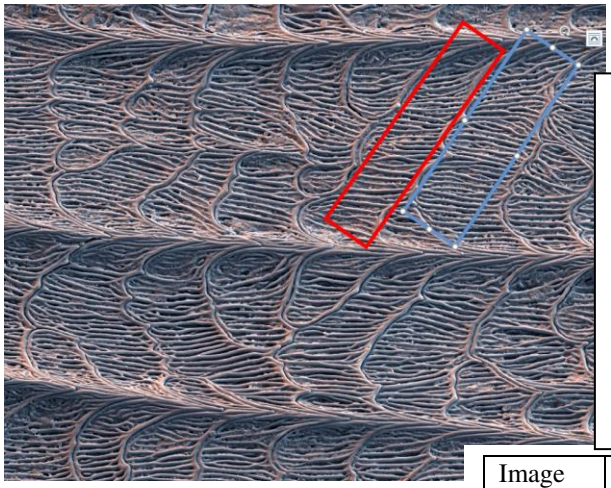

Credit: Eye of Science / Science Source

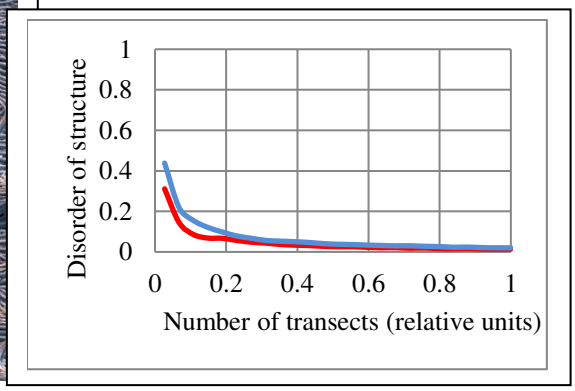

Image category	Disorder of image structure	Disorder (y) as a function of the number of transects (x)
	0.042	$y = 0.0144x^{-0.864}$
	0.063	$y = 0.0212x^{-0.873}$

Figure 19. Structural disorder in snake skin

PeerJ Preprints | https://doi.org/10.7287/peerj.preprints.27451v2 | CC BY 4.0 Open Access | rec: 5 Jan 2019, publ: 5 Jan 2019

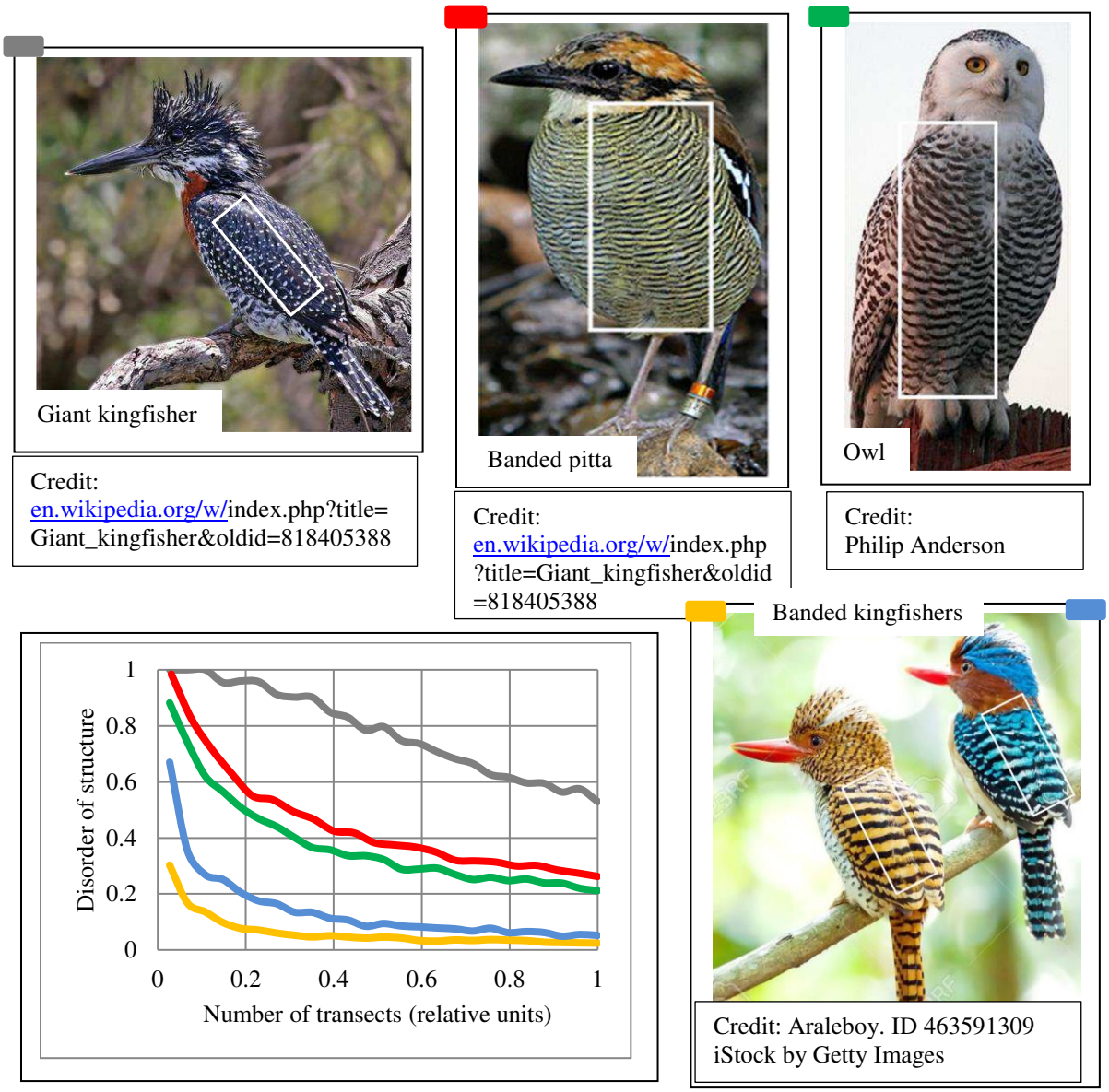

Color code	Image category	Disorder of image structure	Disorder (y) as a function of the number of transects (x)
	Giant kingfisher	0.7591	$y = -0.5248x + 1.049$
	Banded pitta	0.4277	$y = 0.2866x^{-0.406}$
	Owl	0.3590	$y = 0.2331x^{-0.424}$
	Banded kingfisher	0.1299	$y = 0.0561x^{-0.722}$
	Banded kingfisher	0.0574	$y = 0.0261x^{-0.682}$

Figure 20. Structural disorder in bird plumage patterns. Plumage patterns in banded pitta, kingfisher, and owl (Fig. 20) offer examples of layered systems in bird plumage. DStr shows significant diversity in the structure of these layered systems: DStr(giant kingfisher) = 0.7591; DStr(banded kingfisher) = 0.0574. This result inspires us to ask whether parameters of layered structures might serve as phenotypic characteristics (Gluckman and Mundy, 2016). Model M = {BF, G(N), $T_{M,N}$} could be used to test this hypothesis (i.e., examine the structural characteristics of birds' plumage patterns with respect to state of the environment).

PeerJ Preprints | https://doi.org/10.7287/peerj.preprints.27451v2 | CC BY 4.0 Open Access | rec: 5 Jan 2019, publ: 5 Jan 2019

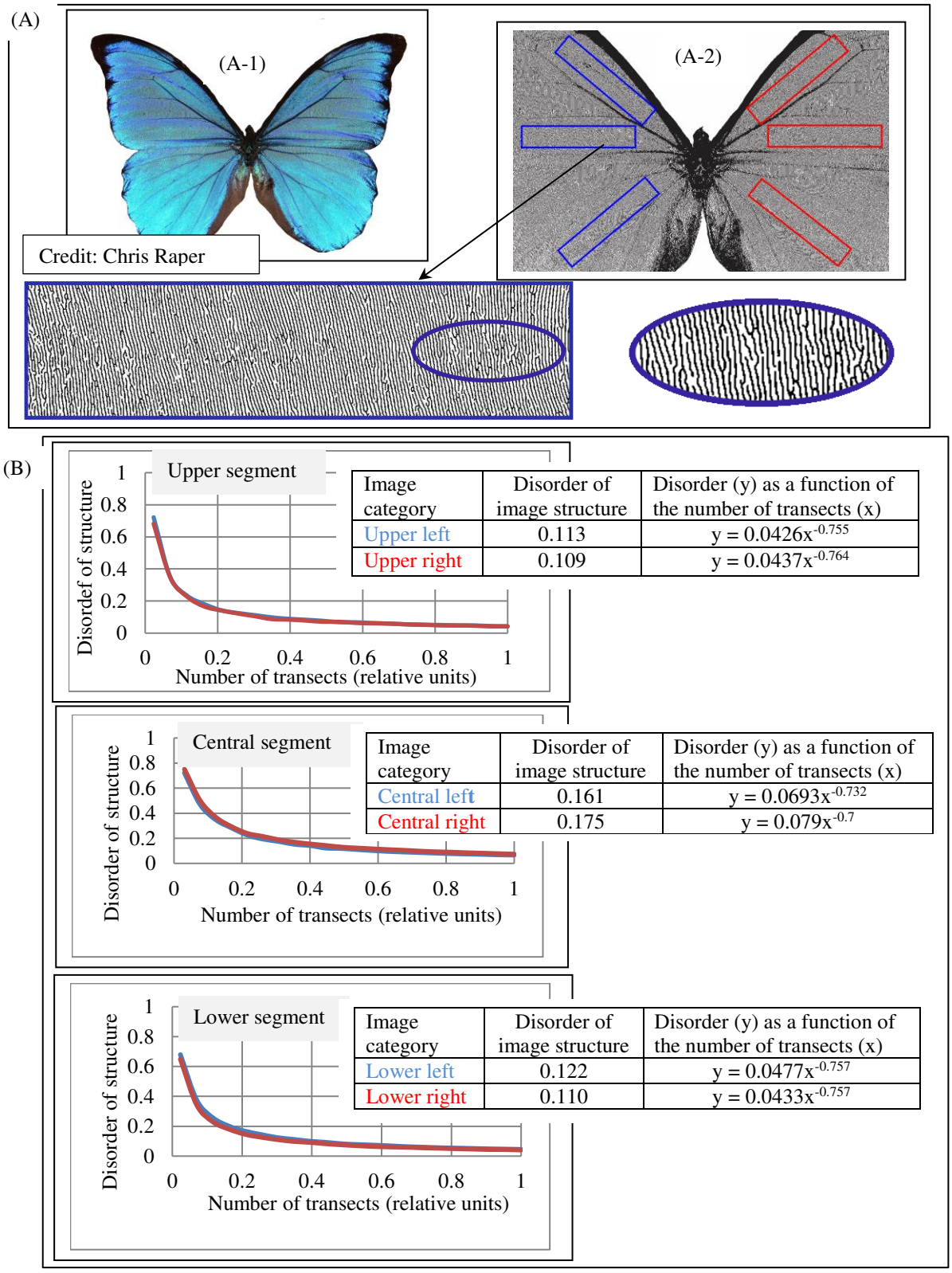

Image category	Disorder of image structure	Disorder (y) as a function of the number of transects (x)
Upper left	0.113	$y = 0.0426x^{-0.755}$
Upper right	0.109	$y = 0.0437x^{-0.764}$

Image category	Disorder of image structure	Disorder (y) as a function of the number of transects (x)
Central left	0.161	$y = 0.0693x^{-0.732}$
Central right	0.175	$y = 0.079x^{-0.7}$

Image category	Disorder of image structure	Disorder (y) as a function of the number of transects (x)
Lower left	0.122	$y = 0.0477x^{-0.757}$
Lower right	0.110	$y = 0.0433x^{-0.757}$

Figure 21. Morphology of butterfly wing. (A) Sampling areas in Morpho butterfly wing. (B) Structural disorder in butterfly wing. See next page.

PeerJ Preprints | https://doi.org/10.7287/peerj.preprints.27451v2 | CC BY 4.0 Open Access | rec: 5 Jan 2019, publ: 5 Jan 2019

Figure 21. Morphology of butterfly wing. (A) Sampling areas in Morpho butterfly wing. (B) Structural disorder in butterfly wing

Photonic systems of biological objects generate interest among scientists and engineers across various disciplines due to their unique ability to manipulate color using micro-structured surfaces (Starkey and Vukusic, 2013; Parker, 2000). Many photonic surfaces in flowers and animals exhibit lamellar structures (Vukusic and Sambles, 2003), such as the scales arranged in anisotropic layered patterns on the surfaces of morpho butterfly wings (Fig. 21A). We use DStr to compare the anisotropic characteristics of left and right wings. Figure 21B reports the results of DStr calculations for six sampling areas. The left and right wings of Morpho butterfly have similar structural characteristics: DStr is equal to 0.132 and 0.131, respectively. Could DStr be a characteristic of blue color nuances in Morpho butterflies? Do male and female Morpho butterflies have similar structural characteristic DStr? How do local/global structural anomalies in butterfly wings with respect to DStr affect butterfly color? Model M = {BF, G(N), $T_{M,N}$} could be used to answer these questions.

PeerJ Preprints | https://doi.org/10.7287/peerj.preprints.27451v2 | CC BY 4.0 Open Access | rec: 5 Jan 2019, publ: 5 Jan 2019

(A)

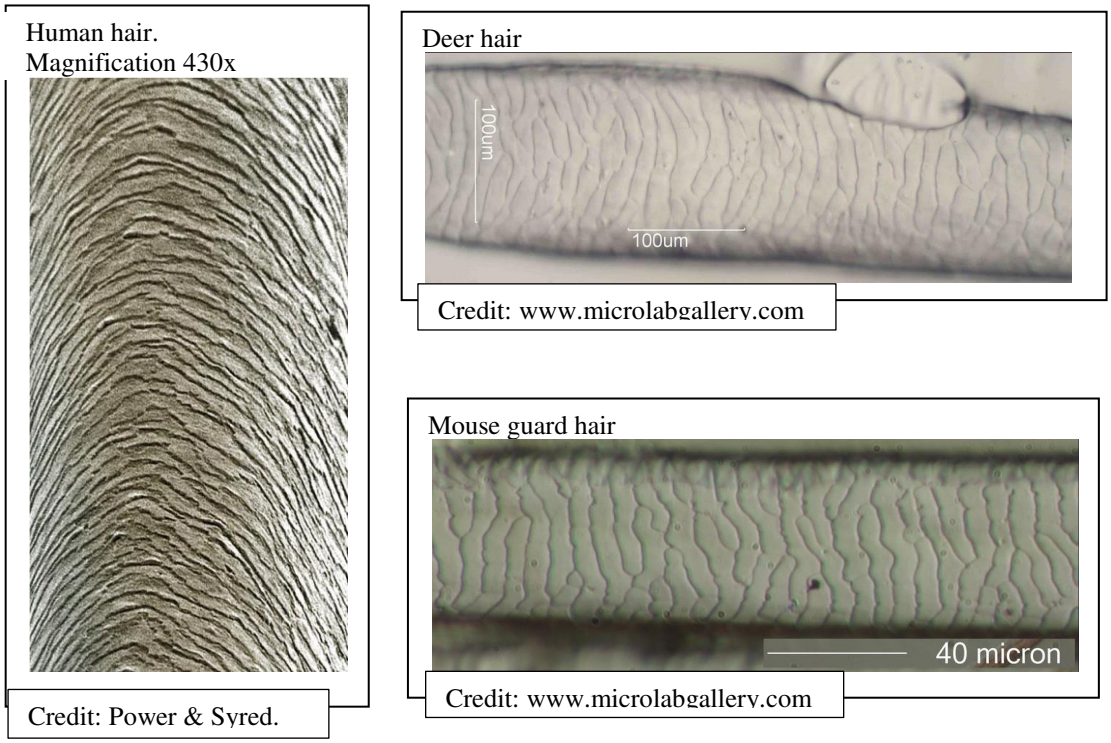

Hair category	Disorder of image structure	Disorder (y) as the function of the number of transects (x)
Human	0.3397	$y = 0.2142x^{-0.407}$
Deer	0.1595	$y = 0.0621x^{-0.69}$
Mouse	0.0515	$y = 0.0117x^{-0.933}$

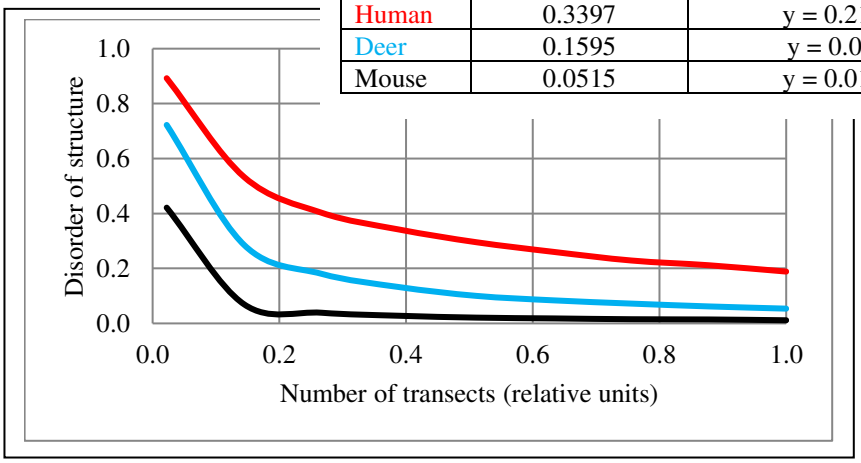

Figure 22. Morphology of hair microstructure
Figure 22A. Structural disorder in human and animal hairs
Figure 22B. Structural disorder as a function of sampling density

The layered microstructures of human hair are much more complicated than those of some animals (Fig. 22A), which is confirmed by DStr(human), DStr(deer), DStr(mouse), and the corresponding charts for "structural disorder of hair = f(number of transects)." Figure 22B (next page) shows that high sampling density accounts for more structural details than low sampling density.

PeerJ Preprints | https://doi.org/10.7287/peerj.preprints.27451v2 | CC BY 4.0 Open Access | rec: 5 Jan 2019, publ: 5 Jan 2019

(B)

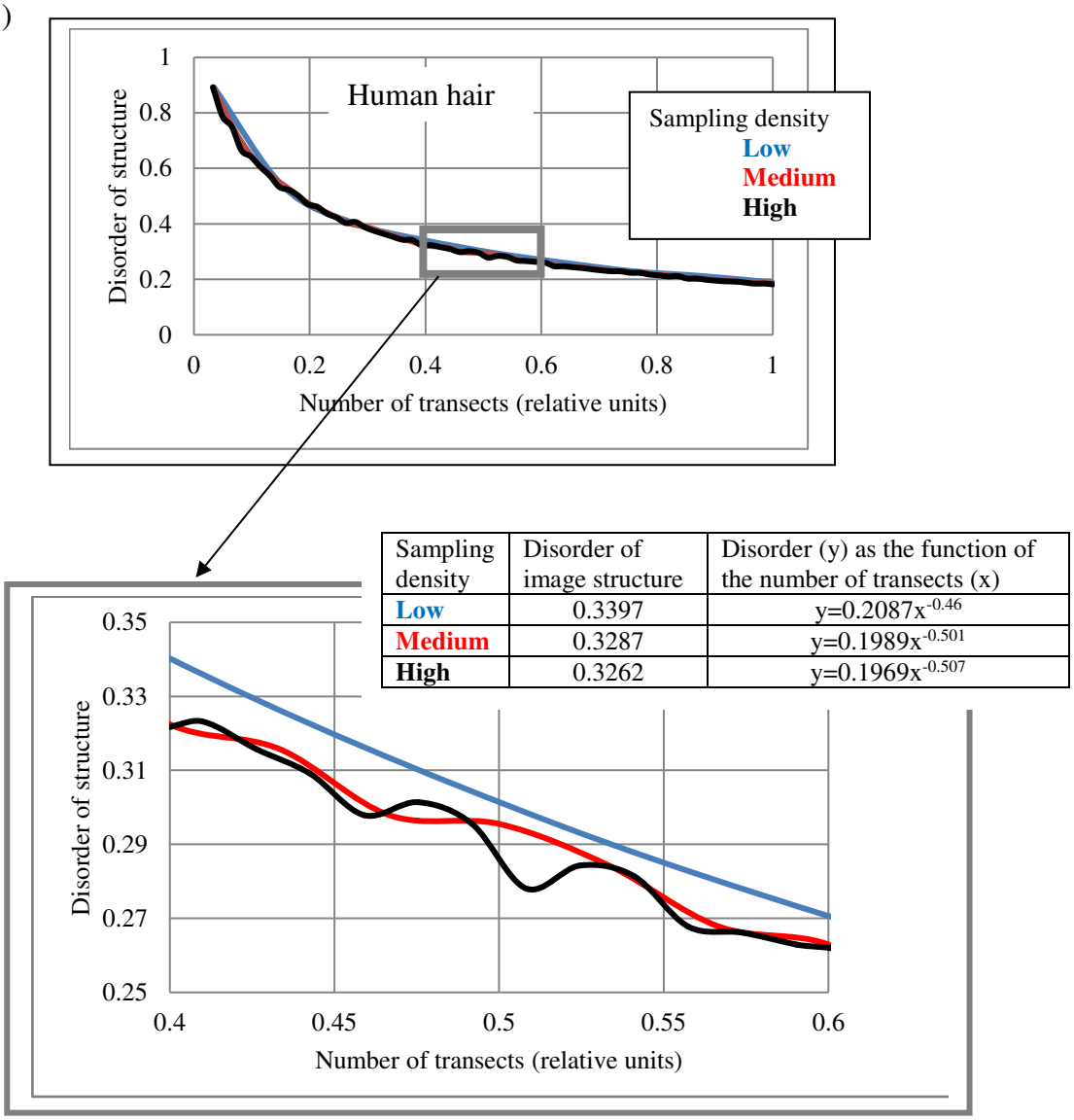

Sampling density	Disorder of image structure	Disorder (y) as the function of the number of transects (x)
Low	0.3397	$y=0.2087x^{-0.46}$
Medium	0.3287	$y=0.1989x^{-0.501}$
High	0.3262	$y=0.1969x^{-0.507}$

Figure 22B. Structural disorder as a function of sampling density

PeerJ Preprints | https://doi.org/10.7287/peerj.preprints.27451v2 | CC BY 4.0 Open Access | rec: 5 Jan 2019, publ: 5 Jan 2019

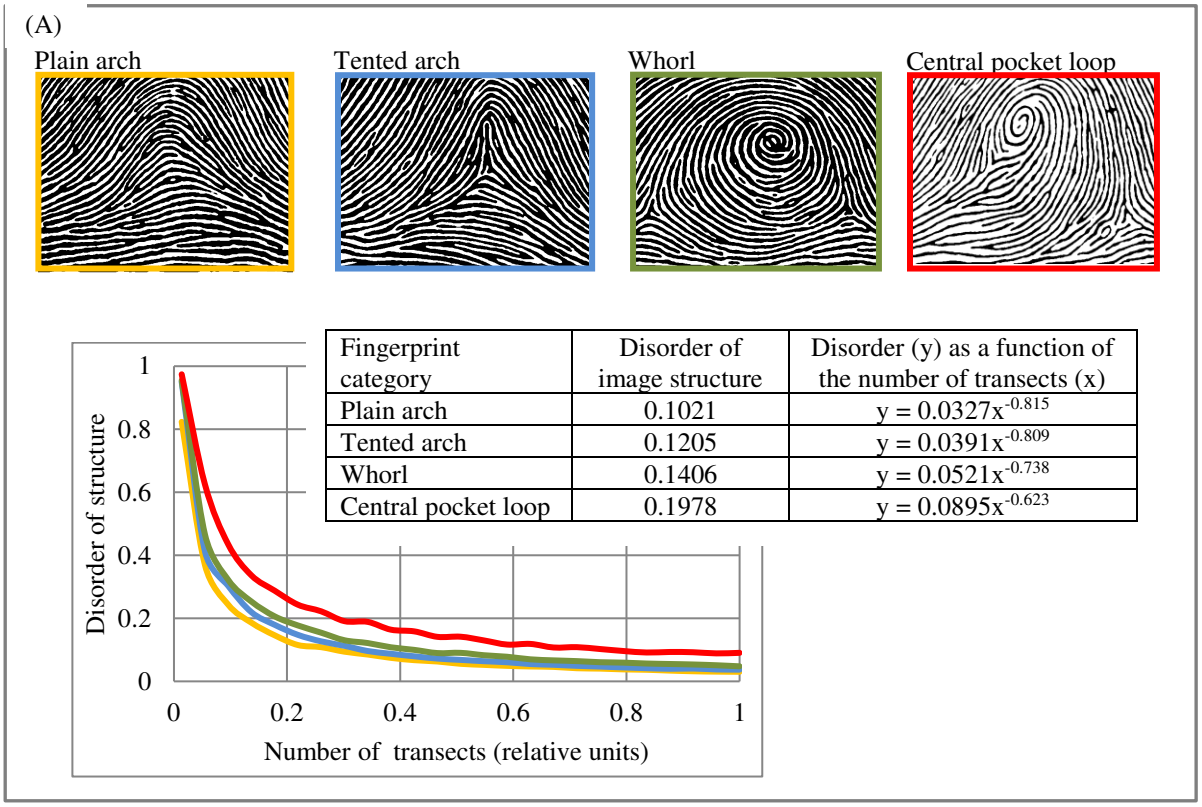

Fingerprint category	Disorder of image structure	Disorder (y) as a function of the number of transects (x)
Plain arch	0.1021	$y = 0.0327x^{-0.815}$
Tented arch	0.1205	$y = 0.0391x^{-0.809}$
Whorl	0.1406	$y = 0.0521x^{-0.738}$
Central pocket loop	0.1978	$y = 0.0895x^{-0.623}$

Figure 23. Morphology of fingerprints
Figure 23A. Structural disorder in four categories of fingerprints
Figure 23B. Structural disorder as a function of number of transects

As Figure 23A indicates, the four basic categories of fingerprint patterns have distinctive structural characteristics that vary from DStr(plain arch) = 0.1021 to DStr(central pocket loop) = 0.1978. Distinctions between DStr among different categories of fingerprints substantially depend on the number of transects used to calculate DStr (Section 2.2). To define the number of transects that allow maximal differences among DStr in the four categories of fingerprints, we plot the chart (Fig. 23B) as DStr(central pocket loop) − DStr(plain arch) = f(number of transects). Nine transects allow the maximal possible differences between two categories of fingerprints; that is, DStr(central pocket loop) − DStr(plain arch) = 0.253, which is 2.6 times more than the DStr(central pocket loop) and DStr(plain arch) comparison if equation (2) is used to calculate DStr. Sampling density and number of transects could complement DStr in forensic identification.

PeerJ Preprints | https://doi.org/10.7287/peerj.preprints.27451v2 | CC BY 4.0 Open Access | rec: 5 Jan 2019, publ: 5 Jan 2019

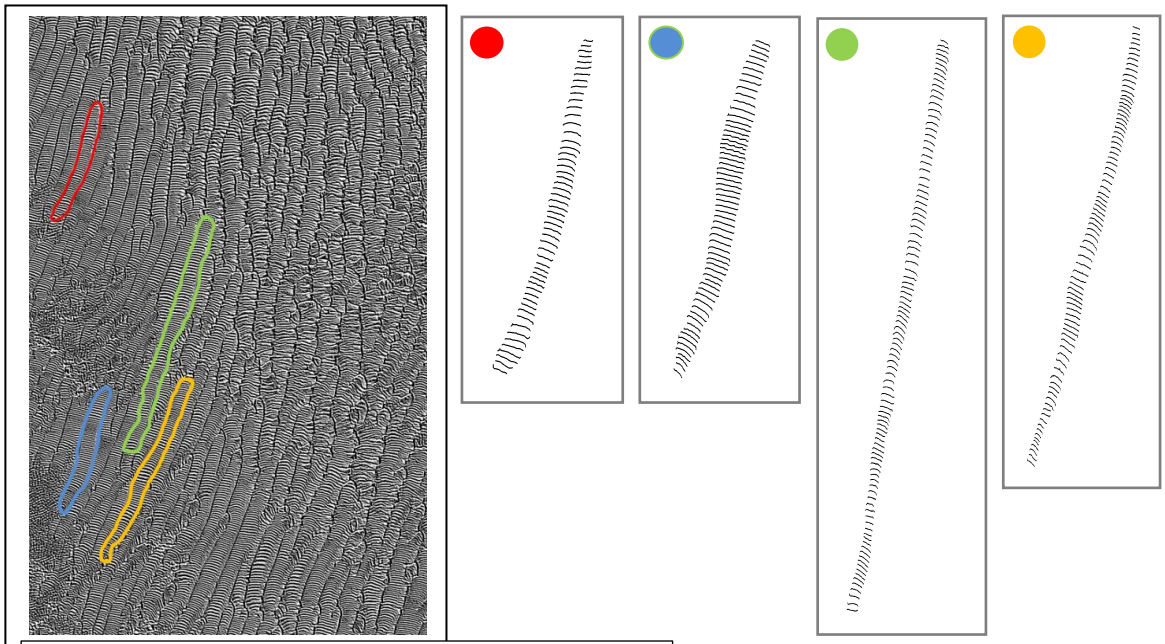

Credit: NASA/JPL/Univ. of Arizona. PSP_006609_1330

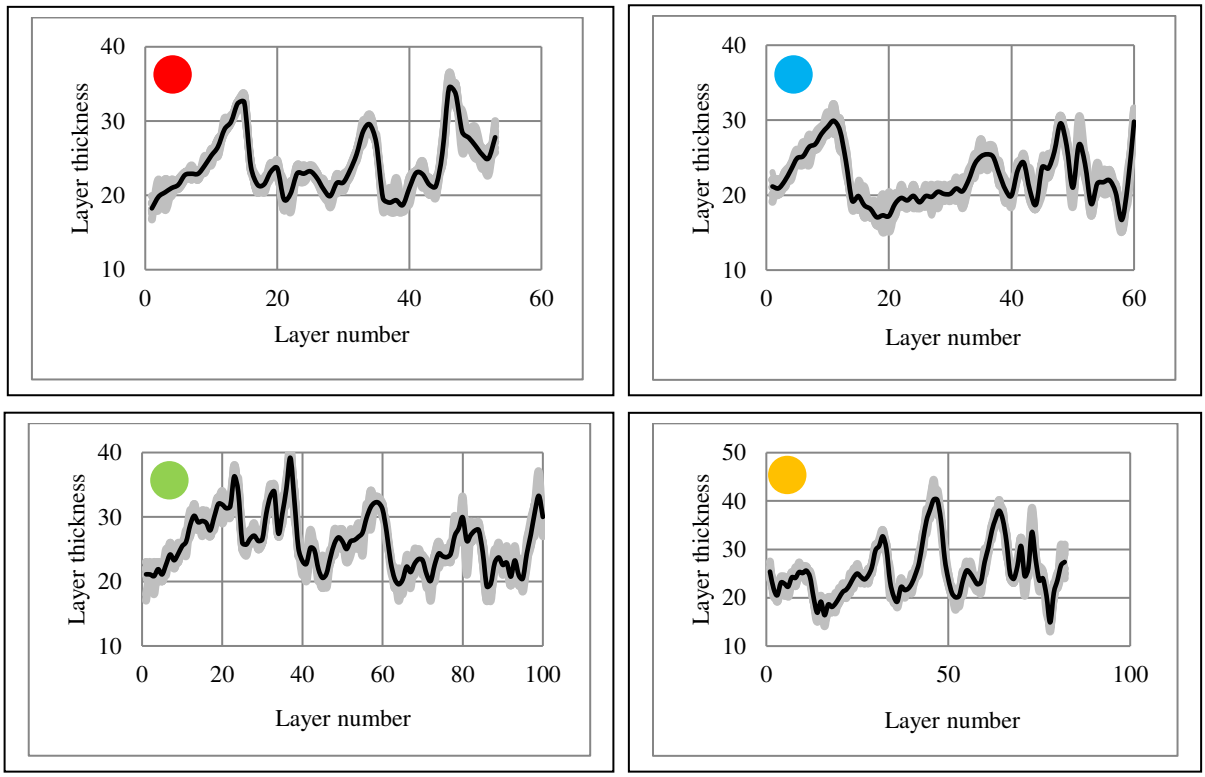

Figure 24. Layer thickness variability across a 2-D plane: Martian surface
See text next page

PeerJ Preprints | https://doi.org/10.7287/peerj.preprints.27451v2 | CC BY 4.0 Open Access | rec: 5 Jan 2019, publ: 5 Jan 2019

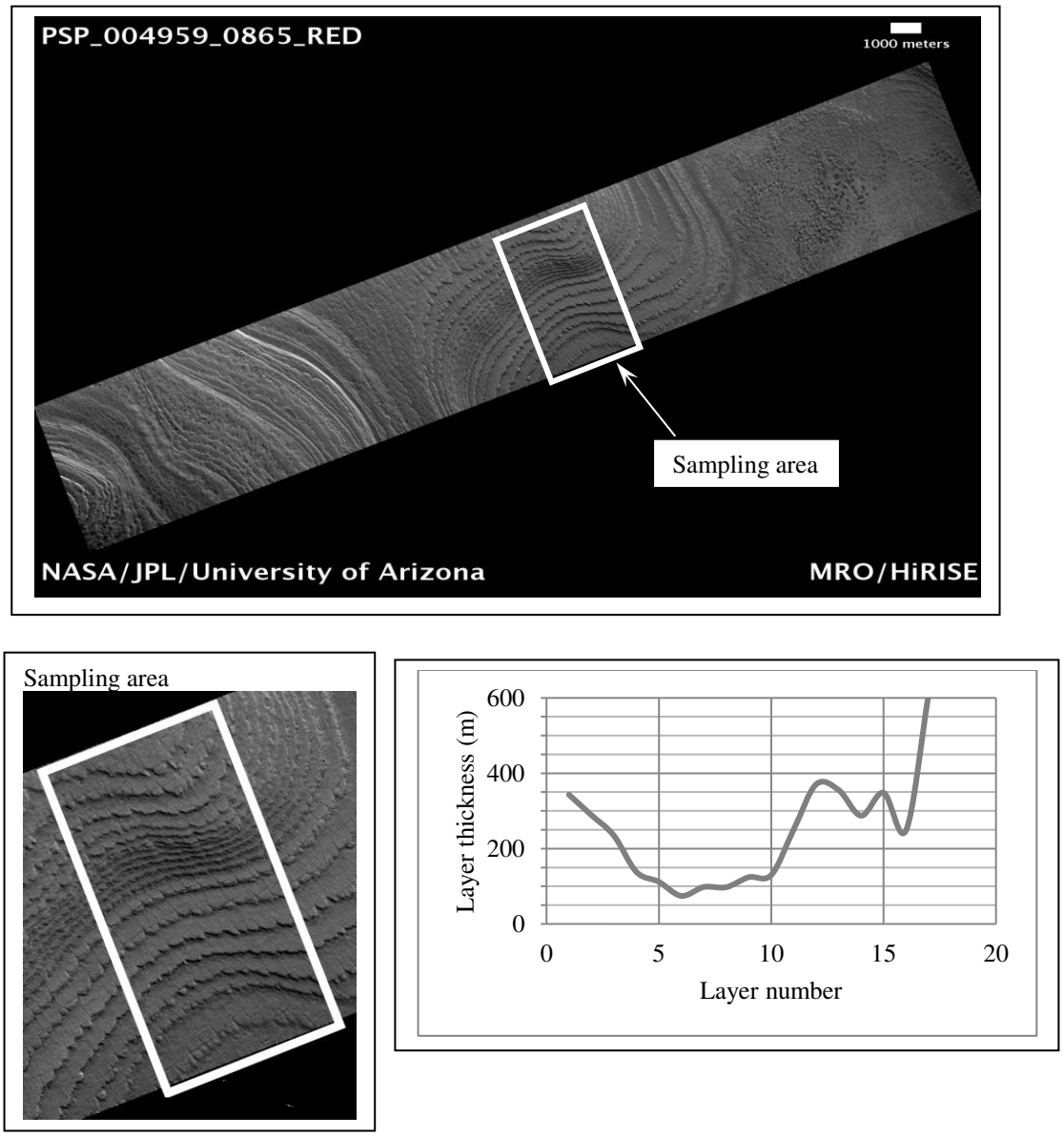

Figure 25. Layer thickness variability across a 2-D plane: South Pole of Mars

Dune fields are an example of the layered patterns that exist throughout nature. Dune spacing (i.e., layer thickness) is a basic morphological characteristic of dune systems (Lancaster, 2009). Figures 24 and 25 show layered fragments of the surface of Mars that have isotropic structure (i.e., all fragments have DStr = 0), which allows us to describe the variability of layer thickness across the 2-D sampling area with high accuracy. Several transects are used to calculate average thickness of each layer. Charts of "layer thickness vs. layer number" show cyclic trends in the variability of layer thickness across the sampling area (Fig. 24 and 25). Similar cyclic trends in anisotropic structures are also observed on Mars and Earth (Smolyar et al., 2016).

PeerJ Preprints | https://doi.org/10.7287/peerj.preprints.27451v2 | CC BY 4.0 Open Access | rec: 5 Jan 2019, publ: 5 Jan 2019

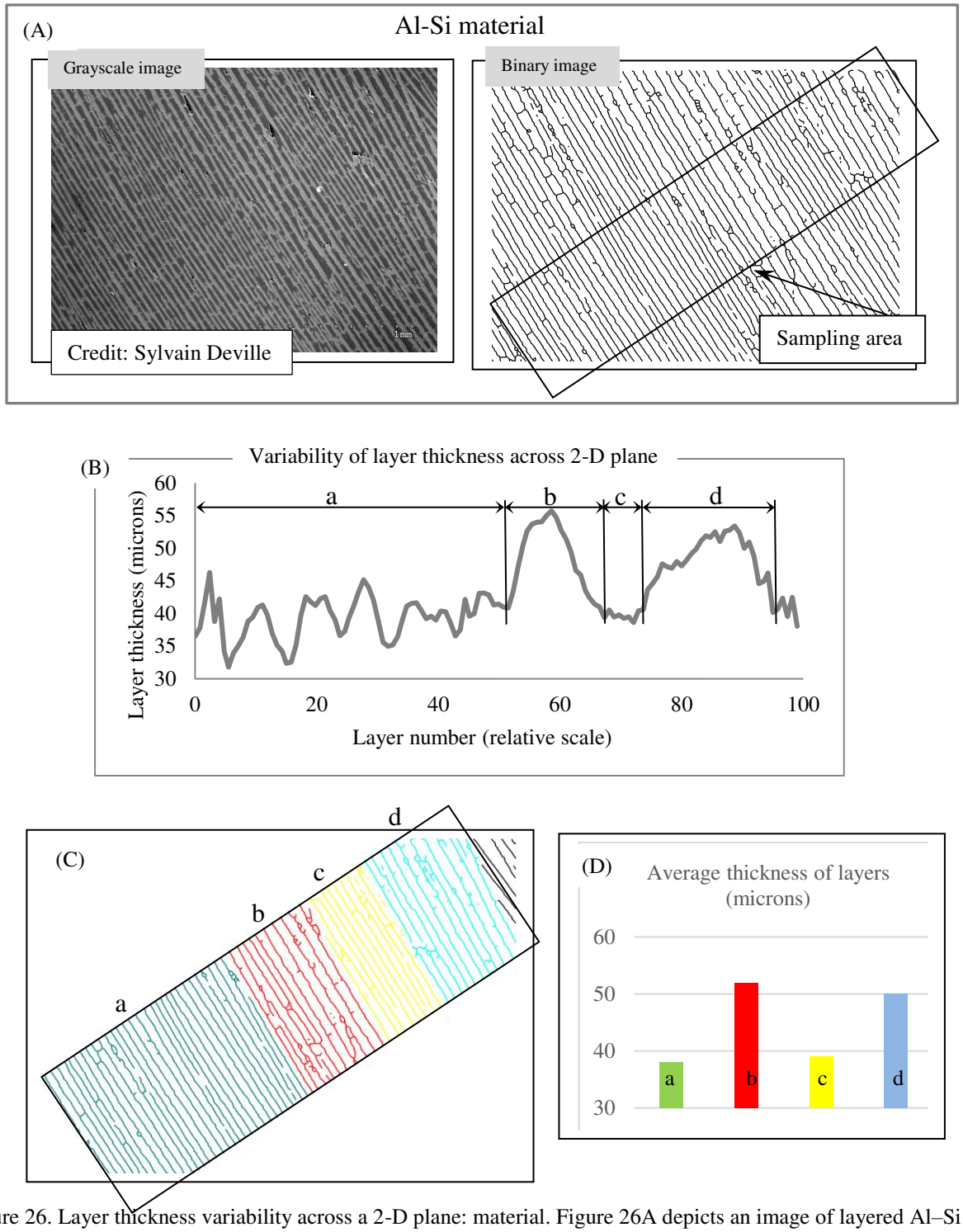

Figure 26. Layer thickness variability across a 2-D plane: material. Figure 26A depicts an image of layered Al–Si composite with anisotropic structure. The chart of "layer thickness vs. layer number" shows cyclicity in the variability of layer thickness across the sampling area (Fig. 26B), which is divided into parts A, B, C, and D (Fig. 26C) according to the uniform distribution of layer thickness in each part (Fig. 26D). It follows that the chart of "layer thickness vs. layer number" provides a more detailed description of a layered pattern's morphological characteristic than average layer thickness.

PeerJ Preprints | https://doi.org/10.7287/peerj.preprints.27451v2 | CC BY 4.0 Open Access | rec: 5 Jan 2019, publ: 5 Jan 2019

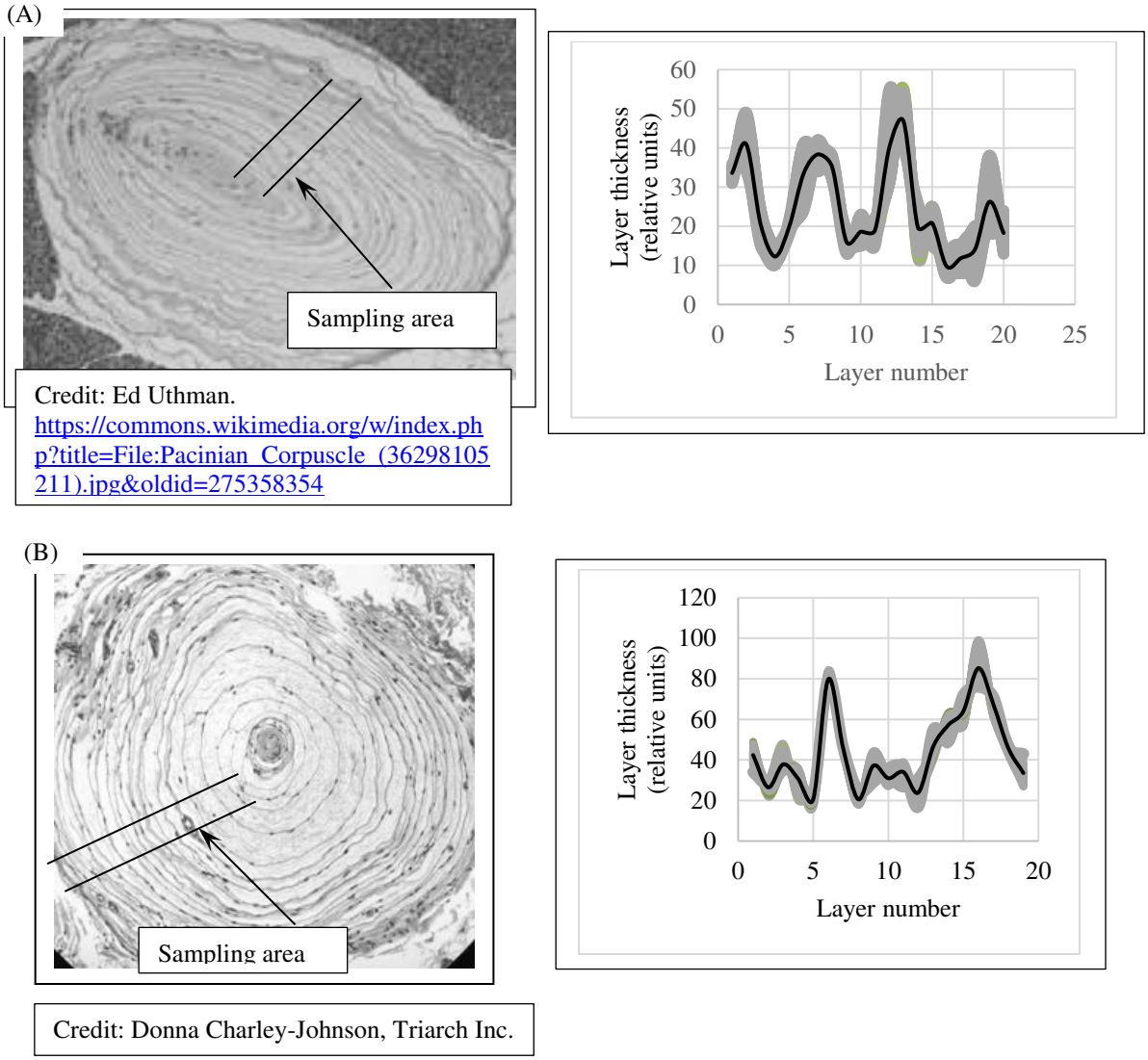

Figure 27. Layer thickness variability across a 2-D plane: Pacinian corpuscle

PeerJ Preprints | https://doi.org/10.7287/peerj.preprints.27451v2 | CC BY 4.0 Open Access | rec: 5 Jan 2019, publ: 5 Jan 2019

Credit: http://en.wikipedia.org/w/index.php?title=Banded_pitta&oldid=746065080

Credit: Philip Anderson

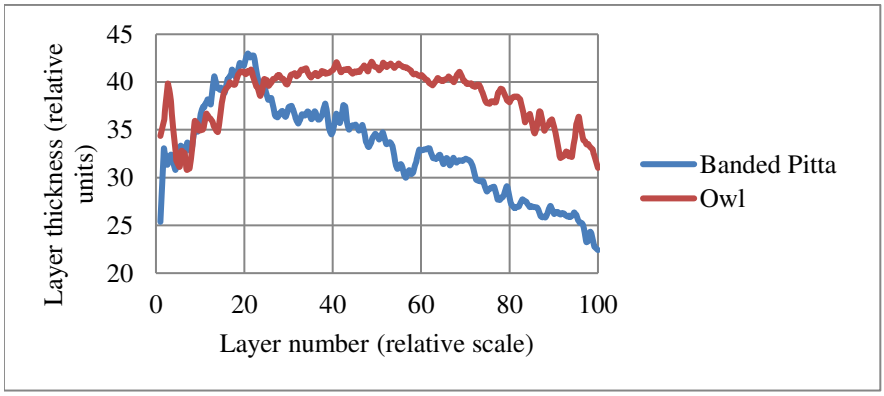

Figure 28. Layer thickness variability across a 2-D plane: banded pitta and owl feathers. The chart of "layer thickness vs. layer number" exhibits non-random trends in the variability of layer thickness across bird feathers (Fig. 28). The chart and DStr could potentially serve as morphological characteristics of birds with application to the study of their life cycles. Striped patterns are often used to distinguish bird species from one another. In particular, shrikes and their relatives are recognizable to birders by the peculiar differences in the thickness and layering of their striped patterns, many of which are simply black and white. Furthermore, there are often marked differences in the morphological features of feathers between males and females of the same species, a dimorphism that is recognized both by the animals themselves and by human observers (Gluckman 2014).

PeerJ Preprints | https://doi.org/10.7287/peerj.preprints.27451v2 | CC BY 4.0 Open Access | rec: 5 Jan 2019, publ: 5 Jan 2019

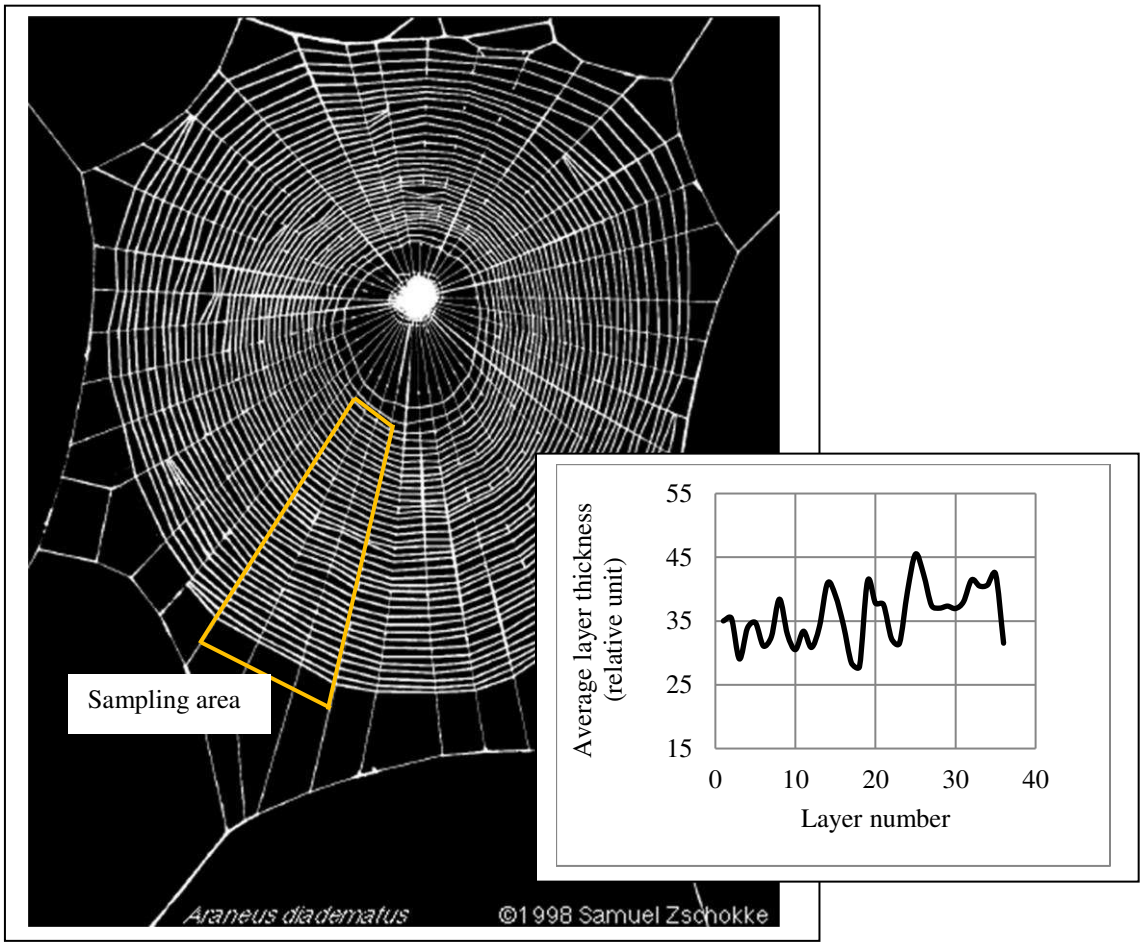

Figure 29. Layer thickness variability across a 2-D plane: spider web

The morphology of orb (circular) spider webs (Fig. 29) is frequently studied not only because of their superior mechanical properties but also as a source of information about spiders' construction behaviors (Sensenig et al., 2010; Eberhard, 2014; Soler and Zaera, 2016). The orb web represents a layered system with structural anisotropy: "One of the most relevant structural traits of orb webs is their mesh width" (Zschokke and Nakata, 2015, p. 661). Mesh width (i.e., layer thickness) is used to understand the construction features of web systems and relate them to spiders' behavior. For instance, Zschokke and Nakata (2015, p. 661) point out that "a closer look at the orb webs reveals that mesh widths are not the same throughout the entire web." Charts describing the variability of mesh width across the sampling area (Fig. 29) confirm this statement and indicate cyclicity in the variability of mesh width across the sampling area. Thus, $M = \{BF, G(N), T_{M,N}\}$ could be used to generate a new set of structural characteristics describing the anisotropy of an orb web and its segments.

PeerJ Preprints | https://doi.org/10.7287/peerj.preprints.27451v2 | CC BY 4.0 Open Access | rec: 5 Jan 2019, publ: 5 Jan 2019

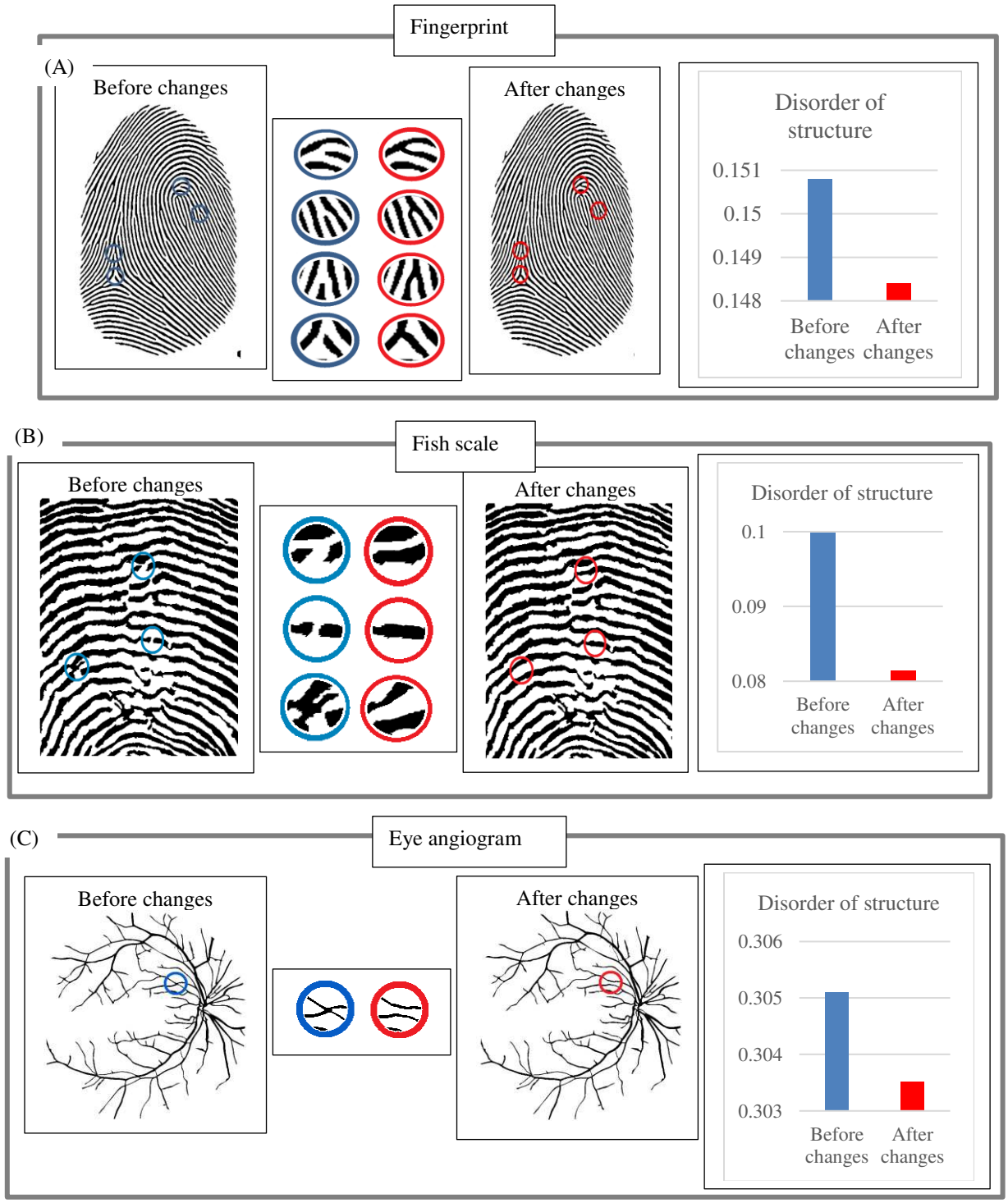

Figure 30. Sensitivity of parameter DStr to changes in layer structure.
See next page.

PeerJ Preprints | https://doi.org/10.7287/peerj.preprints.27451v2 | CC BY 4.0 Open Access | rec: 5 Jan 2019, publ: 5 Jan 2019

We examine how minor changes in layer structure affect DStr, using fingerprint (Fig. 30A), fish scale (Fig. 30B), and an eye angiogram (Fig. 30C) as test objects. Let us denote characteristics of images before and after structural changes by DStr(before changes) and DStr(after changes). We describe the link between DStr(before changes) and DStr(after changes) and structural changes in images in quantitative terms using the following procedure: First, we describe the difference between DStr(before changes) and DStr(after changes) on a relative scale (%). All changes in layer structure are marked in red. We denote the difference as Parameter-1. Second, we describe (in %) the difference (in pixels) between the images before and after changes. To do so, we calculate the number of black pixels in an image before changes (total pixels before changes) and the total number of pixels that change color (white to black or vice versa) as a result of structural changes (total pixel change). The ratio (%) of "total pixel change/total pixels before changes" allows us to calculate the magnitude of structural changes in an image. This ratio is denoted Parameter-2. The relation between Parameter-1 and Parameter-2 allows us to estimate the sensitivity of DStr to structural changes in the image. Results of calculating Parameter-1 and Parameter-2 are

	Parameter-1	Parameter-2
Fingerprint	0.55%	0.072%
Fish scale	3.80%	0.150%
Eye angiogram	0.32%	0.077%
Average	1.56%	0.10%

The average ratio between Parameter-1 and Parameter-2 is 1.56:0.1, which implies that a 1% structural change in layers results in a 15.6% change in DStr. This result provides evidence that minor changes in layer structure are accompanied by substantially greater changes in DStr values.

PeerJ Preprints | https://doi.org/10.7287/peerj.preprints.27451v2 | CC BY 4.0 Open Access | rec: 5 Jan 2019, publ: 5 Jan 2019

	Degree of disorder of layer structures											
	0	>0-0.1	0.1-0.2	0.2-0.3	0.3-0.4	0.4-0.5	0.5-0.6	0.6-0.7	0.7-0.8	0.8-0.9	0.9-1	
	Geology											
Mars surface	•		•	••	•							Fig. 5, 24
Tidal ripples					•		•					Fig. 8
Vertical section					•••							Fig. 7
	Geology. Structural anomaly											
Mars surface		•	•									Fig. 6A
Earth sand ripples				•		•						Fig. 6B
	Atmosphere											
Clouds			•	•								Fig. 9
USA at night										•		Fig. 11A
Hubble sky											•	Fig. 11B
Lightenings			•		•							Fig. 10
	Materials											
Alloy			•									Fig. 12A
Ion-induced ripples		•										Fig. 12A
Pearlite steel				•		•						Fig. 12A
Black diamond			••	•								Fig. 12B
	Medicine											
Bones		•	•									Fig. 13
Aorta					•••	•						Fig. 14
Eye angiogram			•		•							Fig. 15
	Forensic											
Fingerprints			•••									Fig. 23
Hairs		•	•		•							Fig. 22A
	Plants											
Flower			•••	•	•							Fig. 16
Leaf	•								•			Fig. 17
	Animals											
Fish skin			•••									Fig. 18
Snake skin		••										Fig. 19
Birds coloration		•	•		•	•			•			Fig. 20
Butterfly wing			•••									Fig. 21B
	0	>0-0.1	0.1-0.2	0.2-0.3	0.3-0.4	0.4-0.5	0.5-0.6	0.6-0.7	0.7-0.8	0.8-0.9	0.9-1	
	Degree of disorder of layer structures											

Figure 31. Overview of experiments: structural disorder in patterns formed in nature and beyond

PeerJ Preprints | https://doi.org/10.7287/peerj.preprints.27451v2 | CC BY 4.0 Open Access | rec: 5 Jan 2019, publ: 5 Jan 2019

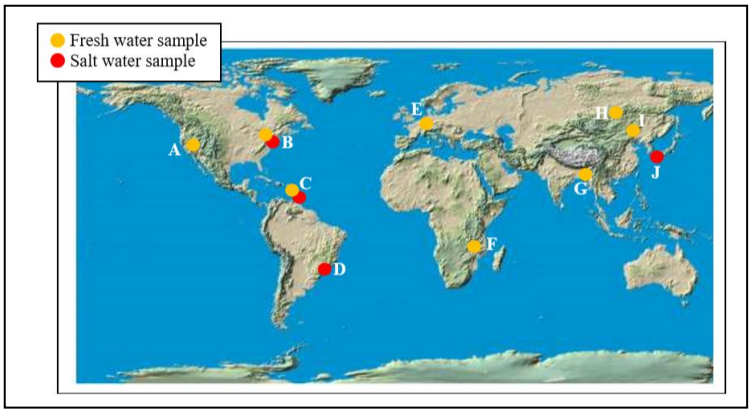

Area code	Sample ID*	Water category	Water sources	Place	Country	Coordinate
A	1	🟡	Well-2	Fresno, CA	USA	36°39’13"N, 119°39'49"W
A	2	🟡	Well-3	Fresno, CA	USA	36°38’57"N, 119°37'51"W
A	3	🟡	Snow	Lassen Volcanic Nat. Park	USA	40°28’27.3"N, 121°30'21.7"W
A	4	🟡	Snow	Crater Lake Nat. Park, CA	USA	42°54'32"N, 122°04'25"W
B	5	🟡	Tap, 0-min	Middletown, NY	USA	42º27' N, 74º25'W
B	6	🟡	Tap, 5-min	Middletown, NY	USA	42º27' N, 74º25'W
B	7	🟡	Delaware R.	Pleasant Park Hill, PA	USA	40°2'27.51"N, 4°59'31.04"W
B	8	🔴	Shore	Sea Island City, NJ	USA	39°11'34.4"N, 74°39'23.7"W
B	9	🟡	Canandaigua lake	State Marine Park, NY	USA	42°52'32.40"N, 77°16'36.50"W
C	10	🟡	Rain	Bathsheba	Barbados	13°12'42.18"N, 9°31'4.46"W
C	11	🔴	Shore	Oistins,	Barbados	13°3'39.86"N, 9°32'25.35"W
D	12	🔴	Shore	Rio de Janeiro	Brazil	22.977854°S, 43.187257°W
E	13	🟡	Nidda river	Frankfurt	Germany	50°9'46.10"N, 8°39'7.99"E
F	14	🟡	Malawi lake	Malawi Lake National Park	Malawi	12°10'60.00" S 34°21'59.99" E
G	15	🟡	Rain	Karachi	Pakistan	24.8427554°N, 67.06103329°E
H	16	🟡	Baikal lake	Khuzhir, Irkutsk Oblast	Russia	53°12'11"N, 107°20'27"E
I	17	🟡	Rain	Beijing	China	39°41'21"N, 115°55'23"E
J	18	🔴	Shore	Fukuoka,	Japan	33.596823°N, 130.359027°E

* ID - identification number

Figure 32. Distribution of water samples

PeerJ Preprints | https://doi.org/10.7287/peerj.preprints.27451v2 | CC BY 4.0 Open Access | rec: 5 Jan 2019, publ: 5 Jan 2019

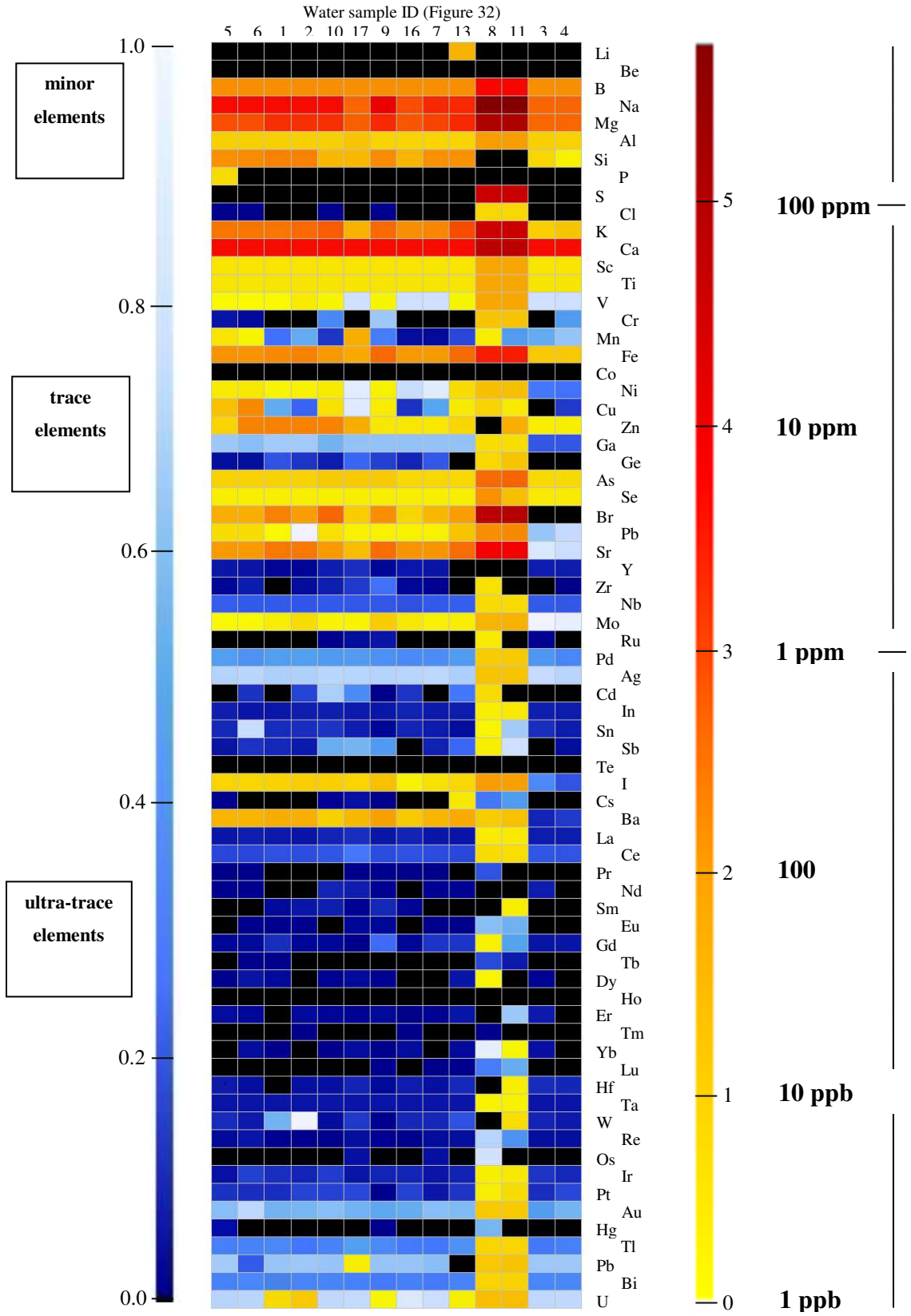

Figure 33. See next page

PeerJ Preprints | https://doi.org/10.7287/peerj.preprints.27451v2 | CC BY 4.0 Open Access | rec: 5 Jan 2019, publ: 5 Jan 2019

3162
3163 Figure 33. Element concentration patterns in (environmental) water. Element symbols are on right vertical
3164 axes. Trace concentrations between not detected (black) and 1 µg/L (white) are shown in shades of blue.
3165 Concentrations above 1 µg/L are represented by warm colors and given in a logarithmic scale and range
3166 from >1 µg/L (yellow) to over 3600 mg/L (dark red)
3167
3168

PeerJ Preprints | https://doi.org/10.7287/peerj.preprints.27451v2 | CC BY 4.0 Open Access | rec: 5 Jan 2019, publ: 5 Jan 2019

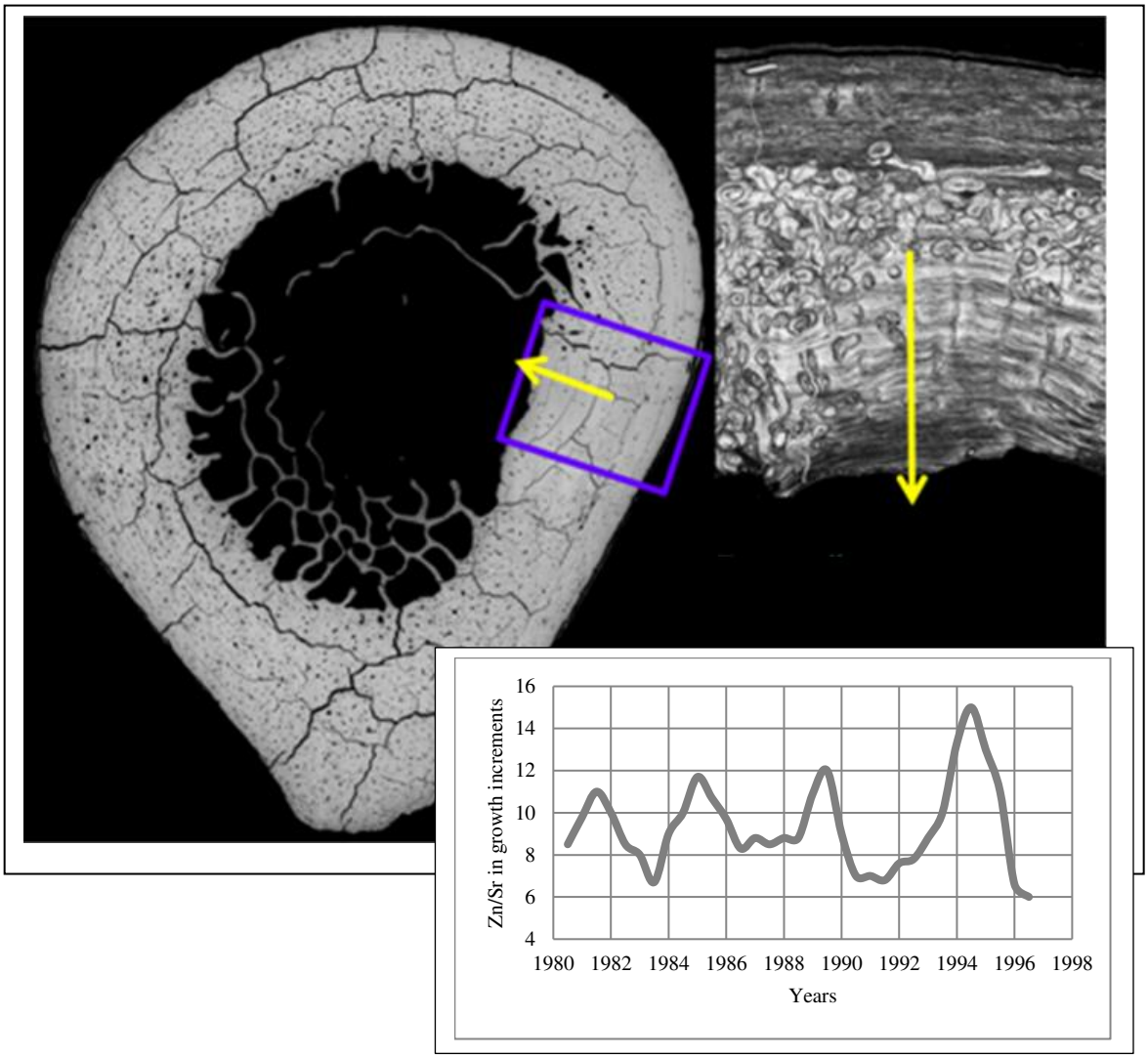

Figure 34. Zn/Sr ratio over 15 years of lamella bone

We discovered that the lamellar increments of bone are formed on the same interval at which the growth increments in enamel, the striae of Retzius, are formed (Bromage et al., 2009). Striae of Retzius may be calibrated in absolute time, and in this fisherman that period was 8 days. Roughly 15 years of continuously formed lamellar bone were available from years for which we have meteorological data. In the example shown in Figure 34, we demonstrate, for instance, that from 1981 to 1995, the concentration of Strontium (Sr) varies cyclically in its ratio with Zinc (Zn).

PeerJ Preprints | https://doi.org/10.7287/peerj.preprints.27451v2 | CC BY 4.0 Open Access | rec: 5 Jan 2019, publ: 5 Jan 2019

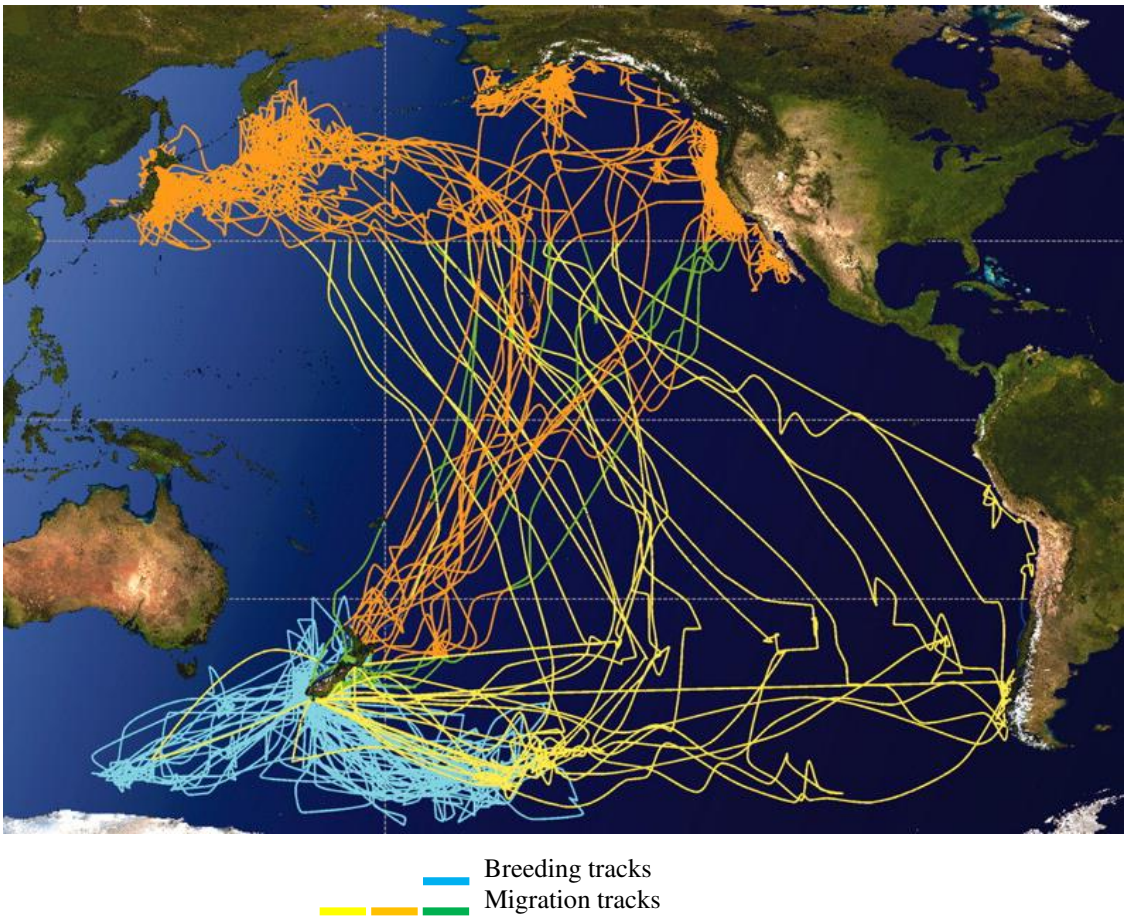

Credit: Shaffer, et al. PNAS ©, August 22, 2006, 103

Figure 35. Sooty shearwaters migration routes across Pacific Ocean

Examples in which marine data could relate to the structure of living organisms are birds' and turtles' morphology and their migration patterns across the world ocean (Fig. 35). Although the focus of the present work is the quantitative description of morphology of layered anisotropic patterns, nevertheless a proposed method could be potentially extended for processing morphological characteristics of arbitrary images such as birds' feathers, backs, and footprints. New instrumental methods of monitoring birds' and turtles' migration on a global scale (e.g., the ICARUS project) provide us with tools to describe collective birds motion across the world ocean.

PeerJ Preprints | https://doi.org/10.7287/peerj.preprints.27451v2 | CC BY 4.0 Open Access | rec: 5 Jan 2019, publ: 5 Jan 2019